Perm National Research Polytechnic University
Department Dynamics and Strength of Machines

Université des Sciences et Technologies de Lille
Laboratoire de Génie Civil et géo-Environnement

Année 2015 **N°**

THESE

Pour obtenir le grade de

Docteur de L'Université Lille1 - Sciences et Technologies

Discipline: Génie Civil

Présentée et soutenue publiquement par

KOSHELEVA NATALIA

Optimization of production and use superconductor products

Sous la direction de

Professeur Isam SHAHROUR

Professeur German KOLMOGOROV

Soutenance le 12 octobre 2015 à l'Université Lille1 - Sciences et Technologies

Devant le Jury Composé de :

Thèse dirigée par :

SHAHROUR Isam, Professeur, Université de Lille 1, Directeur de Thèse

KOLMOGOROV German, Professeur, Perm National Research Polytechnic University, Directeur de Thèse

Rapporteurs : Soulhi Aziz, Professeur, ENSMR, Rabat

Oleg Naimark, Professeur, ICMM of Urals Division of the Russian Academy of Science

Invités: Christian-Eric Bruzek, Chef de projet Cables Supraconducteurs, Nexans, France

Mikhail Tashkinov, Chercheur sénior, Perm National Research Polytechnic University

ABSTRACT

This thesis is devoted to the optimization the process of production of low-temperature superconductor (LTS) as well as high-temperature superconductor (HTS) products. The aim of the work is the optimization of the fabrication process.

Chapter 1 deals with the process of production of low-temperature superconductors. It provides analysis of the heating/cooling phenomena in the fabrication process. The chapter also proposes a method for determining the optimum angles of tools used in the fabrication of low-temperature superconductor.

Chapter 2 provides a general presentation of the high-temperature superconductors (HTS). The history of development of this material is summarized. The chapter gives a particular focus on the 2nd Generation of HTS. After a presentation of the structure of the high-temperature superconductor, the fabrication process and the challenges, we present the need for the use of numerical model on the design and fabrication of HTS.

Chapter 3 presents a simplified model for HTS beams. This model is based on the classical beam theory together with the discretization of each layer in small sub-layers working under purely axial stresses. The model takes into consideration the plastic behavior of the HTS constitutive materials. This model was implemented using MATLAB software. It presents also the validation of this model by its confrontation to finite element analyses as well as its use in the optimal design of HTS.

Chapter 4 presents the verification of the numerical model presented in the previous chapter for high-temperature multilayer 2G. The verification is carried out on a bending beam test conducted on a high-temperature superconductor tape. The test was presented first. The comparison of the numerical and experimental results allows the validation of the simplified model on experimental tests.

RÉSUMÉ

Ce travail de thèse est consacré à l'optimisation du processus de fabrication des supraconducteurs à basse température (SBT) et à haute température (SHT). Le but est l'optimisation de fabrication de ces produits.

Le premier chapitre est dédié au processus de production des SBT. La recherche concerne le problème de réchauffement de la surface des fils par les forces de friction lors du processus d'étirage. Le processus de réchauffement/refroidissement génère des contraintes résiduelles. Cet aspect a été traité dans ce chapitre. On y présente également une méthode pour déterminer les angles optimaux des outils utilisés dans la fabrication des supraconducteurs.

Le deuxième chapitre donne une présentation générale des SHT. On donne d'abord l'historique de ces produits, ensuite les développements en cours et les perspectives. Il présente aussi le processus de fabrication de ce matériel et ses défis. Le chapitre traite en particulier des SHT de deuxième génération et montre l'intérêt de l'emploi de la modélisation numérique.

Le troisième chapitre présente un modèle simplifié pour le comportement mécanique des SHT. Ce modèle est basé sur la théorie classique des poutres associée à une discrétisation de la poutre en sous-couches travaillant en traction-compression. Ce modèle prend en compte le comportement plastique des composantes de la poutre SHT. Le modèle a été implémenté dans un environnement MATLAB. La validation du modèle est effectuée par sa confrontation à des analyses par éléments finis. Le modèle est ensuite utilisé pour l'analyse des configurations industrielles dans un but d'optimisation.

Le quatrième chapitre présente la vérification numérique du modèle décrit dans le chapitre précédent sur un essai de flexion effectuée en laboratoire sur une bande «poutre» en SHT. La comparaison entre les résultats numériques et les données expérimentales montre le bon fonctionnement du modèle développé.

ACKNOWLEDGMENTS

I would like to sincerely thank supervisors of my thesis: Professor Isam Shahrour for his generosity, patience, thoughtfulness, excellent skills in cooperation work and good guidance throughout this thesis; and Professor German Kolmogorov for his endurance, thoughtfulness and willingness to help that were deeply appreciated. It has been a pleasure to have them as supervisors. My gratitude and appreciation for all members of my committee and especially for my committee chairman.

I am very grateful to the administration of Perm National Research Polytechnic University and International Office for enabling me an opportunity to make my phD in collaboration with Lille-1 University and their support in realisation of this program. I would like to thank the financial support of Russian Federation President's Scholarship and Scholarship of French Government (Doctoral scholarships Vernadski) that helped me to realise myself in my scientific carrier .

I would like to express my sincere thanks to Chef de projet "Cables Supraconducteurs" Nexans France Company Christian-Eric Bruzek for his co-operation, encouragement, friendly attitude and for numerous fruitful discussions.

I would like to express my thanks and gratitude to all my friends and colleagues in the LGCgE. You support granted me the ability and willing to complete this thesis. The friendship atmosphere, your concerns and assistance in different ways help me to overcome all difficulties throughout the period of my studies.

My heartiest thanks to my Russian friends: Anastasiia and Roman I, Mikhail and Irina T. that was in touch with me all these period. I am grateful to them not only for their big support, but also for a lot of productive discussions about my research, critical comments and suggestions, which helped me to make further improvements.

Finally, I would like to say big thanks for all my family, especially for my lovely parents, for their patience, love, support, and encouragement throughout my entire graduate study.

CONTENT

GENERAL INTRODUCTION

The work is devoted to the optimization process in the production of low-temperature superconductor (LTS) products as well as high-temperature superconductor (HTS) products.

Relevance of the work. The ambitious project ITER (International Thermonuclear Experimental Reactor) starts in 1990. This large-scale scientific experiment aims at the study of controlled thermonuclear reaction development of the industrial reactors of the future. ITER is one of the most complex scientific and engineering projects in the contemporary world. This project aims at producing in laboratory and in industrial conditions the Sun process: nuclear fusion of isotopes of hydrogen – deuterium and tritium, which leads to the formation of reactionless helium and the generation of large quantity of energy. To provide a huge amount of energy, which produces the nuclear fusion of isotopes of hydrogen, special current-carrying elements is required. Development and introduction of high technologies play significant part in solving this problem (Shikov, et al., 2003). Such processes include superconducting technologies – the technologies concerning the application of superconductor phenomenon (Ginzburg & Andrushin, 2006), i.e. electrical resistance loss at cooling to low temperatures.

Superconducting alloys or compositions cannot be used for practical purposes directly: it is necessary to create on their basis wires for the production of magnetic systems and other electrical devices, as superconductors work as a rule in unstable state. Superconductors must provide operating parameters: high critical temperature, high critical magnetic field and current density, certain mechanical properties. They must be highly corrosion stable, be stable to cyclic temperatures and voltage change, exposure to radiation and other exposures.

There are two main kinds of superconductor materials which are widely used in ITER: low-temperature (LTS) (Aymar, 2002) and high-temperature (HTS) (Kaizhong, et al., 2012).

The aim of the work: is the optimization of the technological bases of creation of low-temperature and high-temperature superconductor product in order to achieve the high quality manufacturing standards and reduce number of manufacturing problems.

To achieve the aims the following specific tasks were investigated:

- Determination of critical velocities of drawing of some metals providing items production on conditions of residual thermoplastic stresses prevention;
- Analysis of obtained results for copper, titanium, zirconium;
- Theoretical justification of pressing technology of low-temperature superconductor blank consisting of superconducting material core and copper jacket, in the form of:
  - monolithic blank with the given mechanical characteristics;
  - bimetal assembly blank;
  - trimetal assembly blank.
- Optimization and improvement of production technology of low-temperature composite superconductors for achievement of necessary production output at compliance with quality requirements;
- Mechanical modeling high-temperature superconducting tape from conditions of saving durability of a superconductor low-plastic composition layer in case of elastoplastic deformation during the manufacturing bending process;
- Development of numerical simulations for elastoplastic behaviour of high-temperature superconducting multi-layered tape;
- Optimisation the stresses inside the tape based on the principle of neutral axis.

Scientific novelty. At the first time, based on thermos-elasticity equations, temperature modes resulting in the appearance of thermoplastic deformations and the possible residual stresses formation were established. The critical drawing velocities for

such metals as copper, aluminium, titanium, steel, zirconium were obtained from the conditions of contact heating.

Theoretical justification of pressing technology of low-temperature superconductor blank consisting of superconducting material core and copper jacket, in the form of monolithic blank with the given mechanical characteristics, bimetal assembly blank and trimetal assembly blank was shown.

For 2G high-temperature tape the simplified numerical model that allows to find the optimal design was created. The main condition that requires keeping the neutral axis close to the superconductive layer were taken into consideration. The main principle of this model is the combination of the classical beam theory with the discretization of each layer in small sub-layers working under purely axial stresses. The best geometry of the HTS tape with the condition of reducing the mechanical stresses was found.

On the defence are made:

- Determination of critical velocities of drawing of some metals providing items production on conditions of residual thermoplastic stresses prevention;
- Theoretical justification of pressing technology of low-temperature superconductor blank consisting of superconducting material core and copper jacket, in the form of monolithic blank with the given mechanical characteristics (Kolmogorov, et al., 2011), bimetal assembly blank (Kolmogorov, et al., 2013) and trimetal assembly blank (Kolmogorov, et al., 2014);
- The main principle of the simplified numerical model that allows to find the optimal design for 2G HTS tapes as well as the validation of these model by its confrontation to finite element analyses and experimental.

The practical significance**:** The result of this thesis work could be easily implemented and used in industrial environment, in particular:

- to make an improvement in the pressing technology of low-temperature superconductor blank;
- to make a prediction and to find a right geometry for the high-temperature materials of second generation for different industrial applications.

Approbation of work: The results were presented and discussed at the following conferences and meetings:

1. VI Russian conference of students "National treasure of Russia" (2012, Moscow, Russia);
2. Russian competition of research works of students and phD students in the field of technical science.(2012, St. Petersburg, Russia);
3. Russian scientific conference of young scientists “Science. Technology. Innovation” (2012, NGTU, Novosibirsk, Russia);
4. XVIII Winter School on Continuous Media Mechanics (2013, Institute of Continuous Media Mechanics, Ural Branch of Russian Academy of Sciences, Perm, Russia);
5. «6-eme Journee de Doctorants. Mecanique, Genie civil, Energetique et Materiaux» (2013; Université de Valenciennes, France);
6. «7-eme Journee de Doctorants. Mecanique, Genie civil, Energetique et Materiaux» (2014; Université Lille-1, France);
7. XIX Winter School on Continuous Media Mechanics (Institute of Continuous Media Mechanics, Ural Branch of Russian Academy of Sciences, Perm, Russia, 2015);
8. International Conference on Mechanics of Complex Solids and Fluids (ICMCSF) (2015; Université Lille-1, France);
9. 12th European Conference on Applied Superconductivity (2015, Lyon, France).

Publications: On the topic of the thesis are published four articles in peer-reviewed Russian and in the international journals, 13 abstracts and articles in scientific collections, three patents.

Personal contribution of the author: All calculation and the results that were presented in the paper were obtained by the author or with his direct participation. The experimental test was done by author of the thesis in the Laboratoire de Génie Civil et géo- Environnement of Lille-1 University. The test samples of 2G HTS tape were provided by the Chef of the project & Nexans Fellow expert Chrictian-Eric Bruzek (Nexans Company, France).

The work was done: within the framework of agreement pursuant to a co-tutorial thesis between Université des Sciences et Technologies de Lille (Lille -1 University) in the Laboratoire de Génie Civil et géo- Environnement and Perm National Research Polytechnic University (PNRPU) in the Department of Dynamics and Strength of machines. The work was done with financial support of Russian Federation President's Scholarship and Scholarship of French Government (Doctoral scholarships Vernadski).

In the chapter 1 the optimization process under LTS materials the main attention has been given to developing drawing technology such metals as copper, aluminum, steel, titanium, and zirconium as well as the temperature regimes during drawing. In order to prevent the residual stresses in superconducting wire products, the problem of the friction forces in the process of drawing was investigated and limiting velocity values of drawing have been studied.

Also the important role in the fabrication process of low-temperature superconductors is played by pressing. In order to make an optimization the minimum consumption of energy should be provided during pressing. A new method for determining the optimum angles of technological tools for pressing billets of low-temperature superconductor such as monolithic piece, bimetallic composite billets, trimetal composite billets were described.

In the chapter 2 high-temperature superconductors of second generation were developed for different industrial applications, in particular for those in high energy density, nuclear, fusion and plasma applications. The optimisation of production of HTS

is devoted to industrial challenges during their manufacturing. The layered internal structure of HTS in combination with extremely weak adhesion between their layers could lead to degradation of the HTS by delamination. Moreover, in some applications, the superconducting tape is submitted to bending. And it is known that ceramic HTS tapes, which transmit power, could lose their conduction property by mechanical and thermomechanical stresses. Therefore, to solve this challenge issue the a simplified model for high-temperature superconductor tape was proposed.

Chapter 3 describes the main principle of this model is the combination of the classical beam theory with the discretization of each layer in small sub-layers working under purely axial stresses. This model was implemented using MATLAB software.

The validation was done using COMSOL Multiphysics software. After validation our model question of the optimal design of HTS was taken into account. The best geometry of the HTS tape with the condition of reducing the mechanical stresses was found.

Also the model was validated by experimental test in chapter 4. The validation test was shown in comparison with prediction of numerical model (HTS_Analysis program) that was implemented using MATLAB software. The texture analysis machine was used to make experimental test, because 2G HTS samples have a very small and specific thickness. During test analysis force – deflection dependence was obtained.

The HTS_Analysis program prediction and analysis of test result give us information about such important characteristics as critical forces, deflection, influence of boundary condition. All these parameters will help to construct the HTS tape with condition of respect of the high quality manufacturing standards. The recommendation about improvement and optimization the fabrication process can be easily given after HTS_Analysis program simulation.

Volume and structure of the thesis: The thesis is stated on 102 pages of text, illustrated with 7 tables and 46 figures. Bibliography contains 100 references. The work consists of general introduction, four main chapters, general conclusion and references.

CHAPTER 1. Superconductors cables for ITER

The chapter 1 is devoted to the optimization process in the production of low-temperature superconductor products.

The paper deals with contact heating of wire workpiece surfaces problem because of the friction forces in the process of drawing. In the limiting case, thermoplastic condition of the workpiece is transferring into thermoplastic condition. Under the further cooling of the workpiece, it may have undesirable residual stresses. In the plastic deformation appearance conditions the allowable values of contact heating and the corresponding heating rate of drawing have been worked out. For some metals the limiting velocity values have been received.

The paper also proposed a method for determining the optimum angles of technological tools for pressing billets of low-temperature superconductor, which is consist of superconducting core material and the copper shell to form, in look: monolithic piece with the above mechanical properties, bimetallic composite billets, trimetal composite billets.

In a basis of optimization tension of pressing that provides the minimum consumption of energy during pressing is necessary. The technological parameters affecting the pressing force are revealed. Influence of an extract and factor of a friction on values of optimum angles is shown.

1.1. Introduction

History of construction of ITER

The ambitious project ITER (International Thermonuclear Experimental Reactor) starts in 1990. This large-scale scientific experiment aims at the study of controlled thermonuclear reaction development of the industrial reactors of the future. ITER is one of the most complex scientific and engineering projects in the contemporary world. This project aims at producing in laboratory and in industrial conditions the Sun process: nuclear fusion of isotopes of hydrogen – deuterium and tritium, which leads to the formation of reactionless helium and the generation of large quantity of energy.

In 1978 in the Soviet Union built first TOKAMAK with superconducting system (Fig. 1.1). The idea of the creation of such thermonuclear synthesis installation based on superconductors belongs to "KURCHATOV INSTITUTE" (Sherbakov, et al., 2012).

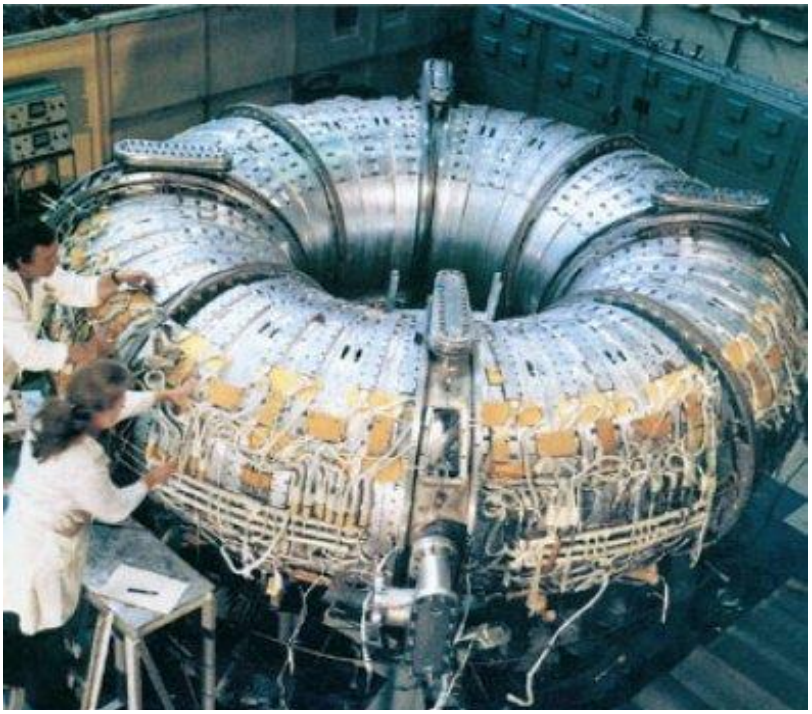

Fig. 1.1. First in the world TOKAMAK with superconducting system.

In 1985, the former Soviet Union built the 2nd Generation of TOKAMAK. The USA with European Community and Japan started worked in this field. In June 2005 the partners of the ITER decided to locate it at Cadarache, in France.

To provide a huge amount of energy, which produces the nuclear fusion of isotopes of hydrogen, special current-carrying elements is required (Ginzburg, 1999). Development and introduction of high technologies play significant part in solving this problem (Shikov, et al., 2003). Such processes include superconducting technologies – the technologies concerning the application of superconductor phenomenon (Ginzburg & Andrushin, 2006), i.e. electrical resistance loss at cooling to low temperatures. Schematic diagram of the International thermonuclear experimental reactor is shown in Fig. 1.2.

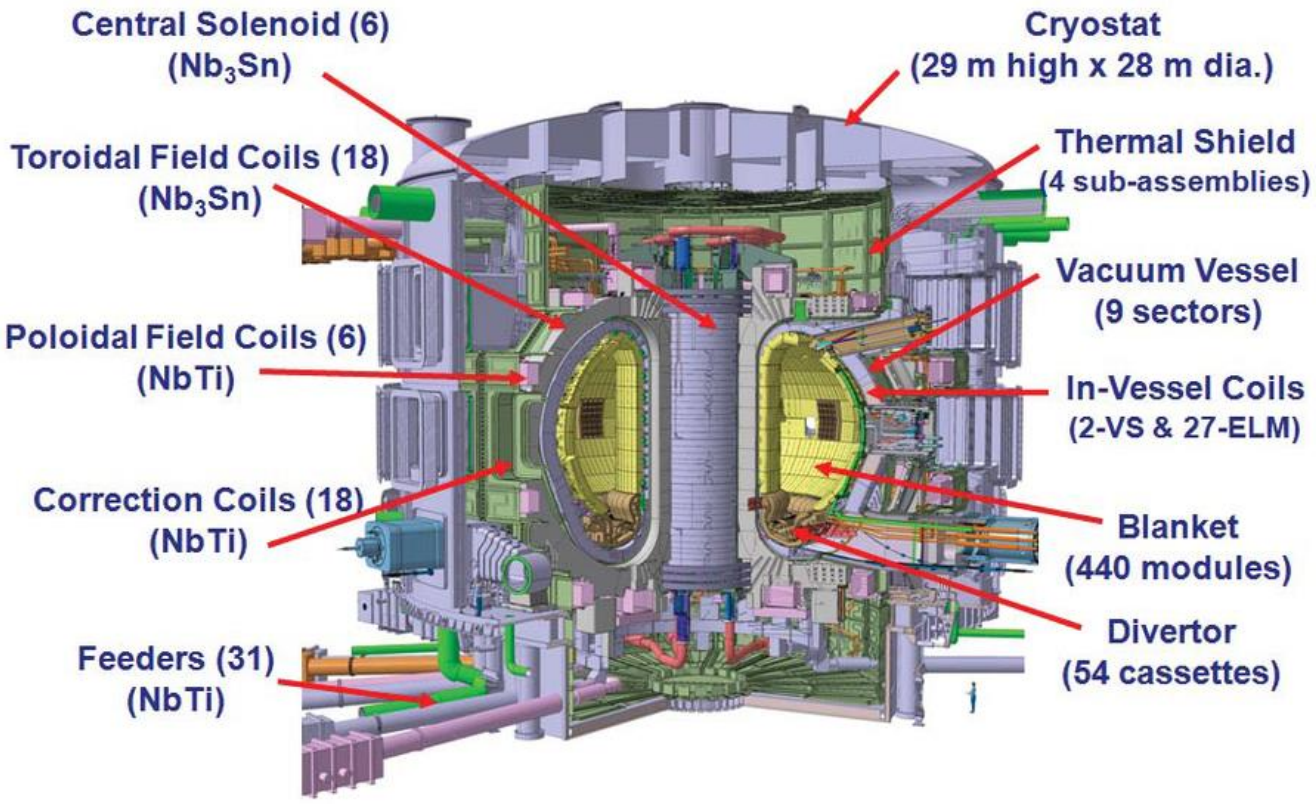

Fig. 1.2. Schematic diagram of the components of ITER tokamak.

Superconducting alloys or compositions cannot be used for practical purposes directly: it is necessary to create on their basis wires for the production of magnetic systems and other electrical devices, as superconductors work as a rule in unstable state.

Superconductors must provide operating parameters: high critical temperature, high critical magnetic field and current density, certain mechanical properties.

They must be highly corrosion stable, be stable to cyclic temperatures and voltage change, exposure to radiation and other exposures.

There are two main kinds of superconductor materials which are widely used in ITER: low-temperature (LTS) (Aymar, 2002) and high-temperature (HTS) (Kaizhong, et al., 2012).

1.2. Low temperature superconductors

1.2.1. Introduction

The low-temperature superconductors are produced in the form of long-length (up to 16 km) wires and bands allowing the production of large-scale products for different purposes – such as cryo-engines, medical diagnostic tomographs, transformers, thermonuclear fusion units etc.

The materials for the LTS superconducting wires are primarily of niobium-titanium alloys, as well as here is a compound Nb_3Sn (Kolmogorov, et al., 2011). Fig. 1.3 presents a variety of design of superconducting products.

Mechanical and electromagnetic disturbances may give rise to the destruction of superconducting state especially in conditions when operating temperature is close to the critical temperature of the superconductor. To prevent this phenomenon, superconductor stabilization is necessary. The technical superconductor is a composite system consisting of heterogeneous materials differing by their physicochemical, mechanical and physical properties. Usual, it is multifiber wire where superconducting material fibers are placed in copper or bronze matrix with diffusion barrier layers, reinforcing elements and partitions from material with high electrical resistance

Superconducting current in such cable is distributed by all cores. At parallel connection of the copper and the superconducting conductors all current flows by the

superconductor (JSC «Chepetsky Mechanical Plant», 2014). The design of low temperature superconductor cable is presented in Fig. 1.4.

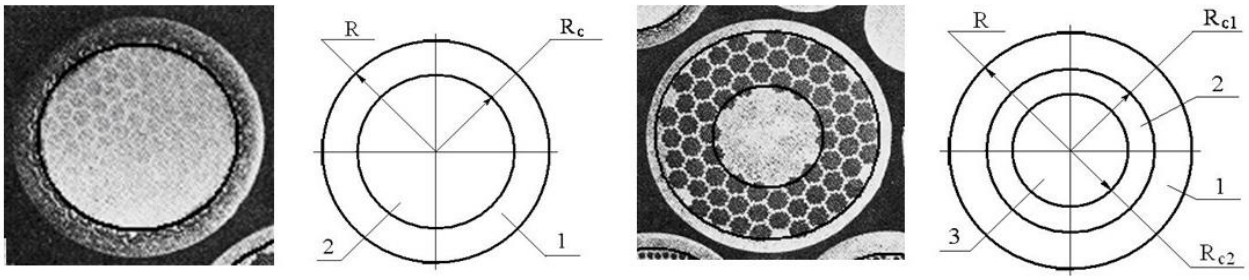

Fig. 1.3. Schematization of construction of superconductors on the basis of NbTi alloys in the form of bi- and trimetal: 1 – is the shell; 2 – is the intermediate layer; 3 – is the core; R – is the conductor radius; R_{c1} – is the external radius of the intermediate layer; R_{c2} – is the core radius.

Superconductors on the basis of NbTi are produced in a stabilized state with copper shell. Many orifices are drilled in the copper block to place superconductor rods. Then the block is drawn into long wire which is cut into pieces and they put into copper block again. This operation is repeated many times. The result is a cable containing up to million superconducting cores, from which electromagnet coils are winded.

Fig. 1.5. shows the superconducting wires production technology, which includes several stages. Two drawing (Perlin & Ermanuk, 1972) and pressing (Perlin & Reitbarg, 1975) technologies are applied during the production of the superconducting composite. They are the most critical steps in the production of superconductors.

Fig. 1.4. Low temperature superconductor cable.

The superconductors' production technology includes cast bar production, pressing and drawing to the final size with intermediate annealing. Drawing and pressing substantially determines the quality of the finished product.

The cross section of the conductor for superconducting magnetic systems is a complex geometric object and may be presented as two- or three layers (bi- or trimetal), which external layer in copper current-stabilizing shell, and the intermediate layer or the

core in composite (Christensen, 1982) consisting of NbTi fibers located in copper matrix. Multifibers superconductors have diameter in the range *0.1-0.6 mm*, length up to *30000 m.* It consists several tens of thousands of superconducting fibers with diameter of *1-50 mcm* twisted around wire axis.

Deformation according to drawing process technology is typical for all composite superconductors production stages, which confirms the necessity to study drawing and pressing process during superconducting products manufacturing (Foner, 1987).

During plastic deformation (Malinin, 1975) of drawing or pressing, residual stresses are induced in the pulled products. These stresses have a negative impact on superconducting products.

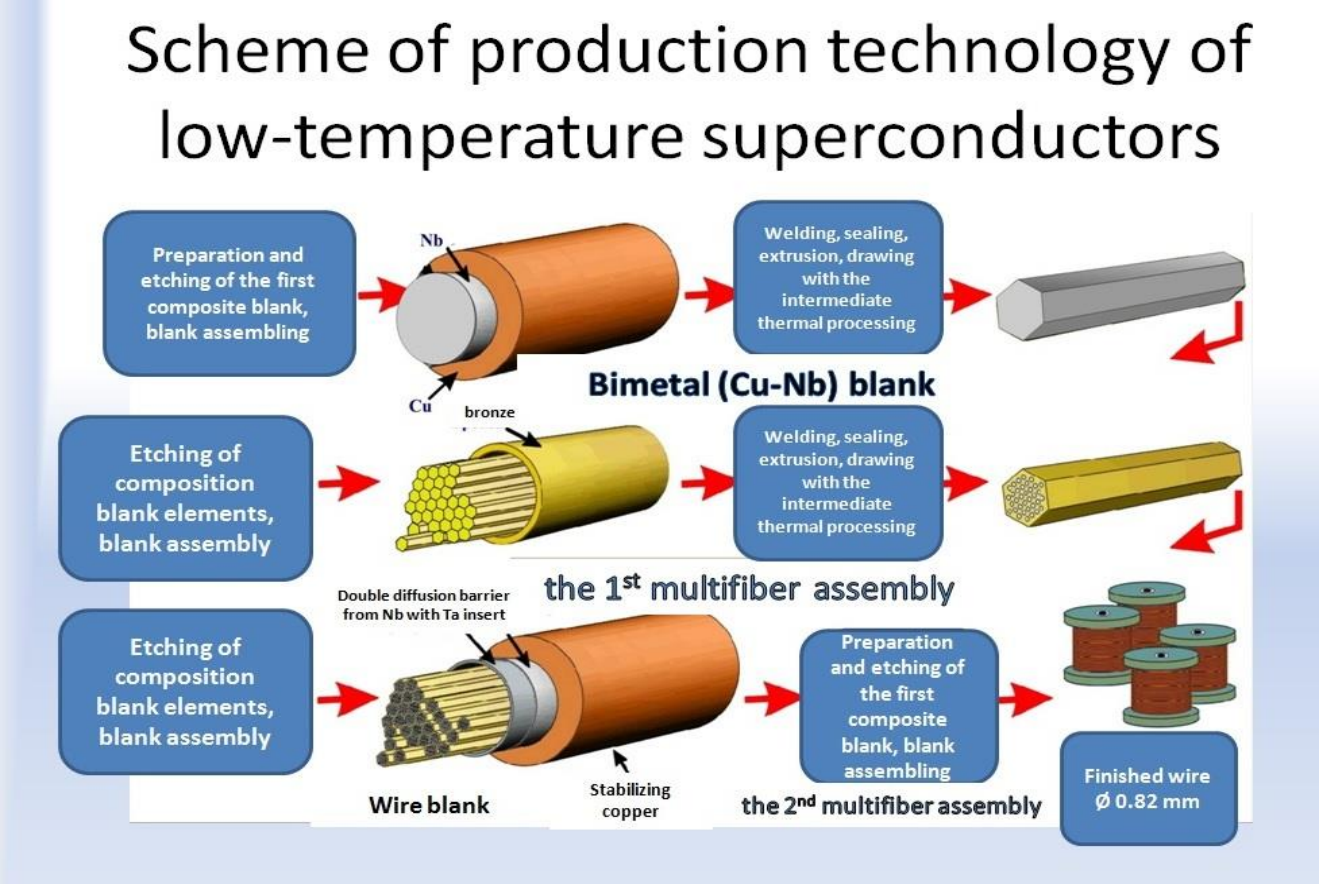

Fig. 1.5. Scheme of production technology of low-temperature superconductors. (JSC «Chepetsky Mechanical Plant», 2014).

Unfavorable wire temperature mode during the plastic deformation leads to the creation of residual stresses during drawing. An undesirable wire surface heating is created by the friction between the product surface and wire-drawing tool (Kolmogorov & Shirobokov, 1995), (Kolmogorov, et al., 1992). The contact heating may be

significant and may lead to thermal stresses, capable of thermoplastic deformations and formation of undesirable residual stresses in the drawn product during the following cooling.

Drawing is a technique of metal processing by pressure when the processed metal in the form of blank with equal cross section is inserted into the channel of drawing tool and is pulled (drawn) through it (Kolmogorov, et al., 2007). This channel has cross sections with the same or close to the form of cross section of the pulled metal but gradually reduced from metal input into the tool to its output. The output channel cross section is always less than the cross section of the pulled stripe. Therefore the latter passing through the drawing tool is deformed and its cross section changes taking after drawing tool the form and the size of the least channel cross section.

The stripe length increases in direct proportion to the cross section decrease. The leading stripe end meant for processing is sharpened before drawing at special machine so that the end comes into the drawing tool and partially comes out from the other side. This end is drawn and winded by special mechanism (Perlin & Ermanuk, 1972).

1.2.2. Production of low-temperature superconductors

The manufacturing technology of superconductors is based on the plastic deformation of metals using metal forming methods, in particular, extrusion of a combined billet and its repeated drawing. The highest labour input is accounted for drawing. The drawing process means drawing a billet through a conical drawing tool, and the total number of stages in superconductor production reaches several dozens.

On the Fig. 1.6 are shown the schematic drawing of the superconductor bimetallic billet. During the drawing process, the plastic deformation is characterized by the draw ratio:

$$\lambda_i = \frac{F_{i-1}}{F_i} = \frac{d_{i-1}^2}{d_i^2}, \qquad (1.1)$$

F_{i-1} and F_i denote the cross-sectional area before and after the pass; d_{i-1} - is the diameter of the billet before entering the drawing tool; d_i - is the diameter of the billet at the output of the tool.

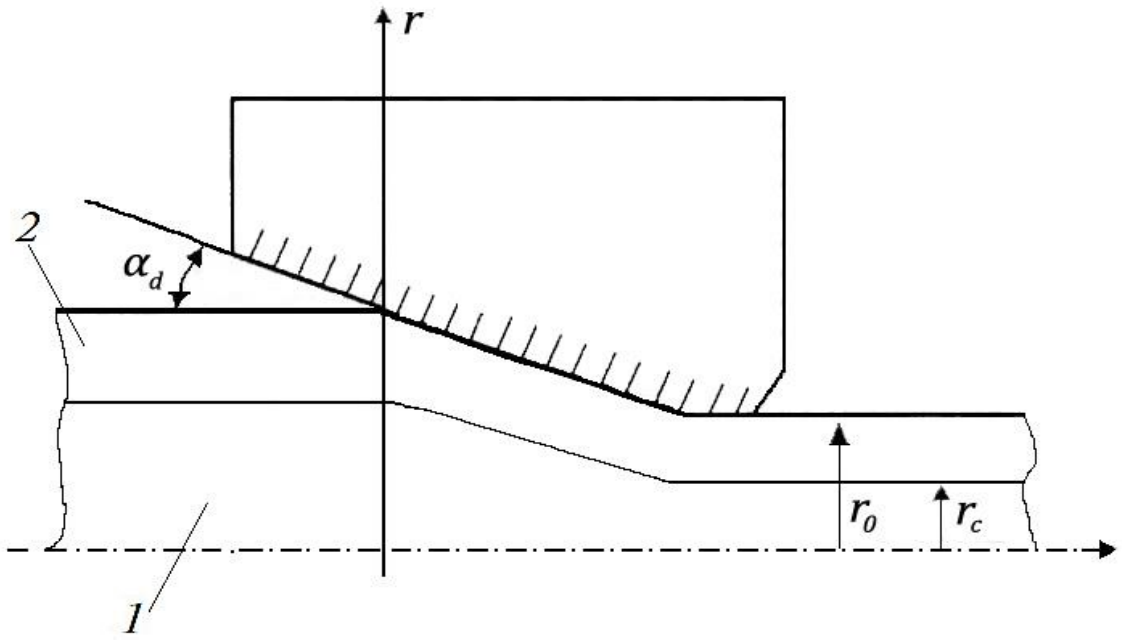

Fig. 1.6. Schematic drawing of a superconductor bimetallic billet: 1 - core; 2 - shell; α_d – inclination angle of a forming of the working cone to the drawing axis; r_0 and r_c - values of the radial coordinate for the shell and the core of the billet respectively.

In repeated drawing the aggregate draw is determined by the area ratio of the original superconductor billet F_0 and the finished superconductor of cross section F_k; the aggregate draw being determined through draw ratios for individual passes by the relation:

$$\lambda_{\Sigma} = \frac{F_0}{F_k} = \lambda_1 \cdot \lambda_2 \cdot \lambda_3 \cdot \ldots \cdot \lambda_n, \tag{1.2}$$

where n is the total number of passes in drawing.

To assess the manufacturing complexity of superconductor products, in the case of realization of equal draw ratios on the route of multiple deformation of the

superconductor billet, the averaged around technological cycle draw ratio λ_{av} is introduced. Then from equation (1.2) for the averaged draw ratio the aggregate draw will be:

$$\lambda_{\Sigma} = \frac{F_0}{F_k} = \lambda_{av}^n . \tag{1.3}$$

From equation (1.3) the number of repeated drawing passes required to produce a superconducting product is determined:

$$n = 2\ln\left(\frac{d_0}{d_k}\right) \Big/ \ln \lambda_{av} , \tag{1.4}$$

d_0 and d_k designate the diameters of the superconductor billet and the finished superconductor, respectively.

From equation (1.1) for the given λ_{av} pass routes are defined:

$$d_i = \frac{d_{i-1}}{\sqrt{\lambda_{av}}} . \tag{1.5}$$

Optimization of the drawing routs allows to achieve the following objectives:

- ✓ reduce the number of the route passes;
- ✓ avoid breakage of long-length billets;
- ✓ improve quality of the surface of superconductor products;
- ✓ increase durability of the drawing tool.

In the processing of metals by pressure it is the deformation degree that largely defines energy-power and technological parameters of plastic deformation.

Reference (Kolmogorov, 1986) gives a formula for determining the average over cross section deformation degree in drawing axisymmetric superconductor products:

$$\varepsilon_{av} = 2\ln\frac{d_0}{d_1} + \frac{4}{3\sqrt{3}}\tan\alpha_d, \tag{1.6}$$

where α_d is the inclination angle of a forming of the tool to the drawing axis, d_0 is the outer diameter before the pass, d_1 is the outer diameter after the pass.

The technology of drawing superconductor composite billets requires knowledge of the deformation temperature conditions. In repeated drawing the billet temperature changes due to the deformation heat up in each pass and are determined by the terms of cooling between passes. Knowledge of the temperature mode is necessary to assess the thermos-elastic state of a multi-component billet and prevent possible shell detachment from the core.

To determine the heat of the metal wire under deformation it is necessary to define the work spent on the deformation, as

$$A = \int_0^{\varepsilon} \sigma_s d\varepsilon, \tag{1.7}$$

If all plastic deformation work is transformed into heat, then the temperature raise for a volume unit of the material element during the adiabatic process of deformation is defined by the equation:

$$\Delta t = A/(c\gamma), \tag{1.8}$$

where c is the specific heat of the drawn metal; γ is the metal density.

In the deformation heat up, the shell may be detached from the core due to the difference of thermo physical properties of their materials. To evaluate the possible detachment and prevent it in the manufacturing process the thermos-elastic state of the bimetallic superconductor billet is considered (see illustration).

The thermos-elastic state of an axisymmetric body is described by the equations of the elasticity theory (Timoshenko & Goodier, 1975):

$$\left.\begin{aligned}\varepsilon_r - \alpha T &= \frac{1}{E}\left[\sigma_r - \nu(\sigma_\theta + \sigma_z)\right];\\ \varepsilon_\theta - \alpha T &= \frac{1}{E}\left[\sigma_\theta - \nu(\sigma_r + \sigma_z)\right];\\ \varepsilon_z - \alpha T &= \frac{1}{E}\left[\sigma_z - \nu(\sigma_r + \sigma_\theta)\right],\end{aligned}\right\}, \tag{1.9}$$

where σ_r, σ_θ, σ_z are normal stress tensor components; ε_r, ε_θ, ε_z are relative deformations in the corresponding direction; α is thermal expansion coefficient; T is temperature; E is modulus of elasticity; ν is Poisson's ratio.

Because of the symmetry the shear strains and the shear stresses are equal zero. In the manufacture of long-length products, the axial deformation is also equals zero ($\varepsilon_z = 0$). From this condition, it follows that:

$$\sigma_z = \nu(\sigma_r + \sigma_\theta) - \alpha E T. \tag{1.10}$$

In view of equation (1.10) the ratios (1.9) are converted to the following:

$$\left.\begin{aligned}\varepsilon_r - (1+\nu)\alpha T &= \frac{1-\nu^2}{E}\left(\sigma_r - \frac{\nu}{1-\nu}\sigma_\theta\right);\\ \varepsilon_\theta - (1+\nu)\alpha T &= \frac{1-\nu^2}{E}\left(\sigma_\theta - \frac{\nu}{1-\nu}\sigma_r\right),\end{aligned}\right\}. \tag{1.11}$$

The strain components are determined from the radial as follows:

$$\varepsilon_r = \frac{du}{dr}, \quad \varepsilon_\theta = \frac{u}{r}, \tag{1.12}$$

The differential equation of thermos-elasticity (Timoshenko & Goodier, 1975) gives the following equation:

$$\frac{d}{dr}\left[\frac{1}{r}\frac{d(ru)}{dr}dr\right]=\frac{1+\nu}{1-\nu}\alpha\frac{dT}{dr}. \tag{1.13}$$

Equation (1.13) is addressed separately for the core, with the average temperature over the cross section Tc and for the shell, with the average temperature over thickness T_0. Temperatures T_c and T_0 are determined from the deformation conditions in the technological tool, with the different ratio of temperatures T_c and T_0 depending on the thermal and mechanical properties of bimetallic billet components.

The set of equations (1.13), (1.11) and (1.12) give:

$$\left.\begin{aligned}
u &= \frac{1+\nu}{1-\nu}\alpha\frac{1}{r}\int Trdr + c_1 r + \frac{c_2}{r};\\
\sigma_r &= -\frac{\alpha E}{1-\nu}\frac{1}{r^2}\int Trdr + \frac{E}{1+\nu}\left(\frac{c_1}{1-2\nu}-\frac{c_2}{r^2}\right);\\
\sigma_\theta &= \frac{\alpha E}{1-\nu}\frac{1}{r^2}\int Trdr - \frac{\alpha E T}{1-\nu} + \frac{E}{1+\nu}\left(\frac{c_1}{1-2\nu}-\frac{c_2}{r^2}\right);\\
\sigma_z &= -\frac{\alpha E T}{1-\nu} + \frac{2\nu E c_1}{(1+\nu)(1-2\nu)},
\end{aligned}\right\}. \tag{1.14}$$

Expressions (1.14) are used independently for the core and for the shell. The constants of integration c_1 and c_2 are determined from the corresponding boundary conditions. For example, for the core, $c_2 = 0$ because $u=0$ when $r=0$. We also assume that at the output of the drawing tool the core and the shell contact without force interaction, i.e. $\sigma_{r|r=r_c}=0$. Defining constants c_1 and c_2, we obtain the formula for the core:

$$\left.\begin{aligned} u_c &= \frac{1+\nu_c}{1-\nu_c}\alpha_c\left[(1-2\nu_c)\frac{1}{r_c^2}\int_0^{r_c} T_c r dr + \frac{1}{r}\int_0^{r} T_c r dr\right]; \\ \sigma_r &= \frac{\alpha_c E_c}{1-\nu_c}\left[\frac{1}{r_c^2}\int_0^{r_c} T_c r dr - \frac{1}{r^2}\int_0^{r_c} T_c r dr\right]; \\ \sigma_\theta &= \frac{\alpha_c E_c}{1-\nu_c}\left[\frac{1}{r_c^2}\int_0^{r_c} T_c r dr + \frac{1}{r^2}\int_0^{r_c} T_c r dr - T_c\right]. \end{aligned}\right\}. \quad (1.15)$$

For the shell, we use boundary conditions to determine integration constants $\sigma_{r|r=r_c}=0$; $\sigma_{r|r=r_0}=0$.

After determining the integration constants, we obtain the solution for the shell:

$$\left.\begin{aligned} u_0 &= \frac{1+\nu_0}{1-\nu_0}\alpha_0\left[\frac{1}{r_0^2-r_c^2}\int_{r_c}^{r_0} T_0 r dr\,\frac{(1-2\nu_0)+r_c^2}{r} + \frac{1}{r}\int_{r_c}^{r_0} T_0 r dr\right]; \\ \sigma_r &= \frac{\alpha_0 E_0}{1-\nu_0}\left[\frac{r^2-r_c^2}{r_0^2-r_c^2}\int_{r_c}^{r_0} T_0 r dr - \int_{r_c}^{r_0} T_0 r dr\right]; \\ \sigma_\theta &= \frac{\alpha_0 E_0}{1-\nu_0}\cdot\frac{1}{r^2}\left[\frac{r^2+r_c^2}{r_0^2-r_c^2}\int_{r_c}^{r_0} T_0 r dr - \int_{r_c}^{r_0} T_0 r dr - T_0 r^2\right]. \end{aligned}\right\}. \quad (1.16)$$

Possible gap between the core and the shell is determined by the size of radial displacements at the core-shell edge. Equation system (1.15) for $r = r_c$ gives:

$$u_c = \frac{1}{r_c} T_c (1+\nu_c)\alpha_c \left(r_0^2 - r_c^2\right). \quad (1.17)$$

Respectively of the expressions (1.16) for the shell when $r = r_c$ yields:

$$u_0 = r_0 T_0 (1+\nu_0)\alpha_0. \quad (1.18)$$

In case of equality of the displacements $u_c = u_0$, - the contact in the bimetallic billet is maintained. When $u_c < u_0$ an undesirable gap appears. The most favourable condition is $u_c > u_0$. It provides contact radial compressive stresses that help increase the metal core plasticity in deformation on subsequent passes. Thus, from the standpoint of thermos-electricity of bimetallic billets in drawing the most favourable ratio is (Kolmogorov, et al., 2011):

$$\frac{1}{r_c} T_c (1+\nu_c)\alpha_c \left(r_0^2 - r_c^2\right) \geq r_0 T_0 (1+\nu_0)\alpha_0 . \qquad (1.19)$$

This ratio is recommended in order to preserve the continuity of a bimetallic billet during drawing. Equations (1.15) and (1.16) may be used to determine the stress state of bimetallic billet components.

The results of the present study is published in work (Kolmogorov, et al., 2013).

1.2.3. Summary

1. The technological principles of low-temperature superconductor production for the magnetic system of the International thermonuclear experimental reactor (ITER) are outlined.

2. Based on thermos-elasticity equations, temperature modes in the superconductor production are established which provide continuity of a bimetallic superconductor billet.

1.2.4. Temperature regime and critical velocities during wire drawing

The basic metallurgical process in the production of superconducting long length products is drawing. It involves pulling a blank through the conical channel of a technological tool (Fig. 1.7.). In this case, residual stresses are formed in pulled metal, and one of their causes is an unfavourable temperature mode of a wire in the course of plastic deformation. Its surface heating due to the effect of external friction forces on a contact surface (a "pulled product–wire drawing tool") is especially undesirable.

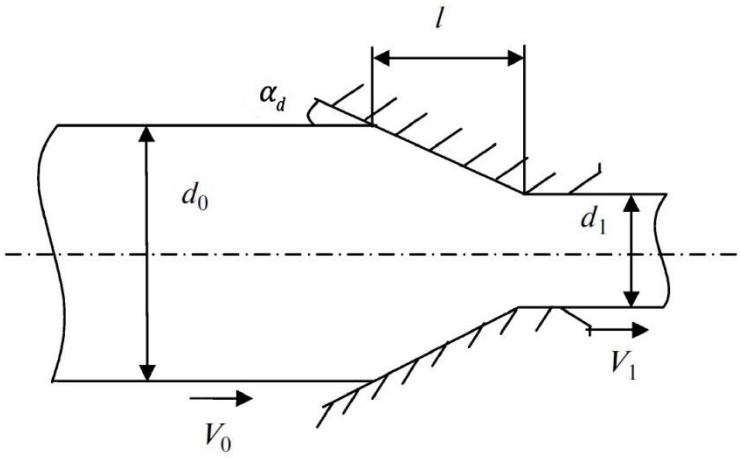

Fig. 1.7. Process of wire drawing.

Contact heating may be significant and lead to the formation of temperature stress capable of causing the temperature plastic deformations and to the formation of undesirable residual stress in the pulled product during cooling. It is known that the surface layer of the pulled product is heated during drawing because of the effect of external friction forces within a deformation area. In this case, the temperature of the contact layer (T_c) is determined by the conditions of drawing and by the thermal properties of the pulled material (Kolmogorov, 1986), (Kolmogorov, et al., 2011):

$$T_c = T_0 + \frac{fK\sigma_y \eta}{c\gamma K_1 (1-\eta)\sin\alpha_d}, \tag{1.20}$$

T_0 - is the temperature of central layers of the wire, (*K*);

f - is the coefficient of friction in the deformation area;

$K\sigma_y$ the mean contact normal pressure in the deformation area, where coefficient *K* determines the average contact pressure in the deformation zone. It depends on the conditions of drawing and the stress pattern. If there is a back tension during drawing *K<1.0*, in the case of the back support *K>1.0*, the traditional drawing *K = 1.0*. In the calculation function, *K = 1.0*;

$\eta = \left(d_0^2 - d_1^2\right)/d_0^2$ - is the relative reduction;

d_0 and d_1 - are wire diameters at the input and output of the deformation area;

c - is the specific heat capacity of the pulled wire material, *J/(kg K)*;

γ - is its density (kg/m^3);

α_d - is the angle of the slope of the generatrix of the operating cone of a drawing die to the drawing axis, (*deg*);

K_1 is the coefficient characterizing a part of heat removed by the wire that is pulled, which depends on the Peclet number $Pe = vd / a$;

a ratio of a deformation area length to mean diameter $l/d = \left(1 - \sqrt{1-\eta}\right)/\left(1 + \sqrt{1-\eta}\right)tg\alpha_d$;

v - is the velocity of the wire in the deformation area, (*m/s*);

$a = \lambda/(c \cdot \gamma)$ - is the thermal diffusivity of the pulled metal;

λ - is the heat conductivity coefficient, (*W/mK*).

As follows from relationship (1.20), the temperature difference determined by the second term of Eq. (1.20) is formed as a result of contact heating between the central and peripheral layers of the pulled wire.

The thermoplastic state of the wire under the conditions of plane deformation (ε_z = 0) corresponds to the following expressions (Timoshenko & Goodier, 1975):

$$\left.\begin{aligned}\sigma_r &= \frac{\alpha E}{1-\nu}\left(\frac{1}{R^2}\int_0^R Trdr - \frac{1}{r^2}\int_0^r Trdr\right);\\ \sigma_\theta &= \frac{\alpha E}{1-\nu}\left(\frac{1}{R^2}\int_0^R Trdr + \frac{1}{r^2}\int_0^r Trdr - T\right);\\ \sigma_z &= \frac{\alpha E}{1-\nu}\left(\frac{2\nu}{R^2}\int_0^R Trdr - T\right),\end{aligned}\right\}, \qquad (1.21)$$

where α- is the linear thermal expansion coefficient of the wire material, (K); E its elasticity modulus (MPa) and ν is the Poisson ratio; R - is the wire radius; $T(r)$ - is the temperature function.

Contact heating is localized within a thin surface layer; therefore, we assume that the temperature distribution over the cross section of the wire due to the effect of external friction forces is described by an exponential dependence of the type $T = T_0 exp(\beta r/R)$, where β is empirical exponent.

Designating the temperature of the wire surface as $T_1 = T_c$, we find exponent β from condition $T_{r=R} = T_1$ and, finally, obtain the temperature function corresponding to the contact heating of the wire during drawing in the following form:

$$T = T_0\left(T_1/T_0\right)^{\bar{r}}, \qquad (1.22)$$

where $\bar{r} = r/R$ - is the dimensionless radial coordinate.

Equations (1.20) (1.22) are used for the computation of the thermo-elastic stresses due to the contact heating. Substituting equation (1.21) into (1.22), we obtain (1.23). Here $\Delta T = T_1 - T_0$ - is the temperature difference between the surface and the center of the pulled wire, which corresponds to the second summand in expression (1.20) in performed computations.

$$\left.\begin{aligned}
\sigma_r &= \frac{\alpha E T_0}{1-\nu}\left\{\frac{1}{\ln\left(1+\frac{\Delta T}{T_0}\right)}\left[1+\frac{\Delta T}{T_0}-\frac{1}{r}\left(1+\frac{\Delta T}{T_0}\right)^{\bar{r}}\right]+\right.\\
&\left.+\frac{1}{\ln^2\left(1+\frac{\Delta T}{T_0}\right)}\left[\frac{1}{\bar{r}^2}\left(1+\frac{\Delta T}{T_0}\right)^{\bar{r}}-\frac{1}{\bar{r}^2}-\frac{\Delta T}{T_0}\right]\right\};\\
\sigma_\theta &= \frac{\alpha E T_0}{1-\nu}\left\{\frac{1}{\ln\left(1+\frac{\Delta T}{T_0}\right)}\left[\frac{1}{\bar{r}}\left(1+\frac{\Delta T}{T_0}\right)^{\bar{r}}-\frac{1}{\bar{r}^2}-\frac{\Delta T}{T_0}\right]+\right.\\
&\left.+\frac{1}{\ln^2\left(1+\frac{\Delta T}{T_0}\right)}\left[\frac{1}{\bar{r}^2}-\frac{1}{\bar{r}^2}\left(1+\frac{\Delta T}{T_0}\right)^{\bar{r}}-\frac{\Delta T}{T_0}\right]-\left(1+\frac{\Delta T}{T_0}\right)^{\bar{r}}\right\};\\
\sigma_z &= \frac{\alpha E}{1-\nu}\frac{2T_0\nu}{\ln\left(1+\frac{\Delta T}{T_0}\right)}\left[1+\frac{\Delta T}{T_0}-\frac{\Delta T}{T_0\ln\left(1+\frac{\Delta T}{T_0}\right)}-\frac{1}{2}\left(1+\frac{\Delta T}{T_0}\right)^{\bar{r}}\ln\left(1+\frac{\Delta T}{T_0}\right)\right]
\end{aligned}\right\} \quad (1.23)$$

The numerical analysis of relationships (1.23) indicates that most temperature stresses arise within wire surface layers ($\bar{r}=1$) where the appearance of residual stresses can be expected; expressions (1.23) for the surface take the form (Kolmogorov & Shirobokov, 1995):

$$\left.\begin{aligned}
&\sigma_{r/\bar{r}=1} = 0;\\
&\sigma_{\theta/\bar{r}=1} = \frac{\alpha E T_0}{1-\nu}\left(\frac{2\left(1+\Delta T/T_0\right)}{\ln\left(1+\Delta T/T_0\right)}-\frac{2\Delta T}{T_0\ln^2\left(1+\Delta T/T_0\right)}-\left(1+\frac{\Delta T}{T_0}\right)\right);\\
&\sigma_{z/\bar{r}=1} = \nu\sigma_{\theta/\bar{r}=1},
\end{aligned}\right\}. \quad (1.24)$$

The last of relationships (1.24) is derived from the Hooke's law for axially symmetrical stress state at $\sigma_{r/\bar{r}=1} = 0$ and $\varepsilon_z = 0$.

The appearance of residual stresses is preceded by the transition of the pulled metal into the plastic state. To evaluate this transition, let us use the criterion of the specific formation energy (the Huber-Mises condition) (Shikov, et al., 2003):

$$\sigma_i = \frac{1}{\sqrt{2}}\sqrt{(\sigma_r - \sigma_\theta)^2 + (\sigma_\theta - \sigma_z)^2 + (\sigma_z - \sigma_r)^2} = \sigma_y, \quad (1.25)$$

where σ_i - is the stress intensity; σ_y - is the yield strength of the pulled metal.

The plasticity condition for the surface layer is simplified:

$$\sigma_\theta \sqrt{1 - \nu + \nu^2} = \sigma_y. \quad (1.26)$$

The above mentioned procedure is used to evaluate the undesirable drawing modes during the production of superconducting long length materials by drawing for a magnetic system of the ITER international thermonuclear experimental reactor. The superconducting composite materials are composed of a central core containing a large quantity of superconducting microfibers of the *Nb–Ti* alloy or pure *Nb* and of a current stabilizing shell of ultrapure copper (Kolmogorov, et al., 2011). In this case, contact heating corresponds to the "copper–drawing tool" friction pair; therefore, these computations correspond to the thermal characteristics of copper. It should be noted that superconducting products are unique in regard to the production technology and prime cost, and the presence of residual stresses in surface layers is extremely undesirable in view of difficult to predict consequences.

From the previous equations the calculation the calculation of the ratio $\Delta T/T_0$ was determined for various values T_0. Fig. 1.8 presents the computed dependence of the ratio $\Delta T/T_0$ on σ_y for various T_0, which was obtained from condition (1.26). The computation was conducted for copper wire $\nu = 0.32$, $\alpha = 1.7 \cdot 10^{-5}$ *degr*$^{-1}$, $E = 1.1 \cdot 10^5$ *MPa*. Fig. 1.8 shows that as σ_y increases, the ratio $\Delta T/T_0$ rises, $\Delta T/T_0$ decreases when T_0 increases.

Using Fig. 1.8, the ratio $\Delta T/T_0$ is determined by the known value of $K\sigma_y \approx \sigma_y$ for a definitive value of T_0 ; the critical value of ΔT, at which the transition of surface layers of the wire into the plastic state, is computed.

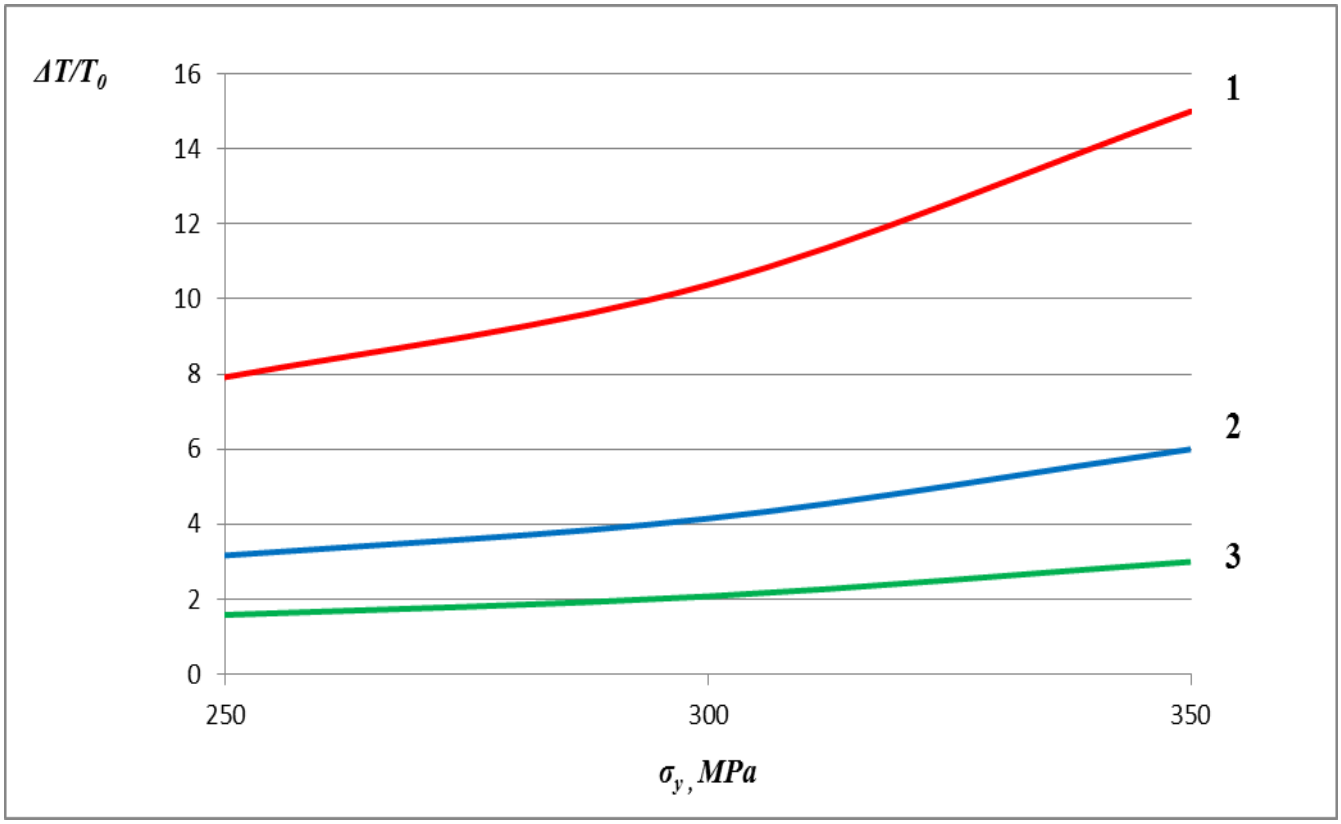

Fig. 1.8. Ratio $\Delta T/T_0$ as a function of mean normal contact pressure in the deformation area at various T_0: **1**- T_0=293 K ; **2**- T_0=323 K; **3**- T_0=373 K.

The critical value of K_1 corresponding to the transition into the plastic state because of temperature stresses, is determined by the values of ΔT found from the second summand in relationship (1.20). In turn, the critical value of the Peclet number is determined by K_1, and the critical velocity of drawing is computed according to formula: $v_{cr} = Pe_{cr}\, a/d$.

Fig. 1.9 presents the computed dependences of the critical drawing velocities on $K\sigma_y$ for different wire diameters d and values of T_0. Computations were carried out η = *0.32* and f = *0.06* corresponding to the conditions of boundary friction.

A similar calculation was conducted for zirconium wire at $\nu = 0.35$, $\alpha = 6.9 \cdot 10^{-6}$ deg^{-1}, $E = 9.7 \cdot 10^5$ MPa and for titanium wire at $\nu = 0.32$, $\alpha = 8.2 \cdot 10^{-5}$ deg^{-1}, $E = 1.16 \cdot 10^5$ MPa. Results are shown in Fig. 1.10 and for titanium wire on Fig. 1.11.

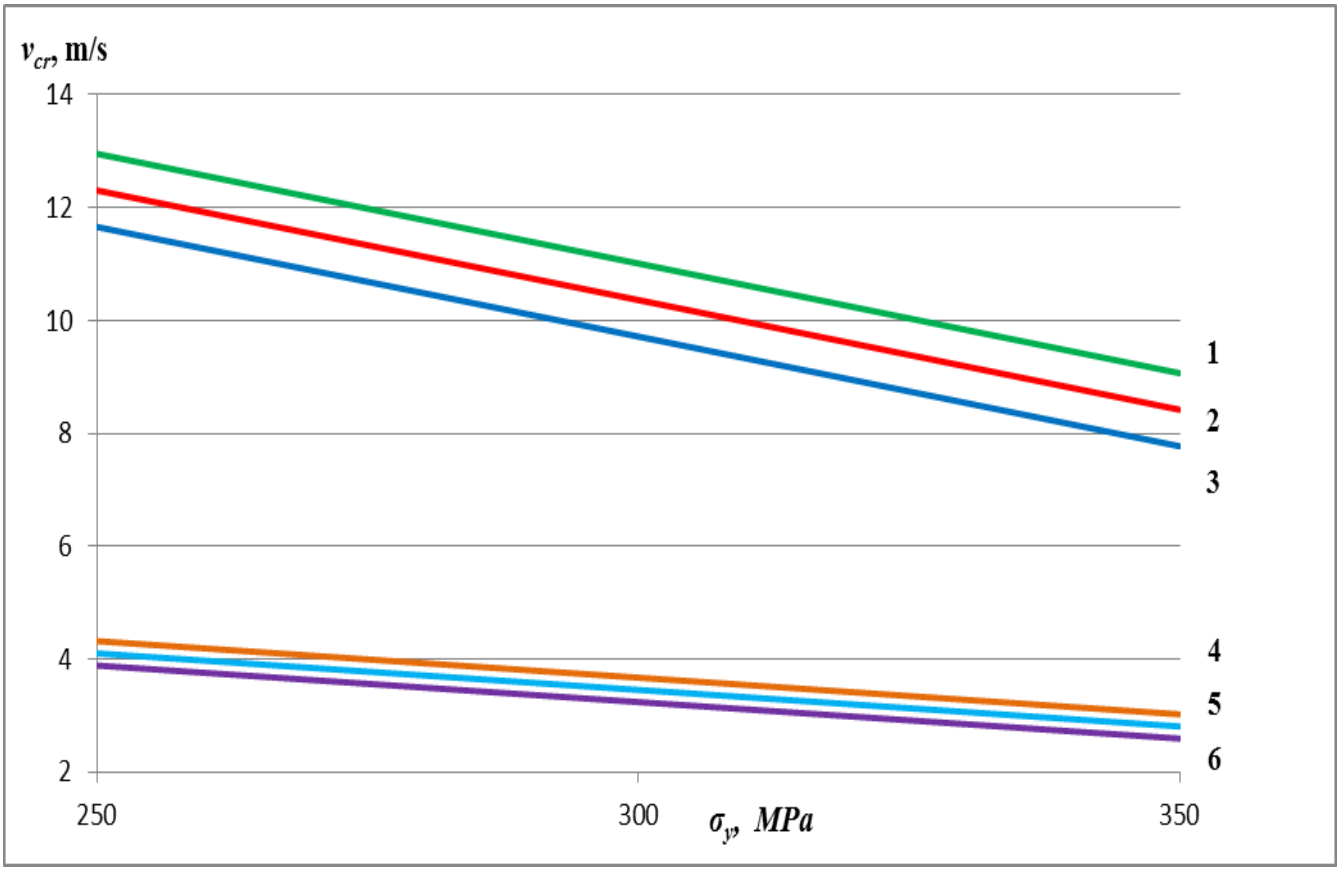

Fig. 1.9. Critical drawing velocities for copper wire as a function of mean normal contact pressure in the deformation area at various T_0 u d: ***1****- $d=10^{-3}$ m, $T_0=373$ K;* ***2****- $d=10^{-3}$ m, $T_0=323$ K;* ***3****- $d=10^{-3}$ m, $T_0=293$ K;* ***4****- $d=2 \cdot 10^{-3}$ m, $T_0=373$ K;* ***5****- $d=2 \cdot 10^{-3}$ m, $T_0=323$ K;* ***6****- $d=2 \cdot 10^{-3}$ m, $T_0=293$ K.*

The dependences shown in Fig. 1.9, Fig. 1.10, Fig. 1.11 allow us to evaluate the drawing velocities; if they are exceeded, undesirable residual stresses appear as a result of the transition of the superconducting products into the plastic state by virtue of thermal stresses appearing due to contact friction forces in the deformation area. It should be noted that critical drawing velocities significantly depend on the friction coefficient *f* in the deformation area.

The provision of the mode of hydrodynamic lubrication allows us to eliminate the negative role of contact heating in the formation of residual thermal stresses.

The results of the present study are published in work: (Kolmogorov, et al., 2011).

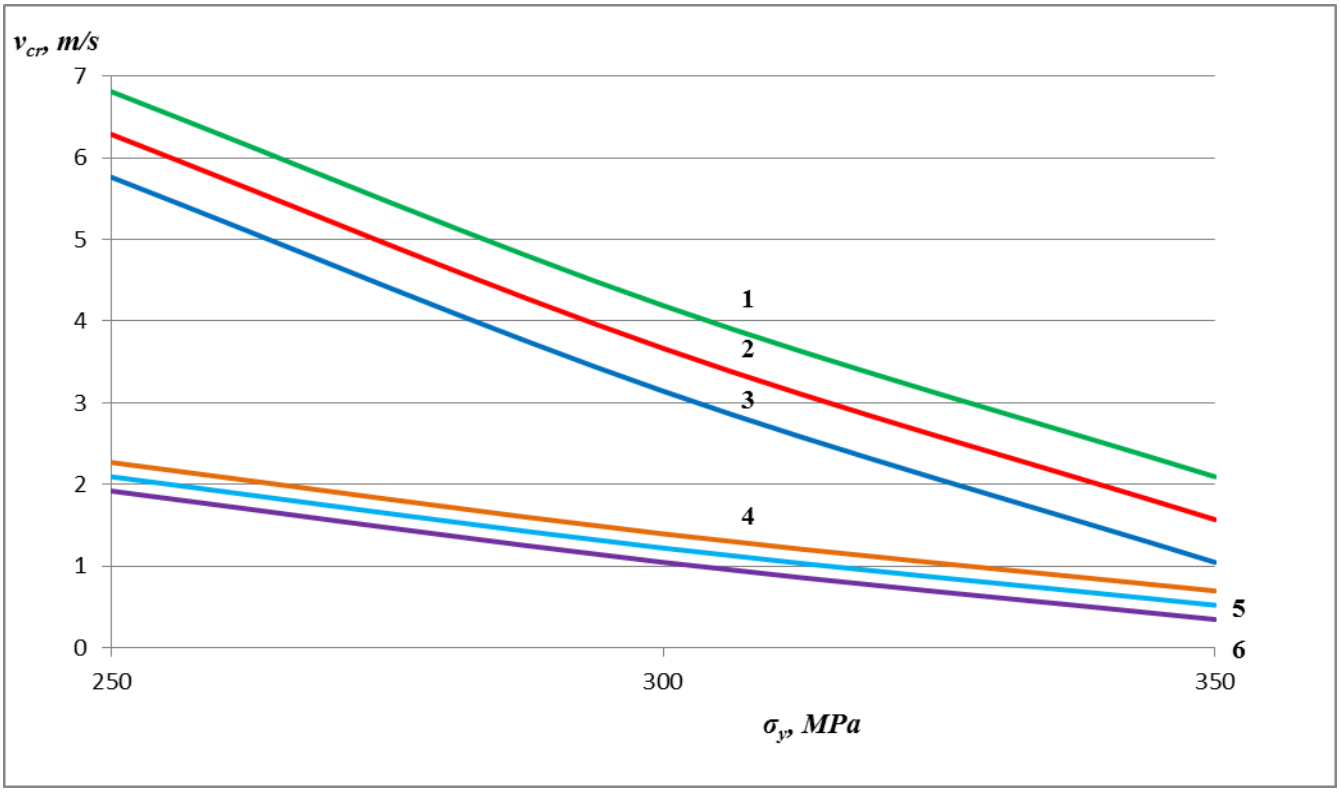

Fig. 1.10. Critical drawing velocities for zirconium wire as a function of mean normal contact pressure in the deformation area at various T_0 u d:
***1**- $d=10^{-3}$ m, $T_0=373$ K; **2**- $d=10^{-3}$ m, $T_0=323$ K; **3**- $d=10^{-3}$ m, $T_0=293$ K; **4**- $d=2\cdot10^{-3}$ m, $T_0=373$ K; **5**- $d=2\cdot10^{-3}$ m, $T_0=323$ K; **6**- $d=2\cdot10^{-3}$ m, $T_0=293$ K.*

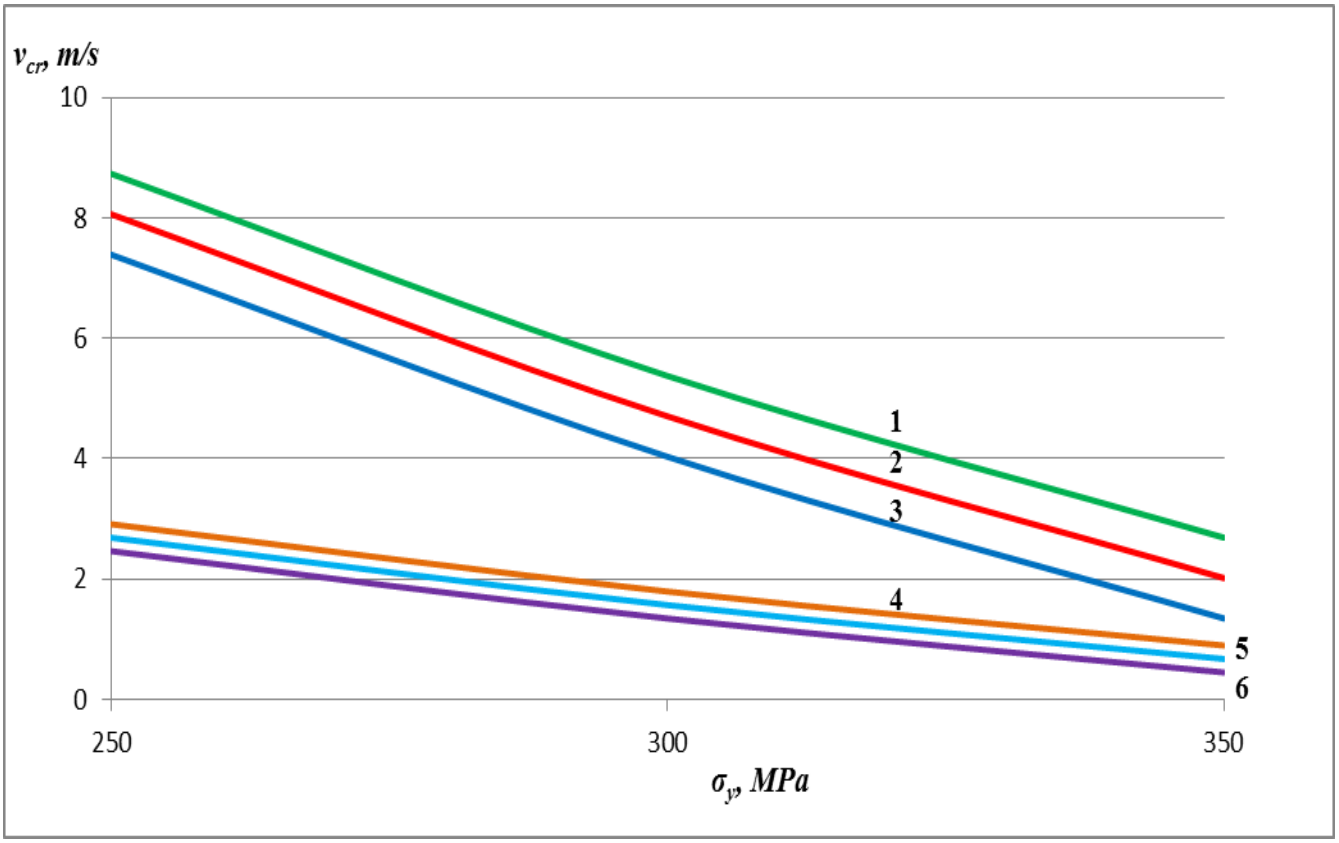

Fig. 1.11. Critical drawing velocities for titanium wire as a function of mean normal contact pressure in the deformation area at various T_0 u d: ***1****- $d=10^{-3}$ m, $T_0=373$ K;* ***2****- $d=10^{-3}$ m, $T_0=323$ K;* ***3****- $d=10^{-3}$ m, $T_0=293$ K;* ***4****- $d=2\cdot10^{-3}$ m, $T_0=373$ K;* ***5****- $d=2\cdot10^{-3}$ m, $T_0=323$ K;* ***6****- $d=2\cdot10^{-3}$ m, $T_0=293$ K.*

1.2.5. Summary

1. Based on thermos-elasticity equations, temperature modes resulting in the appearance of thermoplastic deformations and the possible residual stresses formation are established.

2. From the conditions of contact heating, the drawing velocities during the production of superconducting blanks (which, when exceeded, cause residual stresses in products) are determined.

1.2.6. Optimization of the technological tool geometry at pressing of monolithic blank

Production technology of low-temperature composite superconductors includes specific operations of metallurgical alterations related to metals processing by pressure such drawing as well as pressing.

The matrix of conical form is used for pressing low-temperature superconductor blank for international thermonuclear experimental reactor ITER, which consist in the superconducting material core and copper shell.

Pressing is widely used in metals processing by pressure. The essence of the pressing process concerns the extrusion of material placed into closed volume through the channel formed by the pressing tool (Perlin & Reitbarg, 1975). The pressing is provides increased pressed material plasticity. That is why pressing is widely used in the production of low-plastic hardly-deformed metals and alloys (Kolmogorov & Kuznetsova, 2000).

One of the main parameters in the pressing is the compacting force, it is necessary to have a minimum compacting force in order to decrease the required power. The pressing impression force is the sum of components (Perlin & Reitbarg, 1975):

$$P = T_{cr} + T_m + T_{pl} + T_k + T_{sh} \pm Q, \tag{1.27}$$

where T_{cr}– is the resultant friction force on the container's surface; T_m is the resultant friction force within deformation area on contact surface of press matrix and blank; T_{pl} – is the force of plastic deformation; T_k – is the resultant friction force on the surface of matrix parallel land; T_{sh} – is the force required to overcome friction forces between metal and the pressure pad; Q – is the force of the back pressure or the coiler tension ($\pm Q$).

The total pressing force (1.27) is reduced to the mean pressing stress:

$$\sigma_{pr} = P / F_0, \tag{1.28}$$

F_0 – is the area of the cross section of the initial blank.

Correspondent separate components of equation (1.27) are reduced to the specific normal and tangential stresses of the system of the external forces, which flow pattern is presented in Fig. 1.12.

It is known from pressing practice the existence of optimal angles of the slope of the generatrix of the cone matrix to the pressing axis α_m. T_{pl} and T_M depend on angle α_m. The relationship (1.27) is used for the geometry optimization including the determination of the optimal angle α_m depending on T_{pl} and T_m.

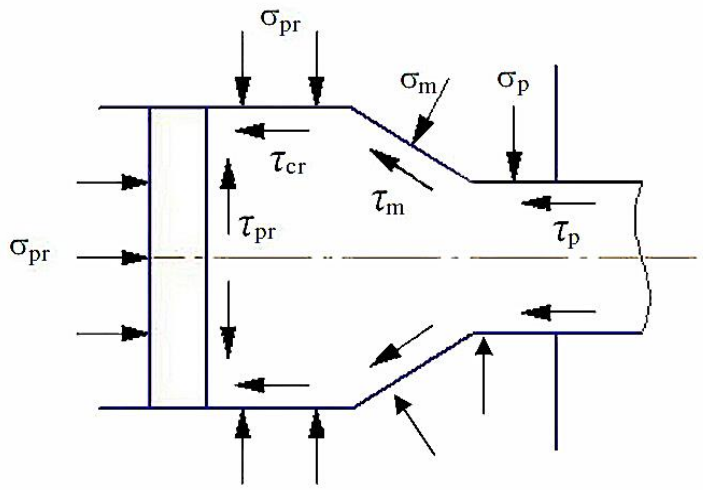

Fig. 1.12. Flow pattern of forces during pressing.

The compacting stress during plastic deformation is equal (Perlin & Reitbarg, 1975):

$$\sigma_{pl} = \int_0^{\varepsilon} \sigma_s d\varepsilon, \tag{1.29}$$

σ_s – is the resistance of the pressed material; ε – is the degree during pressing.

In works (Kolmogorov, 1986) and (Kolmogorov, et al., 2011) the degree of deformation is determined taking into account the elongation and the additional shear at the input and the output of the conical technological tool as follows:

$$\varepsilon_{av} = \ln \lambda + \frac{4}{3\sqrt{3}} \tan \alpha_m, \tag{1.30}$$

$\lambda = R_0^2 / R_1^2$ is the elongation ratio; R_0 and R_1 are the radiuses of the initial blank and press item correspondingly.

For the averaged resistance to deformation the pressing stress component related to the plastic deformation is equal to:

$$\sigma_{pl} = \sigma_s (\ln \lambda + \frac{4}{3\sqrt{3}} \tan \alpha_m). \tag{1.31}$$

The friction forces on the pressing axis for the conical operation surface of the matrix is

$$T_m = \tau_m \cdot F_m \cdot \cos\alpha_m = F_m \cdot f \cdot \sigma_s \cdot \cos\alpha_m, \tag{1.32}$$

f is the friction coefficient in the deformation area; τ_m is the tangential stress; F_m is the surface of conical matrix part.

Based on the geometric ratio for the cone lateral face, representing operating deformation area, we obtain:

$$F_m = \frac{\pi \cdot R_1^2}{\sin \alpha_m} \left(\frac{R_0^2}{R_1^2} - 1 \right). \tag{1.33}$$

Taking into account relationship (1.33), the resultant friction forces on the pressing axis is equal to:

$$T_m = \sigma_s \cdot \pi \cdot R_1^2 (\lambda - 1) \cdot f \cdot \cot \alpha_m . \quad (1.34)$$

The contribution from friction forces overcoming in the deformation area into the total average pressing stress is:

$$\sigma_m = \sigma_s (\lambda - 1) f \cdot \cot \alpha_m / \lambda . \quad (1.35)$$

The optimal angle of the slope of the generatrix to the pressing axis is determined by the minimum of the full pressing stress: only σ_{pl} and σ_m depend on angle α_m, therefore the minimum condition yields:

$$\frac{\partial}{\partial(\tan \alpha_m)} (\sigma_{pl} + \sigma_m) = 0 . \quad (1.36)$$

From the relationships (1.31), (1.33) and (1.35), we obtain:

$$\alpha_m^{opt} = \arctan\left(1.14 \sqrt{\frac{f(\lambda - 1)}{\lambda}} \right). \quad (1.37)$$

Equation (1.37) shows that the optimal matrix angle depends only on the friction coefficient and the elongation.

On the Fig. 1.13 are shown the computed optimal angles at pressing depending on the elongation for various friction coefficients. From this dependence it follows that the optimal matrix angles increase as the elongation ratio λ increases.

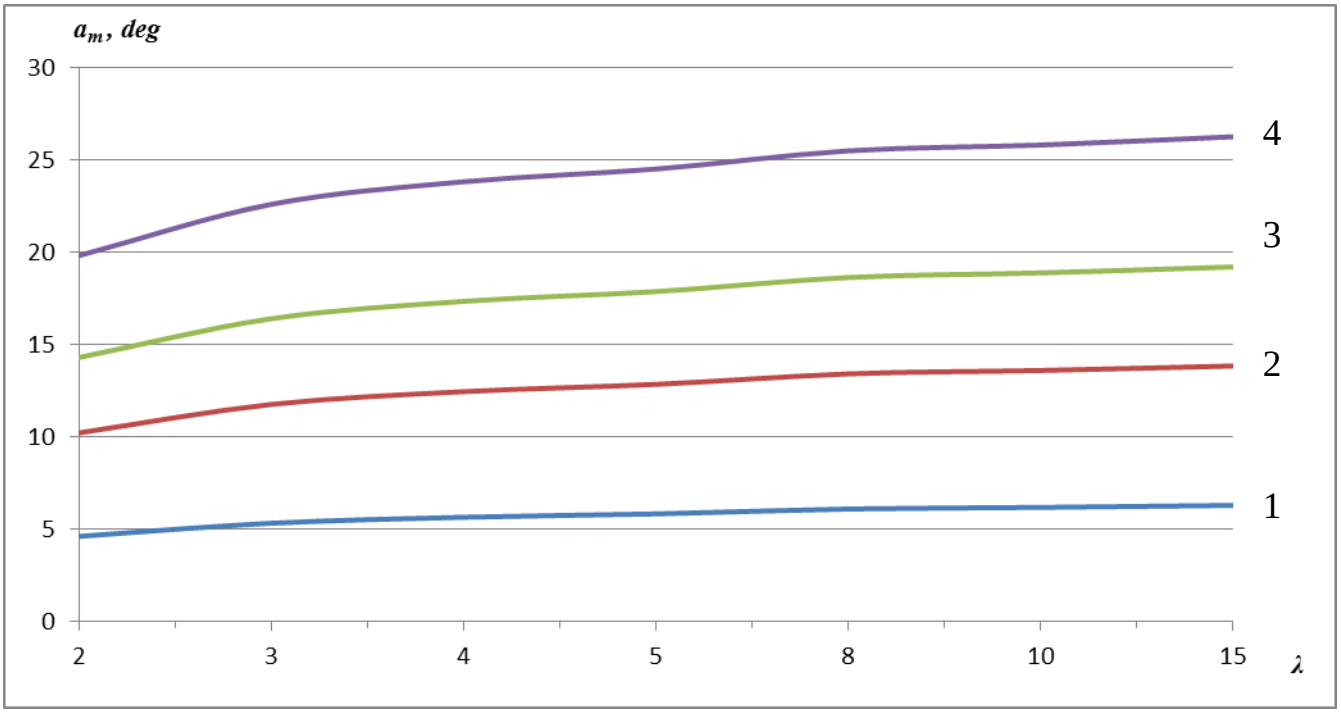

Fig. 1.13. Computed optimal angles at pressing depending on the elongation for various friction coefficients: ***1*** *– f = 0.01;* ***2*** *– f = 0.05;* ***3*** *– f = 0.1;* ***4*** *– f = 0.2.*

The present study results are published in work (Kolmogorov, et al., 2011).

1.2.7. Optimization of technological tool geometry at pressing of bimetal blank

The pressing deformation of the bimetal assembly blank consisting of the core (*Nb-Ti* or *Nb*) and copper shell are presented in Fig. 1.14.

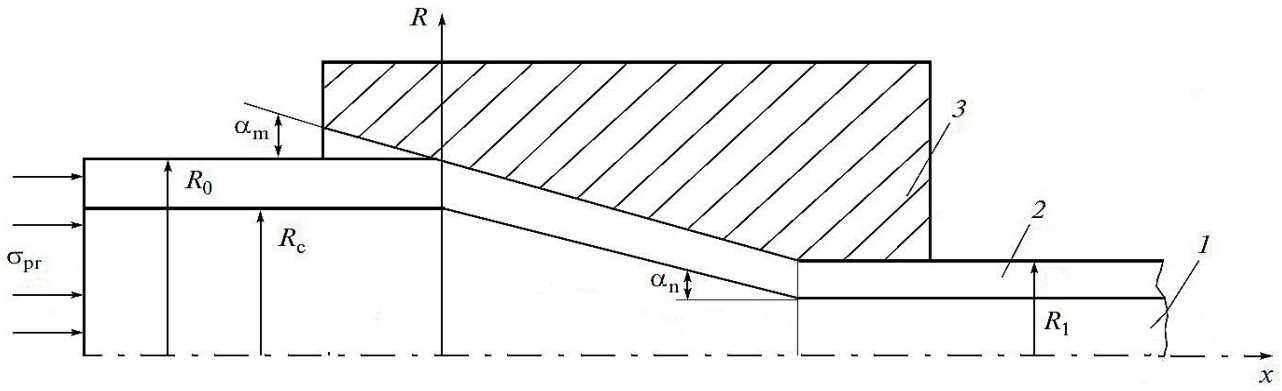

Fig. 1.14. Scheme of pressing of bimetal assembly blank: (1) core; (2) shell; (3) pressing tool.

We consider that during assembly blank pressing, the elongation coefficient for the core is the same as for the shell. The degree of deformation for the central part (core) is equal to (Kolmogorov, 1986):

$$\varepsilon_{av} = \ln \lambda + \frac{4}{3\sqrt{3}} \tan \alpha_n, \tag{1.38}$$

where α_n - is the angle of the slope of the generatrix of the core to the pressing axis; λ – is the elongation. From the geometric ratio of Fig. 1.14, we obtain:

$$\tan \alpha_n = \frac{R_c}{R_0} \tan \alpha_m, \tag{1.39}$$

R_c – is the radius of the core; R_0 – is the external radius of the blank.

Taking into account the relationship (1.39), the average degree of deformation of the core is equal to:

$$\varepsilon_{av} = \ln \lambda + \frac{4}{3\sqrt{3}} \frac{R_c}{R_0} \tan \alpha_m. \tag{1.40}$$

From the relationship (1.40), the average resistance to the deformation of the core is equal to:

$$\sigma_{pl}^c = \sigma_s^c (\ln \lambda + \frac{4}{3\sqrt{3}} \frac{R_c}{R_0} \tan \alpha_m). \tag{1.41}$$

The part of full pressing force of the central part (core) of bimetal blank (Perlin & Reitbarg, 1975) corresponds to the stress (1.41):

$$P_c = \pi R_c^2 \sigma_s^c \left(\ln \lambda + \frac{4}{3\sqrt{3}} \frac{R_c}{R_0} \tan \alpha_m \right). \quad (1.42)$$

Similar computation is performed for the external part (shell) of bimetal blank. The shell pressing stress for averaged resistance to deformation is equal to:

$$\sigma_{pl}^{sh} = \sigma_s^{sh} (\ln \lambda + \frac{4}{3\sqrt{3}} \tan \alpha_m), \quad (1.43)$$

σ_s^{sh} - is the averaged resistance to deformation of shell material.

Correspondingly the part of the total pressing force for deformation is equal to:

$$P_c = \pi \left(R_0^2 - R_c^2 \right) \cdot \sigma_s^{sh} \left(\ln \lambda + \frac{4}{3\sqrt{3}} \tan \alpha_m \right). \quad (1.44)$$

For the shell it is necessary to take into account for the friction forces in the operating part of the deformation area. The projection of the resultant friction force to the pressing axis is equal to:

$$T_m = \sigma_s^{sh} \cdot \pi \cdot R_1^2 (\lambda - 1) \cdot f \cdot \cot \alpha_m, \quad (1.45)$$

R_1 is the radius of the external surface of the bimetal blank.

The contribution of the friction forces overcoming the deformation area to the total average pressing stress is:

$$\sigma_m^{sh} = \sigma_s^o (\lambda - 1) f \cdot \cot \alpha_m / \lambda. \quad (1.46)$$

The optimal angle of the slope of the matrix generatrix to the pressing axis is determined by the minimum of the full pressing stress. Since, α_m depends on σ_{pl}^{c}, σ_{pl}^{sh}, σ_{m}^{sh}, the condition of minimum pressing force could be expressed as follows:

$$\frac{\partial}{\partial(\tan\alpha_m)}(\sigma_{pl}^{c}+\sigma_{pl}^{sh}+\sigma_{m}^{sh})=0. \qquad (1.47)$$

The total pressing stress comprising only values depending on α_m, is equal to:

$$\sigma_{\Sigma}=\sigma_s^c\overline{R}_c^{\,2}\left(\ln\lambda+\frac{4}{3\sqrt{3}}\overline{R}_c\cdot\tan\alpha_m\right)+\sigma_s^{sh}\left(1-\frac{1}{\lambda}\right)\left(f\,\frac{1}{\tan\alpha_m}+\ln\lambda+\frac{4}{3\sqrt{3}}\tan\alpha_m\right), \qquad (1.48)$$

where $\lambda=\frac{R_0^2}{R_1^2}$ - is the elongation; $\overline{R}_c=\frac{R_c}{R_0}$.

After differentiation of expression (1.48) by $\tan\alpha_m$, transformation and reductions we obtain:

$$\alpha_m^{opt}=\arctan\left[1.14\sqrt{\frac{f(\lambda-1)}{\lambda\left(1-\overline{R}_c^{\,2}+\frac{\sigma_s^c}{\sigma_s^{sh}}\overline{R}_c^{\,3}\right)}}\right]. \qquad (1.49)$$

Fig. 1.15 shows the results of calculations according to formula (1.49) for friction coefficient *f =0.1* and ratio $\sigma_s^c/\sigma_s^{sh}=3.33$.

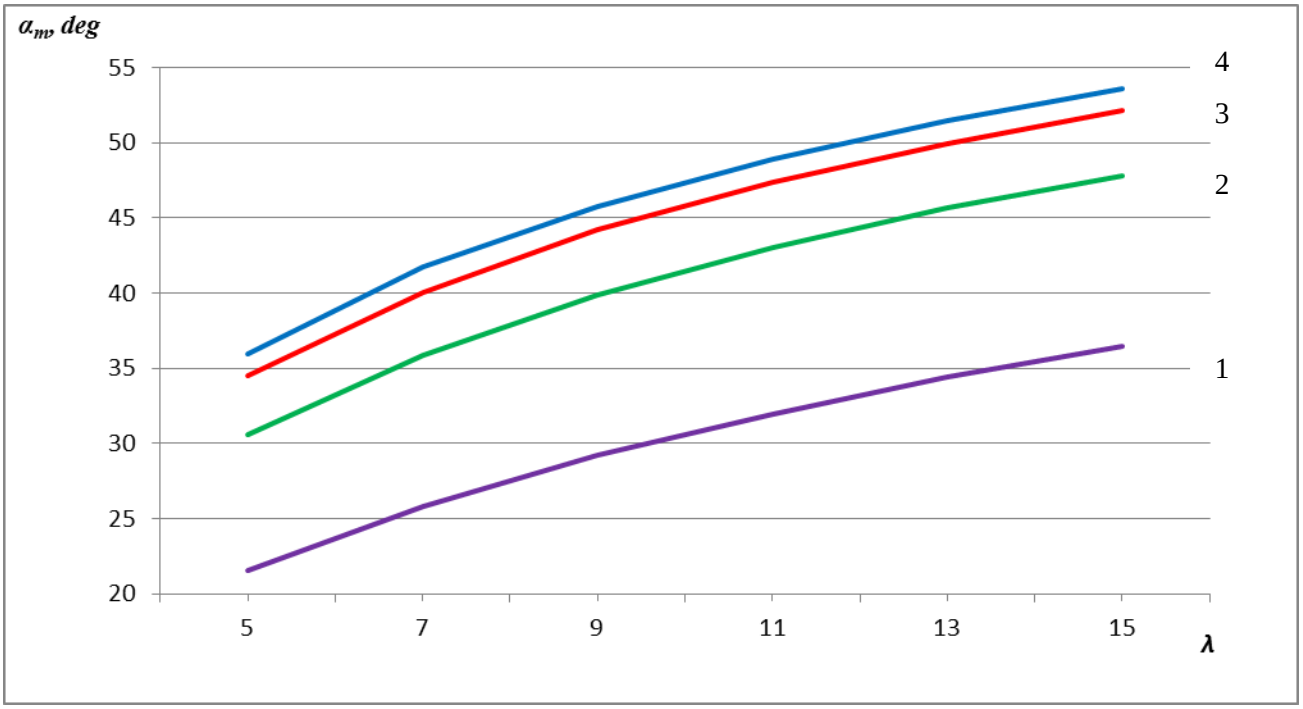

Fig. 1.15. Dependence of the optimal cone angle on the drawing coefficient when pressing the bimetal billet for friction coefficients f = 0.1 and ratio $\sigma_s^c/\sigma_s^{sh} = 3.33$*: **1** – R_c =1; **2** – R_c =0.65; **3** – R_c =0.45; **4** – R_c = 0.25.*

This ratio of deformation resistances of the core and the shell corresponds to hot (873 K) pressing of the superconducting billet, which consists in the niobium core and a copper shell. At this temperature, $\sigma_s^c = 30$ MPa for Nb and $\sigma_s^{sh} = 9$ MPa for copper (Tret'yakov & Zyuzin, 1973).

Fig. 1.15 shows that during bimetal blank pressing the cone angle depends not only on the elongation, but also on the ratio of the blank geometry and the friction conditions.

The present study results are published in work (Kolmogorov, et al., 2013).

1.2.8. Optimization of technological tool geometry at pressing of trimetal blank

The method the determination of the optimal angels of the technological tool at trimetal blank pressing is shown in Fig. 1.16. The optimization is based on the pressing stress providing minimum power inputs during pressing (Kolmogorov, et al., 1991).

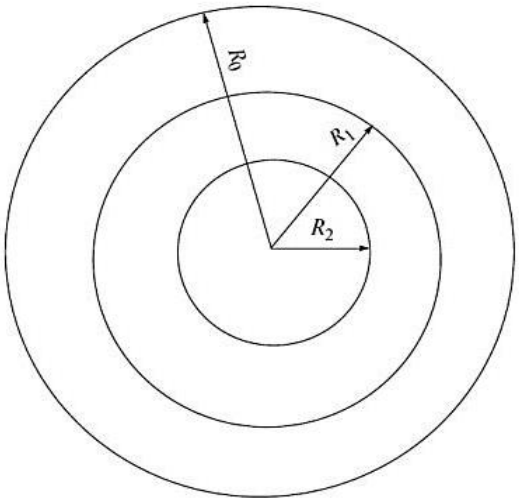

Fig. 1.16. Cross section of a trimetal billet.

Consider that the pressing deformation of the trimetal assembly billet consisting of a copper core with radius R_2, an intermediate layer of the superconducting material (Nb–Ti or Nb) with radius R_1, and a copper shell with outer radius R_0. Fig. 1.16 shows the schematic of the cross section of a trimetal assembly billet and Fig. 1.17 shows the schematic of its pressing.

The degree of deformation, which depends on the drawing coefficient and shear deformations at the inlet into the process tool and at the outlet from it, is determined for each element of this billet (Kolmogorov, 1986).

We assume that the drawing coefficient during the billet pressing is identical for the core, the intermediate layer, and the shell. The average degree of deformation for the core Fig. 1.17 is:

$$\varepsilon_{av} = \ln \lambda + \frac{4}{3\sqrt{3}} \tan \alpha_c , \tag{1.50}$$

α_c is the slope angle of the core generatrix to the pressing axis and λ is the drawing coefficient.

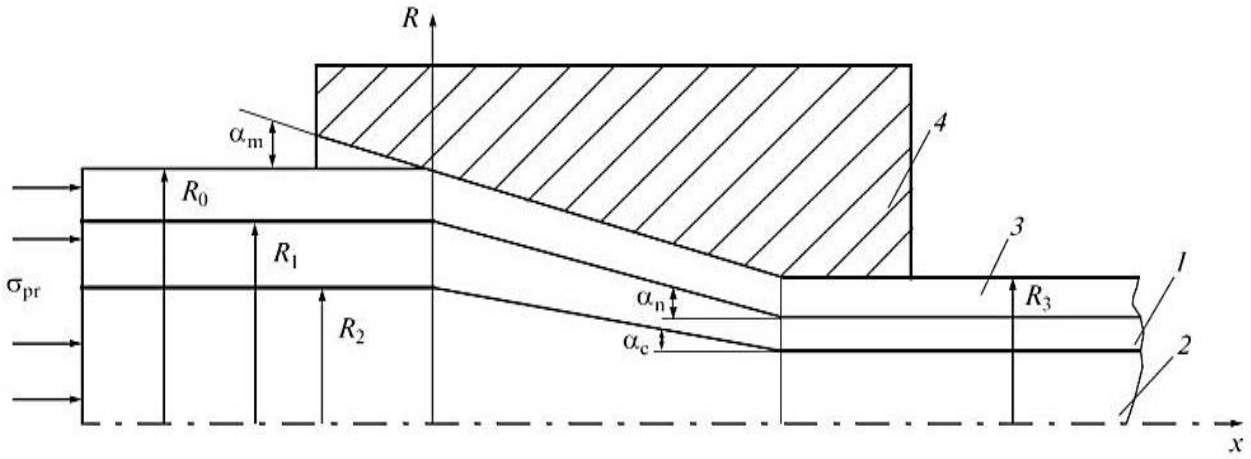

Fig. 1.17. Schematic diagram of pressing the trimetal assembly billet: 1 - Intermediate layer made of the superconducting material (Nb–Ti or Nb), 2 - copper core, 3 – shell, 4 - pressing tool.

It follows from the geometric relationships that:

$$\tan \alpha_c = \frac{R_2}{R_0} \tan \alpha_m . \tag{1.51}$$

In this case, allowing for (1.51), we derive (Kolmogorov, et al., 2011):

$$\varepsilon_{av} = \ln \lambda + \frac{4}{3\sqrt{3}} \frac{R_2}{R_0} \tan \alpha_m , \tag{1.52}$$

$\lambda = R_0^2 / R_3^2$ is drawing coefficient and R_3 is the radius of the outer surface of the trimetal billet.

Similarly, let us derive the degree of deformation for the intermediate layer made of the superconducting material:

$$\varepsilon_{av} = \ln \lambda + \frac{4}{3\sqrt{3}} \tan \alpha_n , \tag{1.53}$$

α_n is the slope angle of the generatrix of the intermediate layer to the pressing axis.

From geometric relationships, we have:

$$\tan \alpha_n = \frac{R_1}{R_0} \tan \alpha_m . \tag{1.54}$$

In this case, allowing for (1.54), the average degree of deformation of the intermediate layer is:

$$\varepsilon_{av} = \ln \lambda + \frac{4}{3\sqrt{3}} \frac{R_1}{R_0} \tan \alpha_m . \tag{1.55}$$

For the shell, we can write:

$$\varepsilon_{av} = \ln \lambda + \frac{4}{3\sqrt{3}} \tan \alpha_m . \tag{1.56}$$

For the averaged value of the core deformation resistance, the stress component associated with the core plastic deformation, allowing relationships (1.52), is equal to:

$$\sigma_{pl}^{c} = \sigma_{s2}^{c} \left(\ln \lambda + \frac{4}{3\sqrt{3}} \frac{R_2}{R_0} \tan \alpha_m \right), \tag{1.57}$$

σ_{s2}^{c} is the average deformation resistance of the core material.

Correspondingly, using for relationship (1.55), we have for the intermediate layer:

$$\sigma_{pl}^{c} = \sigma_{s1}^{c}\left(\ln\lambda + \frac{4}{3\sqrt{3}}\frac{R_1}{R_0}\tan\alpha_m \right), \tag{1.58}$$

σ_{s1}^{c} is the average deformation resistance of the material of the intermediate layer.

Stresses (1.57) and (1.58) correspond to the fraction of the total force of pressing the core and the intermediate layer of a trimetal billet (Perlin & Reitbarg, 1975):

$$P_c = F_2\left[\sigma_{s2}^{c}\left(\ln\lambda + \frac{4}{3\sqrt{3}}\frac{R_2}{R_0}\tan\alpha_m \right)\right] + F_1\left[\sigma_{s1}^{c}\left(\ln\lambda + \frac{4}{3\sqrt{3}}\frac{R_1}{R_0}\tan\alpha_m \right)\right], \tag{1.59}$$

F_1 and F_2 are the cross-section areas of the intermediate layer and the core, respectively.

A similar calculation was performed for the outer part (shell) of a trimetal billet:

$$\sigma_{pl}^{sh} = \sigma_{s0}^{sh}(\ln\lambda + \frac{4}{3\sqrt{3}}\tan\alpha_m), \tag{1.60}$$

σ_{s0}^{sh} is the average deformation resistance of the shell material.

The fraction of the total pressing force is:

$$P_0 = F_0\sigma_{pl}^{sh}, \tag{1.61}$$

F_0 is the cross-section area of the shell, is associated with stress (1.60).

The fraction of the total pressing force consumed for plastic deformation is determined by the sum of (1.59) and (1.61):

$$P_{pl} = \pi\cdot\left(R_0^2 - \left[R_2^2 + R_1^2\right]\right)\cdot\sigma_{s0}^{sh}\left(\ln\lambda + \frac{4}{3\sqrt{3}}\tan\alpha_m \right). \tag{1.62}$$

Friction forces in the working part of the deformation zone should be taken into account for the shell. The projection of the resultant of friction forces on the pressing axis can be written as follows:

$$T_m = \sigma_{s0}^{sh} \cdot \pi \cdot R_3^2 (\lambda - 1) \cdot f \cdot \cot \alpha_m . \tag{1.63}$$

The contribution from overcoming the friction forces in the deformation zone to the total average pressing stress constituted:

$$\sigma_m^{sh} = \sigma_{s0}^{sh} (\lambda - 1) f \cdot \cot \alpha_m / \lambda . \tag{1.64}$$

The optimal angle of the slope of the mold generatrix to the pressing axis is determined from the minimum condition of the total pressing stress; only σ_{pl}^{c}, σ_{pl}^{sh}, σ_m^{sh} depend on angle α_m, Therefore, the condition of minimum pressing force is derived under the following form:

$$\frac{\partial}{\partial(\tan \alpha_m)} (\sigma_{pl}^{c} + \sigma_{pl}^{sh} + \sigma_m^{sh}) = 0. \tag{1.65}$$

The total pressing stress, which includes only magnitudes depending on α_m, is equal to:

$$\begin{aligned} \sigma_\Sigma = {} & \sigma_{s2}^{c} \frac{R_2^2}{R_0^2} \left(\ln \lambda + \frac{4}{3\sqrt{3}} \frac{R_2}{R_0} \tan \alpha_m \right) + \sigma_{s1}^{c} \frac{R_1^2}{R_0^2} \left(\ln \lambda + \frac{4}{3\sqrt{3}} \frac{R_1}{R_0} \tan \alpha_m \right) + \\ & + \sigma_{s0}^{sh} \left(1 - \frac{R_2^2}{R_0^2} - \frac{R_1^2}{R_0^2} \right) \left(\ln \lambda + \frac{4}{3\sqrt{3}} \tan \alpha_m \right) + \sigma_{s0}^{sh} \frac{R_3^2}{R_0^2} (\lambda - 1) f \cdot \cot \alpha_m \end{aligned} \tag{1.66}$$

.

After transformations, expression (1.66) can be written in the form:

$$\sigma_{\Sigma} = \sigma_{s2}^{c}\overline{R_2^2}\left(\ln\lambda + \frac{4}{3\sqrt{3}}\overline{R_2}\cdot\tan\alpha_m\right) + \sigma_{s1}^{c}\overline{R_1^2}\left(\ln\lambda + \frac{4}{3\sqrt{3}}\overline{R_1}\cdot\tan\alpha_m\right) + \\ + \sigma_{s0}^{sh}\left(1-\left[\overline{R_2^2}+\overline{R_1^2}\right]\right)\left(\ln\lambda + \frac{4}{3\sqrt{3}}\tan\alpha_m\right) + \sigma_{s0}^{sh}\frac{1}{\lambda}(\lambda-1)f\cdot\cot\alpha_m \quad , \qquad (1.67)$$

$\lambda = \frac{R_0^2}{R_3^2}$ - is the elongation; $\overline{R}_1 = \frac{R_1}{R_0}$; $\overline{R}_2 = \frac{R_2}{R_0}$.

After the differentiation of the expression (1.67) with respect to tanα_M (allowing for the fact that $\sigma_{s2}^{c} = \sigma_{s0}^{sh}$), transformations and simplifications, we obtain:

$$\alpha_m^{opt} = \arctan\left[1.14\sqrt{\frac{f(\lambda-1)}{\lambda\cdot\left(\frac{\sigma_{s1}^{c}}{\sigma_{s0}^{sh}}\overline{R_1^3} - \left(\overline{R}_1 - \overline{R}_2^3 + \overline{R}_2 - 1\right)\right)}}\right]. \qquad (1.68)$$

Fig. 1.18 shows the results of calculations according to formula (1.68) for friction coefficient *f =0.1* and ratio $\sigma_s^c/\sigma_s^{sh} = 3.33$. This ratio of deformation resistances of the core and the shell corresponds to hot (873 K) pressing of the superconducting billet, which consists of the niobium core and a copper shell. At this temperature, $\sigma_s^c = 30$ MPa for Nb and $\sigma_s^{sh} = 9$ MPa for copper (Tret'yakov & Zyuzin, 1973).

Thus formulas for the determination of the optimal angles at pressing of trimetal low-temperature superconducting products are provided. The friction coefficient, the elongation coefficient influence is shown as well as the ratio of the resistance to deformation of superconducting blank component.

The present study results are published in work (Kolmogorov, et al., 2014).

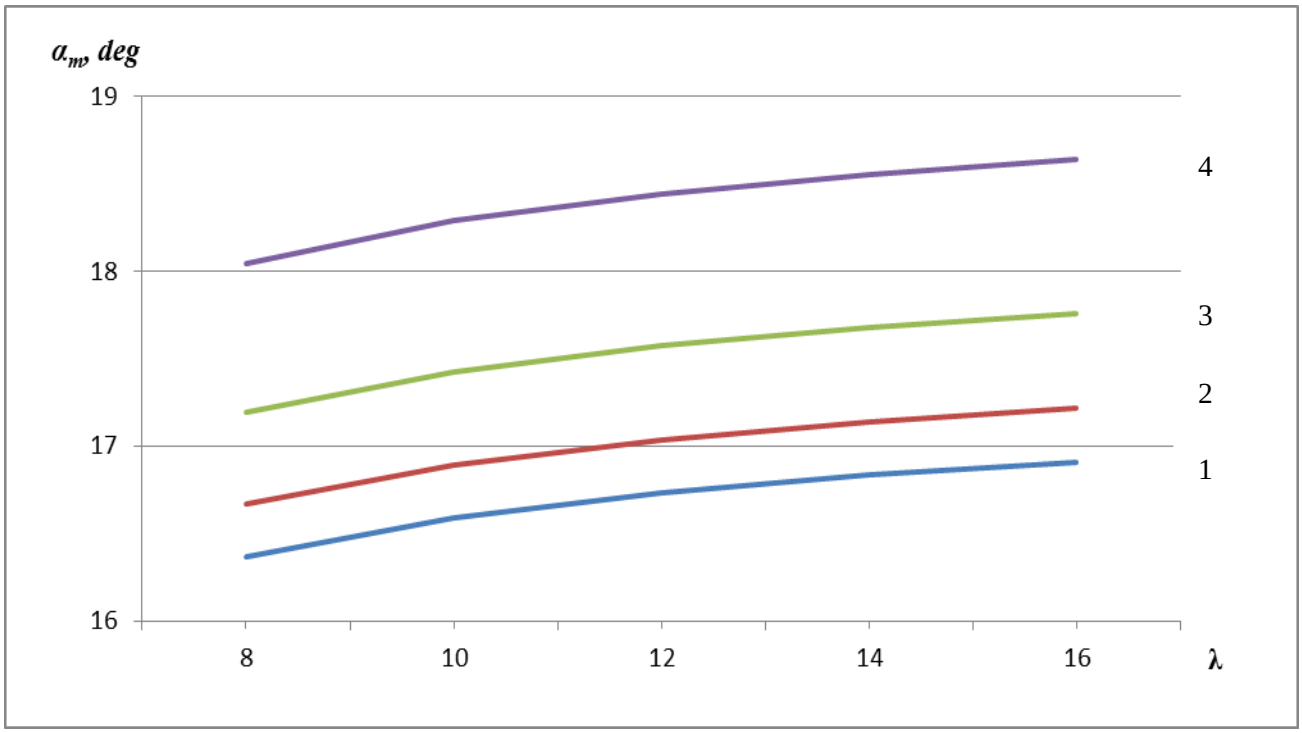

Fig. 1.18. Dependence of the optimal cone angle on the drawing coefficient when pressing the trimetal billet for friction coefficients f=0.1 and $\sigma_{s1}^{c}/\sigma_{s0}^{sh} = 3.3$*:* ***1*** *–* $\overline{R}_1 = 0.5$*;* $\overline{R}_2 = 0.25$*;* ***2*** *–* $\overline{R}_1 = 0.55$*;* $\overline{R}_2 = 0.3$*;* ***3*** *–* $\overline{R}_1 = 0.75$*;* $\overline{R}_2 = 0.5$*;* ***4*** *–* $\overline{R}_1 = 1$*;* $\overline{R}_2 = 0.75$*.*

1.2.9. Summary

1. Optimal angles of molds for pressing the trimetal billet are determined from conditions of the minimum pressing force. Components of the pressing force, which contain the cone angle of process tool, are taken into account in this case;

2. Production parameters that affect the pressing force are revealed. The influence of drawing and the friction coefficient on values of optimal angles are shown;

3. The application of molds with an optimal cone angle makes it possible to lower power inputs for pressing during the production of low-temperature superconducting wares.

1.3. General conclusions

1. The flowsheet of the production process of low-temperature superconductors for international thermonuclear experimental reactor ITER is shown.

2. From the indicated technologies it follows that the main part of the plastic deformation is realized by pressing and drawing.

3. Based on thermo-elasticity equations, temperature modes resulting in the appearance of thermoplastic deformations and the possible residual stresses formation are established.

4. From the conditions of contact heating the critical drawing velocities are determined, which, when exceeded, cause residual stresses in the wire.

5. The results of the work can be applied for development of the drawing technology of such metals as copper, titanium, zirconium.

6. On conditions of minimum compacting force the optimal angles of matrixes for pressing of mono-, bi- and trimetal blank are determined. The compacting force components containing the cone angle of the technological tool are taken into account.

7. The process parameters affecting the compacting force are revealed. The effect of the elongation and the friction coefficient to the optimal angles is shown.

8. Application of the matrix with the optimal cone angle allows to reduce pressing energy intensity during production of the low-temperature superconducting products.

CHAPTER 2. High-temperature superconductors (HTS): Literature review

The chapter 2 provides a general presentation of high-temperature superconductors (HTS). The history of development of the high-temperature superconductor material are shown and summarized. During the history of creation the HTS material of second generation the main disadvantages of first generation of this material are present, in particular the industrial challenges related to their development.

The dynamics of the development the technology of production of HTS of second generation are strongly connected with the cost of this material. The main tendencies and predictions of their cost are shown as well as their future development and perspective of the use in a variety of industrial applications.

The chapter presents also the fabrication process of this material and the challenges of this fabrication. The general structure of the high-temperature superconductor tape is shown. The main usable methods of creation HTS are listed.

The literature review about the main problems and difficulties of creation the HTS of second generation were done. The argumentation of making a research in the field of optimization of the fabrication process was done. The necessity of usage numerical modelling is shown.

2.1. Introduction

2.1.1. History of high-temperature superconductors (HTS)

In the condition of the global energy crisis the scientists work on alternative sources of energy. The international community has major challenges such as providing consumers with reliable and safe electricity, overcoming the under capacity electrical system, increasing the controllability of the electrical networks and optimization of the electrical distribution. Along with this, for example, in electric networks of Russia face the challenge of aging. According to the statistics conducted in 2004, more than 10% of transformers, 6% of reactors and 29% of switches exceeded their service life. It is obvious, that all these factors together talking about the necessity of modernization of electric systems, including the replacement of obsolete equipment with new. But the main challenge is that the new equipment must comply with requirements of the XXI century and the technical and commercial performance: it should be efficient, reliable, fireproof and environmentally acceptable.

Modern science offers new and effective solutions that are based on superconducting technologies, which have been already applied successfully in developed countries. Development in the heavy-current applied superconductivity began in 1961. These developments used low temperature superconductors (LTS) that require the cooling to helium level (4.2 K). Due to the complexity and high cost of the helium cooling systems, the designed devices did not find wide commercial applications. But the discovery in 1986 of high-temperature superconductors (HTSC) created a new story of development in the electrical power industry. So in the middle of the 90s the HTS wires of 1st generation appeared. They were stranded wires on the basis of ceramics bismuth system in a silver shell, produced by the method of "powder-in-tube". Devices based on HTS materials could operate at the level of nitrogen temperature (77 K), which simplified and made cheaper the cooling system.

As a result, superconducting prototypes of all kinds of electrical equipment have been designed, manufactured and tested in the short term. However performance

characteristics of HTS device of first generation (1G HTS wire) at the temperature of liquid nitrogen were relatively low, and the cost - unreasonably high: 1 kA·m HTS wire of the 1st generation was ten times higher than the cost of 1 kA·m copper conductor. To overcome this major difficulty, the leading companies developed new industrial-strength technology HTS wires of 2nd generation. HTS coated conductors were deposited on the long metal tape in a continuous process. The second generation of HTS (2G wires) provides high economic return. At nitrogen temperature, they have performance characteristics (the operating current density and magnetic field), competing with low temperature superconductors. At the same time the cost of 2G HTS wire was equal to that of the copper conductor or below this value.

Experimental devices for HTS wires of 2nd generation were designed. Intensive development were conducted in USA, Japan and Germany. The JSC «Federal grid company of unified energy system» considered the use of advanced superconducting technology as one of the main ways of technical re-transmission and distribution systems of electric power (JSC «Federal grid company of unified energy system», 2011). It is true that superconductors provide a solution for the problems of quality and reliability of electrical networks. The Electric Power Research Institute in USA estimated the economy due to this technology to 30 billions of dollars each year only by eliminating losses of electricity (Kannberg, et al., 2003). However to find a wide usage, the HTS wires of the 2nd generation should be cheaper and more accessible. And what is interesting they should be cheaper in twenty times. This is the most popular phrase in any conference or seminar about superconductors.

Today the HTS tape of 2nd generation is a high tech-product. The part of the material in the product cost is negligible (less than 1%). If we exclude non-technical reasons, it turns out that the cost of the tape is completely determined by the cost of technology used. Also with the development of technology, more efficient technical solutions with decreasing defect rates and with increasing the production should be find, as result the price of the tape should be close to the cost of materials. The same situation was with Nb-Ti and Nb3Sn (LTS wires) (Scanlan, 2001), and also for HTS wire of 1st generation.

Fig. 2.1 shows the data from the SuperPower company that describe the dynamics of changes in the cost of the HTS (Selvamanickam, 2011). Fig. 2.2 shows the HTS material cost reduction over the time which was achieved by Superconductor Technologies Incorporation (Superconductor Technologies Inc, 2013). It is obvious that the price of the wire is decreasing while the companies are trying to improve the properties of HTS tape. According to the report (Hazelton, 2014), the situation with price also will change in future with tendency of decreasing. The complexity of the architecture of these multilayer HTS tapes causes a large number of ways to achieve the desired result. It is shown there that cost will decrease by improving both manufacturing process and performance. It is expected that the performance ratio ($/kA-m) will continue to decrease over the next years by factors of 2-4.

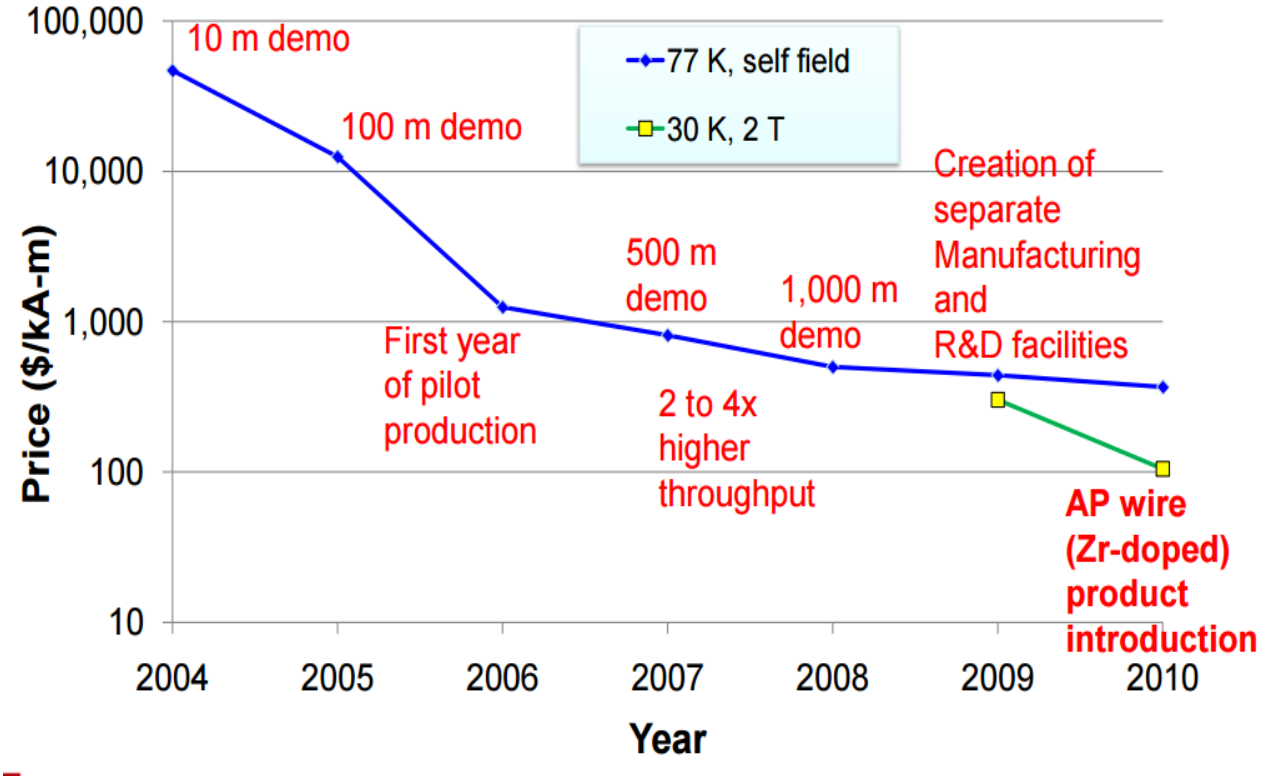

Fig. 2.1.Dynamics of changes in the cost of HTS tape.

By 2016 the SuperPower company wants to increase the critical current of the HTS tape width of 4 mm to 200 A at 77 K in self-field, and up to 1000 A at 30 K in a field of 2 T (working conditions HTS windings in electric machines) (Lehner, 2013). By 2020, it plans to increase the length of a single HTS conductors up to 1000 meters, while today the commercial length is less than 200-300 m.

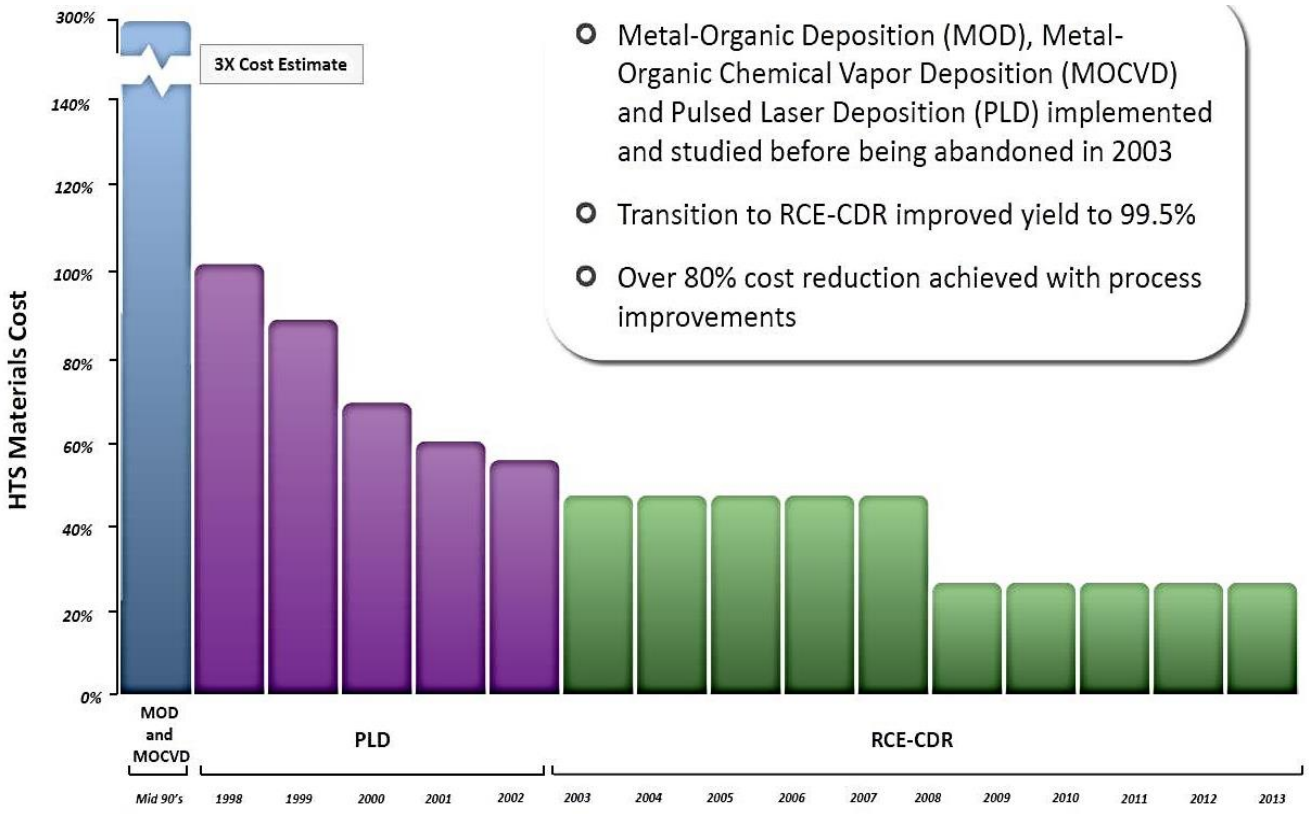

Fig. 2.2.HTS materials cost reduction over the time (Superconductor Technologies Inc, 2013).

Fig. 2.3 shows the prediction of the Superconducting device market and HTS wire market (Lehner, 2013). According to the prognostication of BBC Research, in 2017 the basic consumption of the HTS conductor in 2017 will be in the superconducting cables and current limiters, the contribution of the cost of a superconductor in the cost of the final product and is not determinative. Other superconducting electrical devices such as electrical machinery, transformers and inductive energy storage, according to the forecast BCC Research, have not yet reached the prototype stage and the market will be represented.

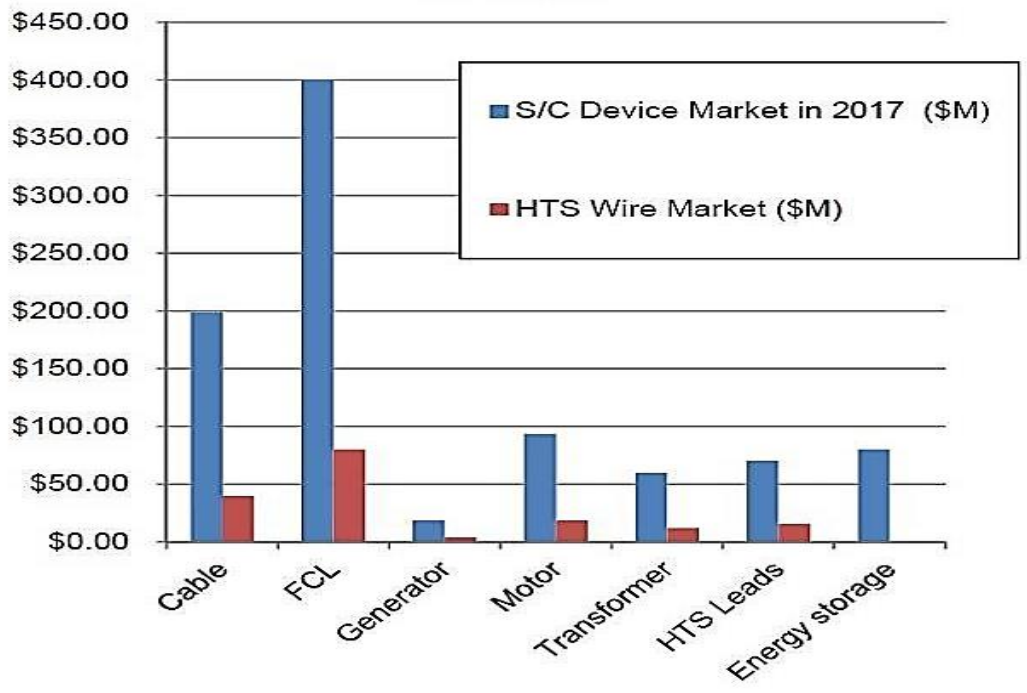

Fig. 2.3. Superconducting device market and HTS wire market prediction.

2.1.2. Perspectives of HTS

The new generation of superconductors conducts electricity with no resistance allowing a substantial energy safe. A significant advantage of the high-temperature superconductors comes from the relatively high operating temperatures. HTS can work at super cooled liquid nitrogen at temperature ranging from 65 to 77 K, that's makes them potentially useful in many areas such as energy, transport and scientific instrumentation technology. It is more interesting to work in the range of temperature 20 - 50 K with hydrogen and helium gas, because critical field and current density of HTSC in this range is very large. In this range of temperature the stability of the wires is considerably higher than in the temperature of liquid helium, due to the higher heat capacity and good thermal conductivity (Bansal, 2008). The work in this range of temperature is substantially less affected by energy loss in the conductor. For small and mobile devices, it is very important to have higher reliability, compactness and lower cost of the cooling system at 20 to 50 K than at 4.2 K. Nowadays HTS tapes of the 2nd

generation are widely used in windings, made of individual tapes, for example, high-field magnets inserts in LTSC (for fields of the order of 25 Tesla). A large gam of high-current applications based on high-temperature superconductors is now in the stage of prototypes. Some of the possible uses of HTSC are present below (National research centre "Kurchatov institute", 2012).

High operating currents are needed for several of HTS devices, but each of them will have their own working conditions for current-carrying element (CCE). For example, for superconducting magnetic energy storage (SMES) (Van der Laan, et al., 2011), (Shikimachi, et al., 2009), we need high operating current and low inductance for high-speed input / output energy at an acceptable voltage at the converter. For different applications operating temperatures of SMES can range from 4.2 K to 65-77 K; field on the windings from 1 T to T 20-25; and currents from 1 kA or even tens of kA at the high speeds of rises/decreases in current mode of input/output energy.

For HTS transformers in the operating temperature range of 77-65 K, current reaches 1 kA at 50-60 Hz in the fields on the winding 0.2-0.3 Tesla. Also HTS power generators exist and may be of two types: with relatively high fields (several Tesla) without iron in the stator and in the rotor (working temperature 20-50 K) and low fields winding 0.2-0.3 T with iron rotor or stator (operating temperatures of 65-77 K). While operating currents are in the projects now, but at the nearest future the level of hundreds of amperes with the prospect of increasing of magnitude in several times are planned. HTS current limiters in the electrical network will operate under alternate currents as well as for direct current in the range from several amperes to several hundreds of kA and at the temperatures of 77-65 K. For SMES can be used the wide (about 12 mm) tape without a stabilizer or a tapes with very thin layer of stabilizer (less than 5 microns of copper).

HTS power line both DC and AC currents should carry from hundreds of amperes and, potentially, to tens of kilo amperes at the temperatures of 77-65 K. The perspectives of flexible HTS power cables are also very huge. For example, the cables of small diameter and weight are planned for use on ships and planes (Van der Laan, et al., 2011), (Van der Laan, et al., 2012). For instance, at the temperature of 55 K in the

condition of flow cooling of helium gas such cables can carry a current with several kA. HTS engines from several megawatts, for example, for the ships – are very perspective because of the high power density per unit of weight and volume. Engines as generators can be divided into two types: the high magnetic field (stator and rotor without iron, the operating temperature from 20 to 50 K) and a low magnetic field (iron stator or rotor with operating temperature 65-77 K).

Magnetic systems of particle accelerators are currently working at temperatures 1.8 K on the basis of low-temperature superconductors (LTS). But in the future, we expect to use HTS coils in order to receive a fields of 10-20 T at 4.2 K with a current of 10 kA and a current density of 400 A/mm2. For tokamak magnetic systems (Bansal, 2008), current requires up to hundreds of kA in fields up to 25 T and this is grand and ambitious plan for the future. In this case, we need a further increase in the current-carrying capacity of current-carrying element. Operating temperatures, apparently, will be in the range of 20-50 K.

Current leads and current feedthroughs are the closest usage in the real and practical application of HTS CCE, operating temperature may range from helium to nitrogen, and the length does not exceed a few meters. Superconducting current-carrying tapes have many engineering applications. They are widely used in creating high-power transmission lines and high-voltage cables, as well as laboratory magnets and current limiters.

2.2. Fabrication process

The modern HTS conductors of the 2nd generation is a tape which includes a superconducting ceramic layer with a thickness of 1-3 microns deposited (via buffer layers) on a substrate (Hastelloy, stainless steel, alloys textured by Ni) with thickness of 50-100 microns. Tapes are coated with a silver layer 1-2 micron in thickness in order to protect and stabilize materials, such as copper or bronze with tens of microns of thick.

The width of the tapes varies from 3 to 10 mm. One of the possible structures of the HTS tape is shown in Fig. 2.4.

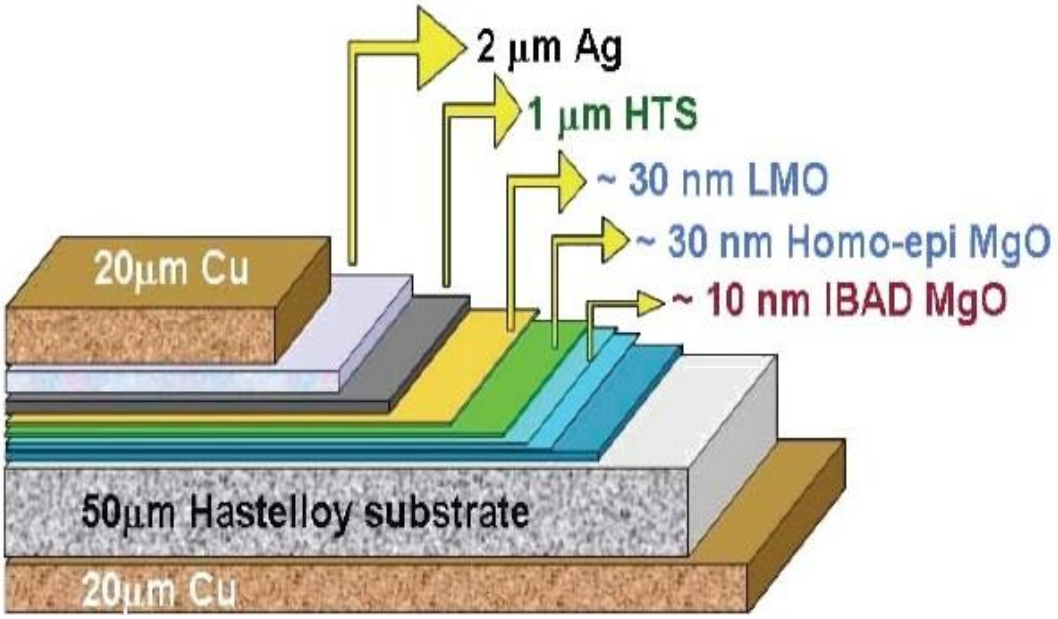

Fig. 2.4. Design of the HTS of the 2nd generation (Selvamanickam, et al., 2010).

The superconducting tape is a multilayer structure that consists of a metal substrate, buffer layer, a superconducting layer and a stabilizing coating. For creating a chemical barrier between the substrate and the HTS and matching their coefficients of thermal expansion (the difference in temperature between the application and the operating temperature can be of over 900°C), it is necessary to produce a buffer layer, as well as creating a texture of HTSC by its epitaxial growth. Texture in the buffer layer is a necessary condition for the epitaxial growth and close lattice parameters of the buffer layer and HTS. To perform all the functions listed above the multiple buffer layers must be used. The report of the (National research centre "Kurchatov institute", 2014) presented main methods of fabrication of HTS.

IBAD methods (Ion Beam Assisted Deposition) was described in (Yu, et al., 1986). It aims at creating niobium films. In the early phase, this method was used for creation the buffer layer by (Iijima, et al., 1991). This method consists in using two beams: the primary target material diffuses, while the auxiliary participates in the

formation of the texture layer (Yamada, et al., 2003). High speed of texturing of magnesium oxide (MgO) allows growing a film with a minimum thickness of the layer (Hühne, et al., 2005) and with minimum roughness (Miyata, et al., 2011) and also with high texture (Groves, et al., 2008). SuperPower Company used this technology to produce the superpower tape with more than 1 km in length (Xiea, et al., 2005). This method is widely used by companies such as Fujikura (Japan), SuperPower and Superconductor Technologies Inc (USA), Sunam Co Ltd. (Korea), International Superconductivity Technology Center (Japan).

Later the method IBAD was modified (Usoskin & Kirchhoff, 2008). The method ABAD (Alternating Beam Assisted Deposition) was developed. It consists in the alternation of the use of primary and auxiliary ion beams. It is necessary to make up 60 cycles of alternation to achieves the required performances, in order to improves texture and roughness values in comparison with the IBAD method (Usoskin & Kirchhoff, 2008), (Obradors & Puig, 2013). German company Bruker uses this method.

The Inclined Substrate Deposition (ISD) was proposed by (Fujino, et al., 1996). It consists in sputtering a target of the buffer layer by laser (Fujino, et al., 1996) or by electron beam evaporation in a vacuum (Bauer, et al., 1999). The main principle of this method concerns the inclination of substrate in a way the pair fall on its surface at an angle of 55°. This allows to achieve values of the texture 9.4 - 11.4, surface roughness of 11.16 - 23.66 nm (Bhattacharya & Xu, 2005) and the tape length up to 40 m (Bhattacharya & Xu, 2005). This method is used by German company Theva.

One of the key factors in the technology of HTS wires of the second generation is the textured metal tape manufacturing. The (National research centre "Kurchatov institute", 2007) give the following requirements for the tape:

- Material of the tape should have a face-centered structure. These materials include such metals as Cu, Ag, Au, Ni, Pd, Pt, Al, Pb, Rh, Ir, as well as many alloys based on them;

- Technology of cold-rolling followed by recrystallization should lead to the formation of acute cube texture. This cube texture should be stable at high temperatures without secondary recrystallization;
- The tape should have good mechanical properties. It is important in both cases: during the deposition on it of coatings at high temperature and in the manufacture of cables and subsequent operation under cryogenic conditions;
- In the case of usage with alternating current, the material of the tape should are not display the magnetic properties at the temperature of HTS use;
- Technology for producing textured layers on such tapes should exist;

The tendency in the development of texted tape is presented by (Bhattacharjee, et al., 2007). Attention was given for obtaining good mechanical properties of the tape such as solid-solution strengthening and multilayer tapes. In these multilayer tapes, one of the layers carries on itself mechanical load, while the outer layer provides a good texture and stability to oxidation. It is necessary to have good understanding of all the process occurring on the surface of the textured tape for the development if higher temperature superconductors of the second generation.

Copper is a good alternative to nickel as a material textured substrate: it provides a good texturing and makes easier the fabrication process. It is also several times cheaper than nickel. The investigation of mechanical properties of copper and its alloys as well as its texturing are discussed in (Sarma, et al., 2003). The work of (Eickemeyer, et al., 2007) aimed at obtaining the textured ribbons with elongated grains in the rolling direction. This elongation reduces the number of intergrain boundaries in the current path. Critical currents in the HTS tapes are significantly anisotropic. This microstructure was successfully obtained in the tape of copper and nickel, microalloyed silver.

2.3. Design process and challenges

Composite superconductor materials have specific mechanical, electrical and thermal properties. The variety of designs of high-temperature superconductor materials leaded to a large variety in technology of their production. The layered structure of HTS in combination with extremely weak adhesion between the layers leads to the fact that the presence of relatively small transverse tensile stress is sufficient to cause delamination of conductor. The production of High-temperature superconductors encountered major difficulties (Van der Laan & Ekin, 2007), (Van der Laan, 2009), (Maeda & Yanagisawa, 2014).

The HTS fabrication process meets two main difficulties. The first concerns the stabilization of 2G tapes having at helium temperature with insufficient capacity and low speed of propagation of normal zones (and complexity increase with increasing magnetic field, the stored energy and inductivity). Up to now, fabrication of THS uses standard approaches for the protection of the windings, such as the use of extra copper stabilization and transition to the resistive coils connected, the use of detection systems of normal zones and output energy of the windings.

In the reference (Song, et al., 2012) presented a comparative analysis of the properties of impregnated and non-impregnated windings. The critical current for impregnated windings after several cycles of cooling-warming can be reduced by 0.3 - 0.4 times from the value of the critical current short sample of HTS tapes. The degradation degree of the critical current of the winding have a correlation with the value of transverse force which appears in the beginning of the delamination in a single HTS conductor under the influence of radial stresses during cooling coil to operating temperature. The conductor delamination is partially exposed because of the difference in the coefficients of thermal deformation of HTS tapes, and epoxy compound material, which is used as frame. As a result this significantly reduces its current carrying capacity. It should be noted that the transverse stresses that’s leads to delamination, is

several times below the maximum of allowable longitudinal tensile stresses for HTS tapes (National research centre "Kurchatov institute", 2013).

The second problem in the HTS fabrication concerns the degradation of the properties of conductors, due to the high mechanical stresses. Thermomechanical and mechanical stresses cause the degradation of the critical current in the HTS conductor (Van der Laan & Ekin, 2008), (Van der Laan, et al., 2010). Experimental studies of the delamination process of HTS conductors 2nd generation were done by (Van der Laan, et al., 2007) and (Gorospe, et al., 2014). They used the technique of stretching in the transverse direction of the conductor. Samples in the form of strips of 10 mm wide and 4 mm were cut from YBCO-tape 40 mm of width. Also YBCO-tape with the original width of 10 mm was studied. In the process of stretching in the transverse direction, a sample voltage was measured. It should be noted that voltage was constant until the beginning of the fall of the critical current. The transverse tensile stress on the sample increased with increments of 0.08 MPa. Other researches on this issue are available in (Zhang, et al., 2011), (Myazato, et al., 2011), (Nishijima & Kitaguchi, 2012) and (Yanagisawa, et al., 2011).

(Van der Laan, et al., 2007) and (Jeong, et al., 2012) showed the necessity to study the mechanicals properties of HTS materials in order to overcome the fragility problem. Fig. 2.4. shows that high-temperature superconducting tape has multilayer structure, consisting of different materials including HTS (YBCO) layer. YBCO coated conductor is a tape, but for some applications, this tape should be submitted to bending. It is known that ceramic HTS tapes, which transmit power, are difficult to bend, because during this operation they can lost their conduction. At the same time, the technology of production HTS magnet tape includes pancake winding and layer winding (Markiewicz & Swenson, 2010).

We find New HTS 2G Round Wires (Bruzek, et al., 2012) (Fig. 2.5). The “round wire” design solved two problems: reducing the diameter of HTS wire and increasing the superconducting section (and current density) (Nexans, 2015). The figure shows the destruction of HTS layer after bending operation. Analysis of this issue requires non-linear numerical modelling.

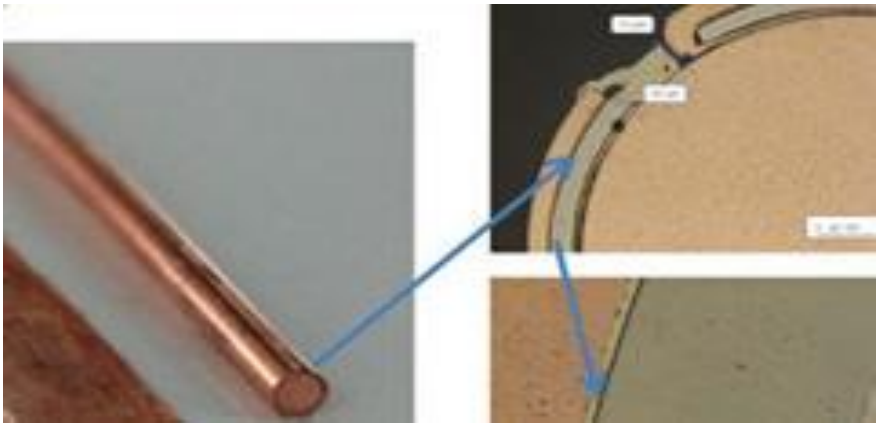

Fig. 2.5. Design of the New HTS 2G Round Wires (Nexans, 2015)

2.4. Conclusion

This chapter gave a global presentation of the High-temperature superconductors (HTS). It described the different phases of the development of this high-tech material. For each phase, the chapter described the industrial challenging as well as the innovation in the technology.

With the 2nd generation of HTS, we have large perspective of industrial application, but yet we have to overcome difficulties related to the fabrication of this material. Indeed, the fabrication stands for the major part of the HTS cost, because the cost of the material is negligible (less than 1%).

The modern HTS conductors of the 2nd generation is a tape which includes a superconducting ceramic layer with a thickness of 1-3 microns deposited (via buffer layers) on a substrate (Hastelloy, stainless steel, alloys textured by Ni) of 50-100 microns in thickness. Tapes are coated with a silver layer 1-2 micron in thickness in order to protect and stabilize materials, such as copper or bronze with tens of microns of thick. The fabrication process of HTS meets two main difficulties. The first concerns the stabilization of 2G tapes having at helium temperature with insufficient capacity and

low speed of propagation of normal zones. The second difficulty concerns the degradation of the properties of conductors, due to the high mechanical stresses.

The design of HTS as well as the optimization of the fabrication process requires the development of numerical models that could consider both the specific heterogeneous geometry of this material, the ultra-small thickness of some layers and the nonlinear behaviour of the constitutive material. Since the development of close-analytical solution seems to be laborious, we have to develop (use) numerical modelling.

In the next chapter we present the numerical modelling of the HTS using both finite element method and a simplified beam-model, which was developed in this work.

CHAPTER 3. Numerical model

The chapter 3 presents a simplified model for HTS beams. This model is based on the classical beam theory together with the discretization of each layer in small sub-layers working under purely axial stresses. The model takes into consideration the plastic behavior of the HTS constitutive materials. This model was implemented using MATLAB software.

It presents also the validation of this model by its confrontation to finite element analyses. This validation was done using COMSOL Multiphysics software. The comparable results of these two programs are shown.

After validation our model the research in the field of the optimal design of HTS was done by the analysis of different industrial configurations. The recommendation about the best configuration is shown as well as the future perspectives were given.

3.1. Introduction

As presented in the second chapter, HTS could be modelled using the beams theory. In the following we present briefly works conducted on simple beams as well as multilayer beams. Then we discuss the necessity to develop specific model for HTS.

3.1.1. Beams' theory

Since beams are largely used in engineering, important works were conducted for developing mechanical model (theory) for their design. The classical beam models are based on the theory of Euler-Bernoulli (Bernoulli, 1751), (Euler, 1744), Saint-Venant (Saint-Venant, 1856), (Feodosyev, 1999) and that of Timoshenko (Timoshenko, 1921), (Timoshenko, 1922). The former didn't take into account the transverse shear deformation, whereas the latter accounted for a uniform shear distribution along the beam cross-section.

A good synthesis of beams' theories can be found in (Carrera, et al., 2011). A general model of thin straight beams for large vibration amplitudes was proposed by (Benamar, et al., 1991). In order to find a set of non-linear algebraic equations, the Hamilton's principle was used. To obtain a numerical solution for the nonlinear problem, the special condition on the contribution of one motion was imposed. Also the investigation of simply supported and clamped-clamped boundary condition was conducted. The analysis subjected to initial axial forces where done for buckling loads of simply supported beams and the natural frequencies were taken into consideration by (Matsunaga, 1996). The research concerning cross-sections of thin rectangular beams aimed at studying the bi-dimensional displacement field. The properties of a Timoshenko beam were analysed in (Van Rensburg & Van der Merwe, 2006). (Attarnejad, et al., 2010) represented the basic displacement functions (BDF), which were obtained by solving the governing differential equations of transverse motion of

Timoshenko beams via the power series method. (Voros, 2009) analysed connections between different vibration modes including the geometry, steady state lateral loads and internal stress resultants. Taking into account small strains and linearized theory of large rotations, a finite element model with seven degrees of freedom per node was developed. The researches in the reference (De Borbon & Ambrosini, 2010) studied thin-walled beams with axial load in order to investigate natural frequencies.

3.1.2. Multilayer beams

Nowadays, multilayer composite materials are widely used in industrial applications such as aerospace (Krasilcikov, 1991), automobile industry, marine, etc (Vasil'ev & Protasov, 1990), (De Lorenzis, et al., 2001). This large use results from the increasing demand for the reduction in the weight of structures and the increase in the resistance. Indeed, the weight saving is a dominant factor in some applications such the transport sectors: high speed trains, high-speed boats, cars etc.

It should be noted that composite multilayer beam is composed of layers of various materials (William & Callister, 2007). Important researches were conducted in this area for the analysis of the mechanical properties of layered beams (Bolotin & Novikov, 1980) (King, 1990), (Golas, et al., 2002) as well as their industrial applications.

(Bareisis & Kleiza, 2009) proposed a mechanical model for the analysis of the multilayer beam bending. (Yaghoobi & Fereidoon, 2010) studied a simply supported beam under uniformly distribution load. He analysed the influence of the material properties of the beam and its thickness ton the location of the neutral axis as well as its deflection. Analytical solution for two-layer beam with different material and geometric characteristics was developed (Schnabl, et al., 2007). This mathematical model was considered the influence of the transverse shear deformation on the displacements in each layer.

(Jonas, 2006) proposed a mathematical relationship for the connection between the position of the neutral layer and of the geometric characteristic of the beam and its stiffness. (Garuckas & Bareisis, 2003) studied the bending of multi-layer beams. He showed that the normal stresses due to bending depend on the position of layers relative to the neutral axis as well as their bending stiffness.

3.1.3. Need for a numerical model for HTS

Consequently, the analysis of the fabrication of these cylindrical wires from HTS tapes constitutes a challenging process issue. It is expected from this analysis to determine the stresses and strains induced into the different layers of the HTS tapes by considering some non-linear mechanical behavior of the different layers. The use of the finite element method for this analysis encounters a major difficulty, because of the very small thickness of some layers. This FEM computation requires very fine meshes and consequently a very long computation time.

In the Fig. 3.1 is presented scheme of the shaping of the HTS tape. Conditionally, this shaping process can be divided into three main steps, like it shown in the Fig. 1: 1 – tape in the normal state; 2 – under the acting forces at the both ends of the tape, the process of the shaping starts; 3 – before the final form of the cylindrical shape (Bruzek, et al., 2012), (Bruzek, et al., 2011).

The design and the optimization of the fabrication process of HTS require a numerical model that can describe easily large bending of HTS. Since HTS materials are composed of thin layers with non-linear behaviour, we have to use advanced numerical model such as the finite element method. In this work, we have started by the use of this method. We have encountered major difficulties, related to the ultra-small size of some layers of the HTS, which requires large meshes and large computation times, with some convergence difficulties in the non-linear domain. After this experience, we started a research work for the development of a simplified model, based

on the beam theory. In the following we present this model as well as its validation and use in industrial applications. And finally we use this model to propose an optimized design of HTS tapes adapted to the cylindrical shaping process.

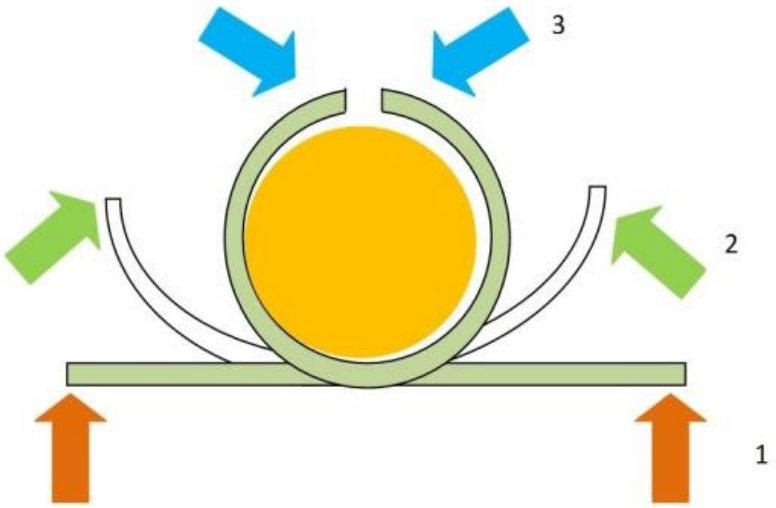

Fig. 3.1. Scheme of the shaping of the HTS beam (Bruzek, et al., 2011).

3.2. Numerical model

The proposed model is based on the bending theory of beams.

The beam section is composed of *m* layers. Each layer (*m*) is characterized by the thickness h_m, Young's Modulus E_m and axial stress strength $\overline{\sigma_m}$. Each layer is subdivided in small sub-layers as illustrated in Fig. 3.2 and Fig. 3.3. Each sub-layer is supposed to be submitted to a purely axial stress σ_i.

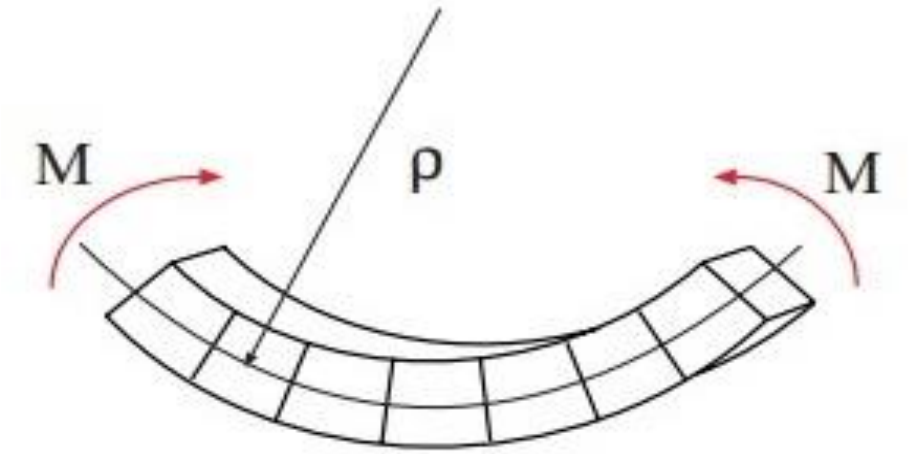

Fig. 3.2. Scheme of a multi-layered bending beam.

We assume that the beam section is submitted to purely bending moment *M* (the axial force *N=0*). The bending moment induces a beam curvature with a rotation of the section around the neutral axis of the beam.

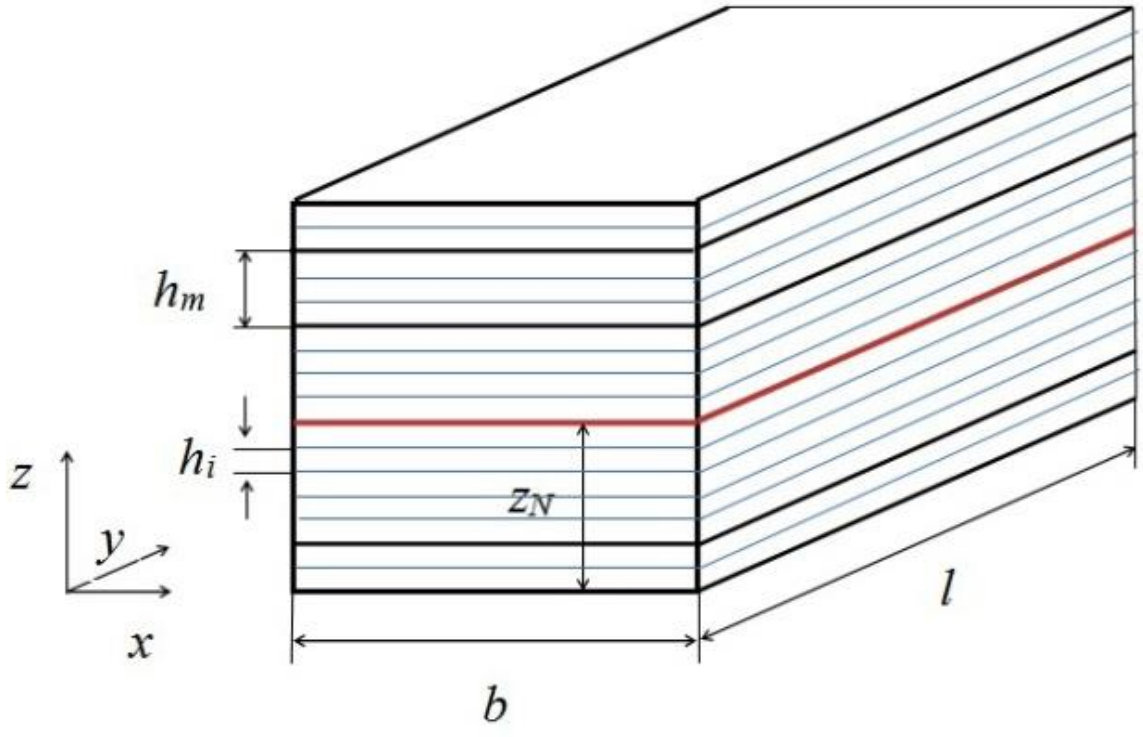

Fig. 3.3. Configuration of the HTS beam section.

3.2.1. Analysis in the elastic area

Axial stress distribution

The section is supposed to be submitted to the curvature (k), which induces the following strain in the section:

$$\varepsilon_i = k(z_i - z_N), \tag{3.1}$$

z_N - is the position of the neutral axis, z_i - is the position of the i-th layer

The corresponding axial stress and force are equal to:

$$\sigma_i = \varepsilon_i E_i, \tag{3.2}$$

$$F_i = \sigma_i A_i, \tag{3.3}$$

A_i is the cross-sectional area of i-th layer.

The location of neutral axis position (z_N) can be obtained using the equilibrium equation in the axial direction:

$$F = \sum_{i=1}^{n} F_i = k \sum_{i=1}^{n} A_i E_i (z_i - z_N) = 0, \tag{3.4}$$

which leads to the following expression:

$$z_N = \frac{\sum_{i=1}^{n} A_i E_i z_i}{\sum_{i=1}^{n} A_i E_i}, \tag{3.5}$$

The bending moment is given by:

$$M = \sum_{i=1}^{n} F_i (z_i - z_N) = \sum_{i=1}^{n} E_i k A_i (z_i - z_N)^2, \tag{3.6}$$

Equation (3.6) gives an explicit relationship between the bending moment and the curvature:

$$k = \frac{M}{\sum_{i=1}^{n} E_i A_i (z_i - z_N)^2}, \tag{3.7}$$

Shear stress distribution

The shear stress distribution is determined from the equilibrium of a small slide of the beam as illustrated in Fig. 3.4. The slide is delimited by the lateral surfaces S_i and S_{i+1} and the lower surface B_i and the free up-surface. The lateral surfaces S_i and S_{i+1} are submitted to the axial force P_i and P_{i+1}, respectively, while the lower surface is submitted to the force $\tau_i dy$.

The equilibrium of the slide allows the determination of the shear stress as follows:

$$\tau_i = \frac{-P_{i+1} + P_i}{dy}, \tag{3.8}$$

P_i stands for the total axial force applied on the section situated above the layer i.

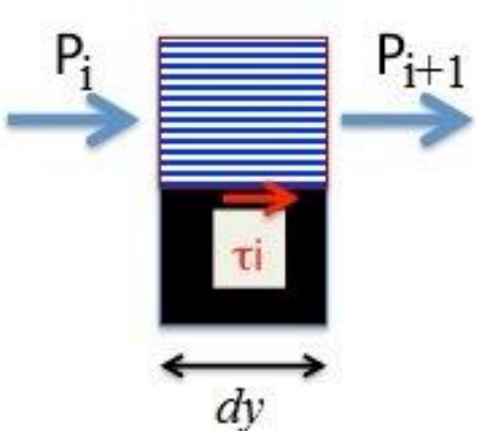

Fig. 3.4. Determination the shear stress.

Beam deflection

According to the beam theory, the deflection (w) is determined by the integration of the following differential equation:

$$k(M) = \frac{d^2 w}{dy^2}, \tag{3.9}$$

3.2.2. Analysis in the plastic area

Axial stress distribution

As in the elastic area, we assume that the rotation of the section around the natural axis induces the following strain:

$$\varepsilon_i = k\left(z_i - z_N\right), \tag{3.10}$$

The corresponding elastic axial stress is equal to:

$$\sigma_i = \varepsilon_i E_i, \tag{3.11}$$

This stress is submitted to the condition of plasticity:

$$\left|\sigma_i\right| \le \overline{\sigma_m} \tag{3.12}$$

With this condition the variation of the axial stress σ_i is not linear with the curvature k. In plastic domain σ_i is constant and depend only the nature of the material, whereas in elastic domain as explained in the previous paragraph σ_i is dependent on k and z.

The corresponding axial force is equal to:

$$F_i = \sigma_m A_i, \tag{3.13}$$

The position of the natural axis (z_N) as well as k are determined from the resolution of the set of equations (3.4) to (3.6) and from (3.10) to (3.13). Since this set of equations is nonlinear, the resolution is conducted using an iterative procedure.

The bending moment is calculated according to the following equation:

$$M = \sum_{i=1}^{n} F_i (z_i - z_N), \tag{3.14}$$

Equation (3.14) gives the nonlinear relationship between the bending moment (M) and the curvature (k).

3.3. Implementation in MATLAB

The model presented was implemented in MATLAB. The program, called (HTS_Analysis), uses a step-by-step analysis. At each step, we impose the curvature increment Δk. The values of the neutral axis (z_N), axial stress (σ_i) and axial stain (ε_m) are determined by the resolution of the nonlinear system of equations (3.4) to (3.6) and (3.10) to (3.13). The shear stress (τ) is computed from equation (3.8), while the corresponding bending moment is determined from equation (3.14). The program provides for the different values of the curvature (k) the corresponding values of the neutral axis (z_N), the axial stress (σ_i), the axial stain (ε_m), the shear stress (τ_i) and the bending moment (M).

The relationship between the bending moment (M) and the curvature *(k)* stands for constitutive law of HTS. It could be used in the general beam theory (Equation 3.9) for the calculation of the beam deflection due to external loading. Since the relationship

between the bending moment and the curvature is nonlinear, a step-by-step approach should be used in the integration of Equation 3.9. At each step, and in each section, we can use the value of the curvature for the determination of the distribution of the stress and strain fields in the beam.

3.4. Validation

3.4.1. Presentation of the validation example

The program (HTS_Analysis) was checked by its confrontation to finite element analyses conducted by COMSOL Multiphysics software. In COMSOL Multiphysics software adaptive meshing and re-meshing was used to overcome the problem of differing length scales. The 3D model used the boundary-mapped mesh. High-resolution solutions with minimum computation requirements were tracked. The mesh resulted in around 5400 elements and 155008 degrees of freedom.

Fig. 3.5 shows the cantilever beam used in the analysis. Its length (l) is equal to 300 μm, while its width (b) is equal to 20 μm. The beam is composed of 4 layers. Table 3.1 summarizes the properties of these layers, which were taken from references (Clickner, et al., 2006) and (Osamura, et al., 2009).

The beam is submitted to an increasing uniform linear force (q).

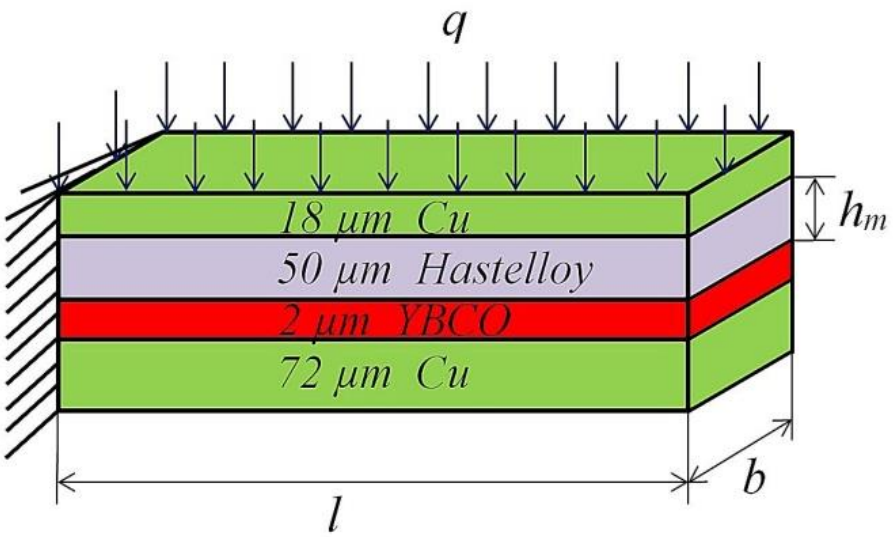

Fig. 3.5. Beam used in the validation of the proposed method.

Table 3.1: Properties of the beam used in the validation of the numerical model.

Number *m*	1	2	3	4
Material	Cu	YBCO	Hastelloy	Cu
Height h(μm)	*72*	*2*	*50*	*18*
Young's modulus E_m (GPa)	*110*	*128*	*192*	*110*
Axial yield stress σ_m (MPa)	*150*	*260*	*478*	*150*

The value of load was increased during calculation from zero till *700 N/m*.

3.4.2. Finite element analysis

Fig. 3.6 shows the variation of the axial stress in the beam with the increase in the load.

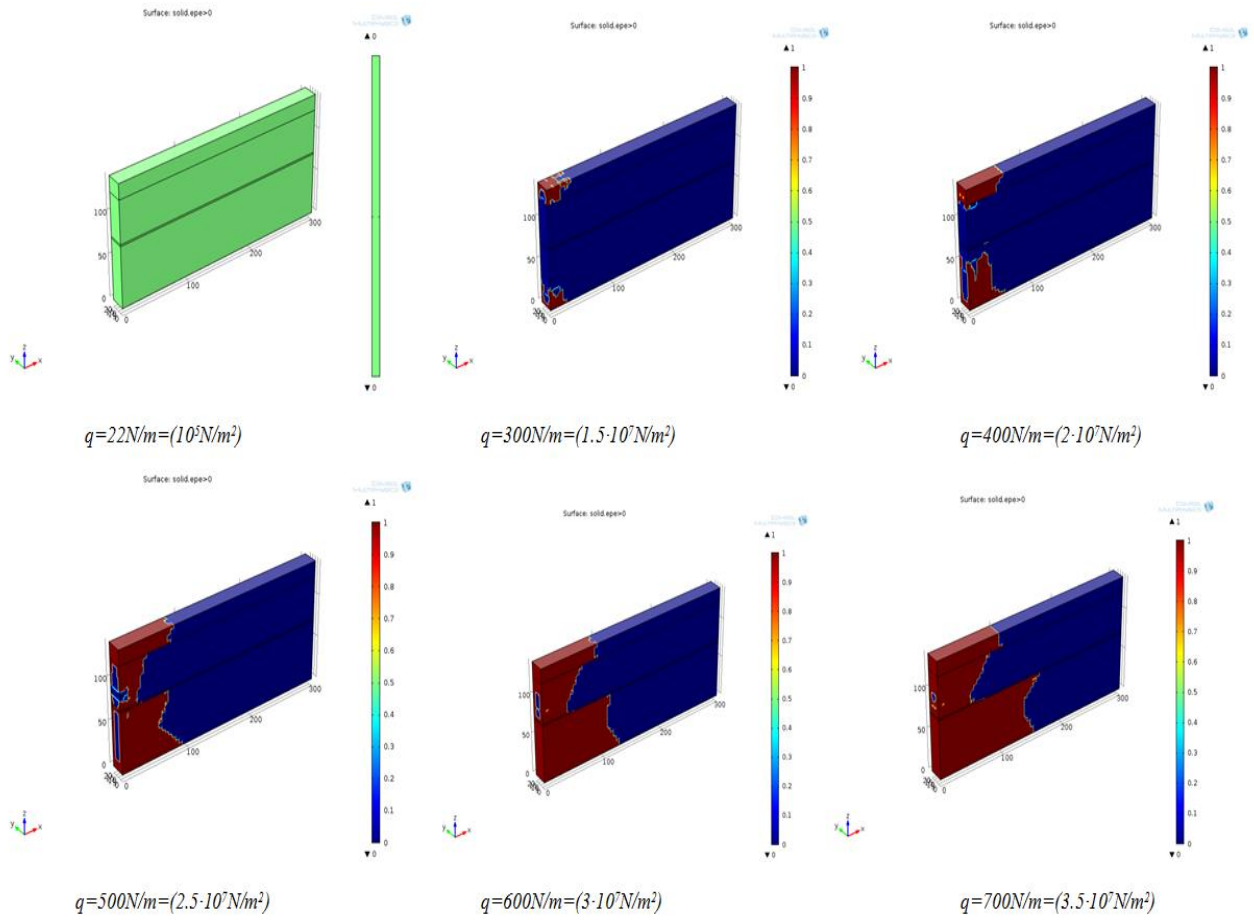

Fig. 3.6. Finite element analysis: Variation of the stresses in the beam.

We observe a high concentration of the stress close to the full-fixed section (left section), which corresponds to the maximum of the bending moment. The distribution of the axial stress in the section does not follow linear variation, because of both the beam heterogeneity (multilayer) and the nonlinear behaviour of the constitutive material. By the end of the loading ($q = 700\ N/m$), about a half of the beam is concerned by plasticity, mainly in the lower and higher parts of the beam.

Fig. 3.7 presents the distribution of the axial stress distribution in the section $l = 35\ \mu m$. In the beginning of the loading ($q = 22\ N/m$), we observe low stresses with linear variation in each layer. With the increase in the load, we observe the apparition of plasticity in the lower layer (Cu) and in the upper one. The apparition of plasticity in these layers is due to their far position from the axe of the beam as well as their low axial strength ($150\ MPa$). By the end of the loading ($q = 700\ N/m$), we observe plasticity in the upper part of the Hastelloy layer.

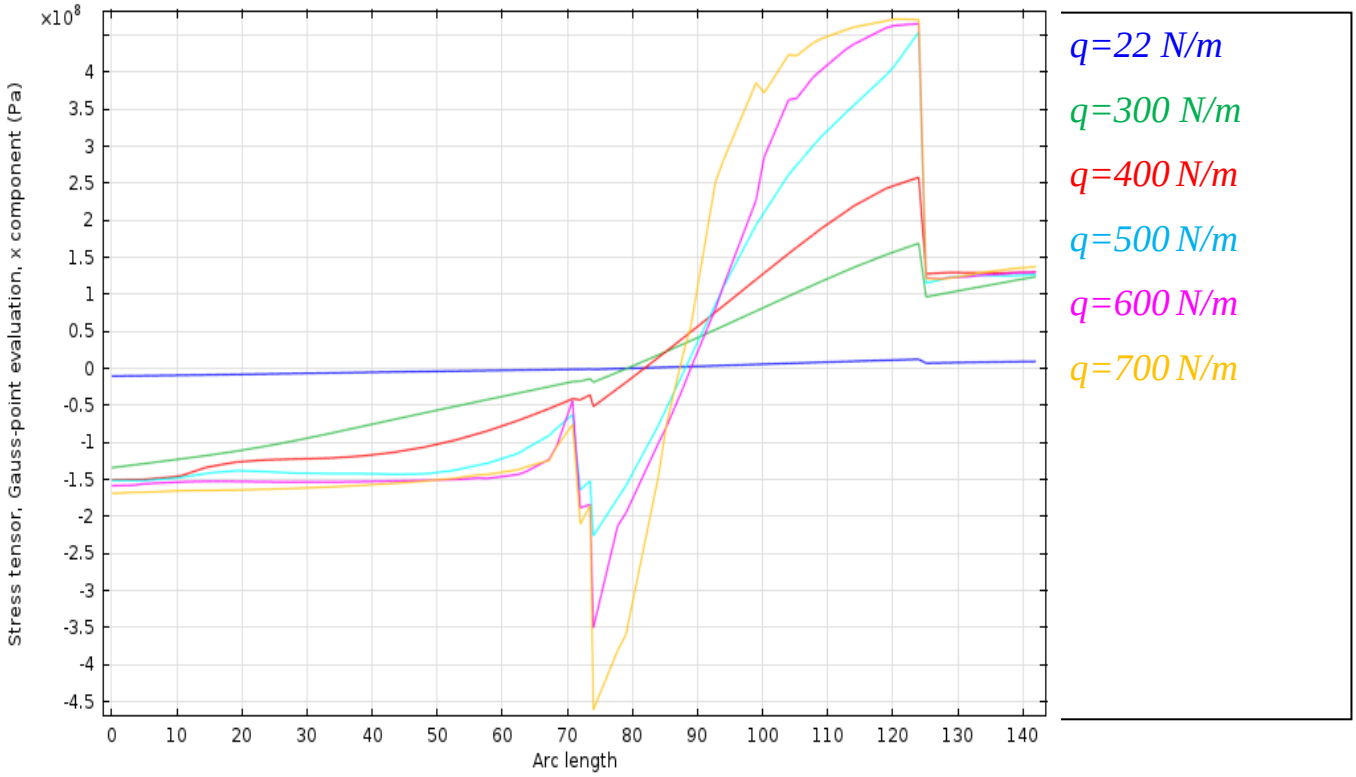

Fig. 3.7. Finite element analysis (COMSOL) variation of the axial stress in the section l= 35 µm.

Fig. 3.8 shows the variation of the shear stress in the section $l = 35\ \mu m$. In the beginning of the loading ($q = 22\ N/m$; elastic area), we observe a conventional distribution of the shear stress: it increases when we go from the beam extremities toward the beam neutral axis. For higher loads, we observe important reduction of the shear stresses in the upper and lower parts of the beam and an increase in the concentration in the central part. This pattern is due to the apparition of plasticity in the upper and lower parts of the beam, which leads limitation of the axial stress in these areas and consequently to close values of the corresponding forces (P_i and P_{i+1}) (Fig. 3.4).

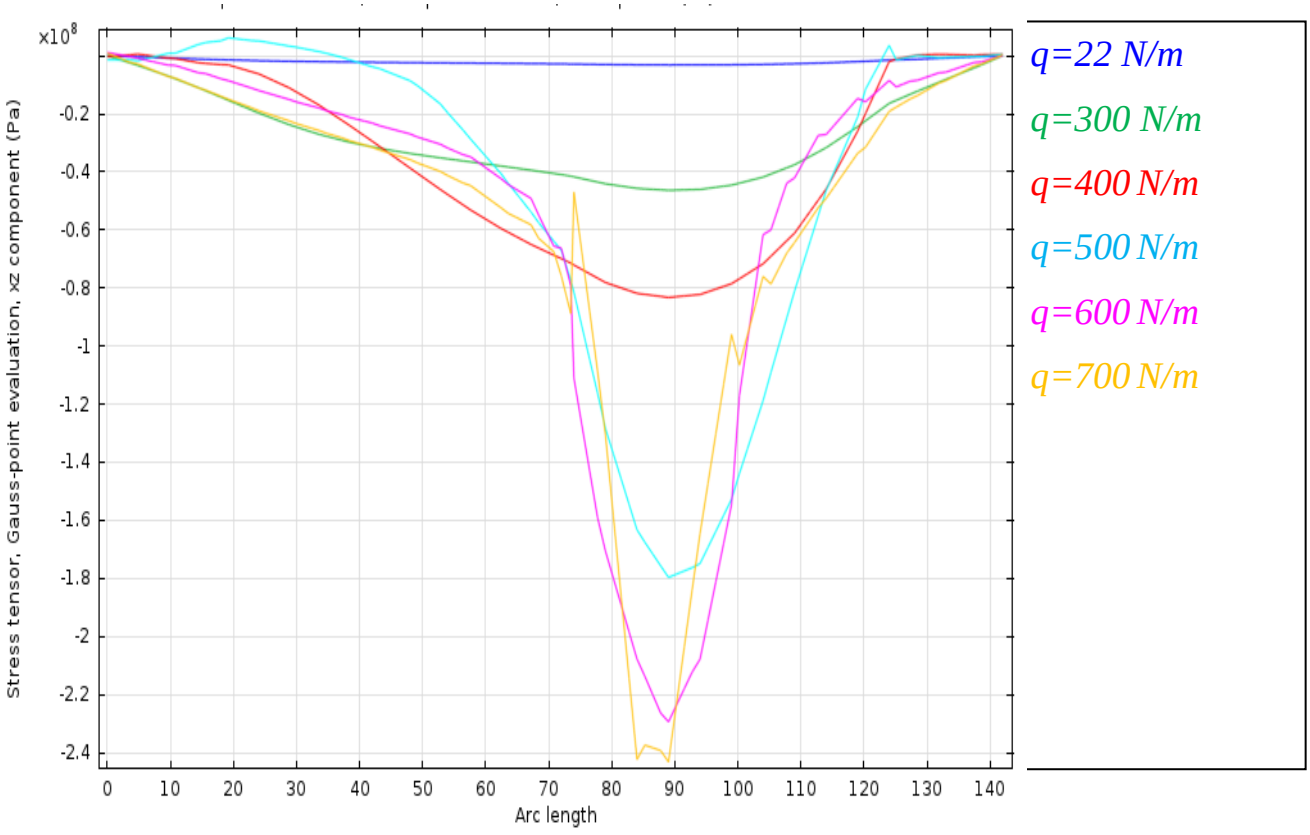

Fig. 3.8. Finite element analysis (COMSOL) variation of the shear stress in the section l= 35 µm.

3.4.3. Comparison COMSOL – Simplified model

Fig. 3.9 and Fig. 3.10 shows a comparison between the results of COMSOL Multiphysics and those obtained by the simplified model (HTS_Analysis).

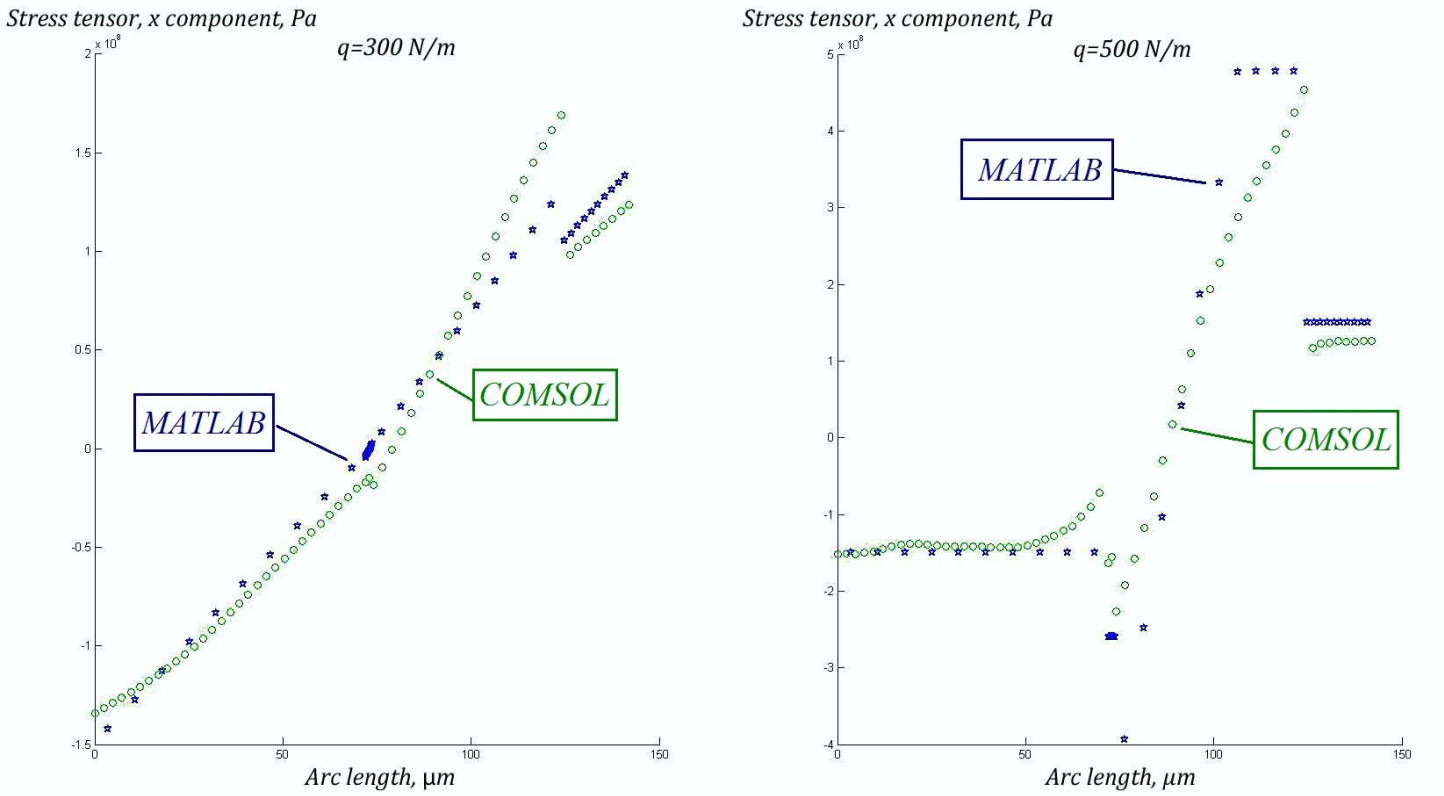

Fig. 3.9. Validation of the simplified model (HTS_Analysis): Distribution of the normal stress in the section l = 35 μm at q = 300 and 500 N/m.

Fig. 3.9 shows the distribution of the normal stress in the section $l = 35\ \mu m$ for two levels of the linear force $q = 300$ and $500\ N/m$. At $q = 300\ N/m$, we observe a linear variation of the normal stress in each layer. The stress remains in the elastic area. The results of the two programs agree well. At $q = 500\ N/m$, the two programs show a linear variation of the normal stress in the second and third layers and plasticity in the 1st and 4th layers.

Fig. 3.10 shows the distribution of the shear stress in the section $l = 35\ \mu m$ for $q = 300$ and $500\ N/m$. At $q = 300\ N/m$, the two programs show conventional variation of the shear stress in the beam section with a maximum near the beam axis, while at $q = 500$

N/m, they show very low shear stresses in the zones close to the extremities of the beam (plastic area) and a concentration of the shear stress in the central part of the section. The results of the two programs agree well.

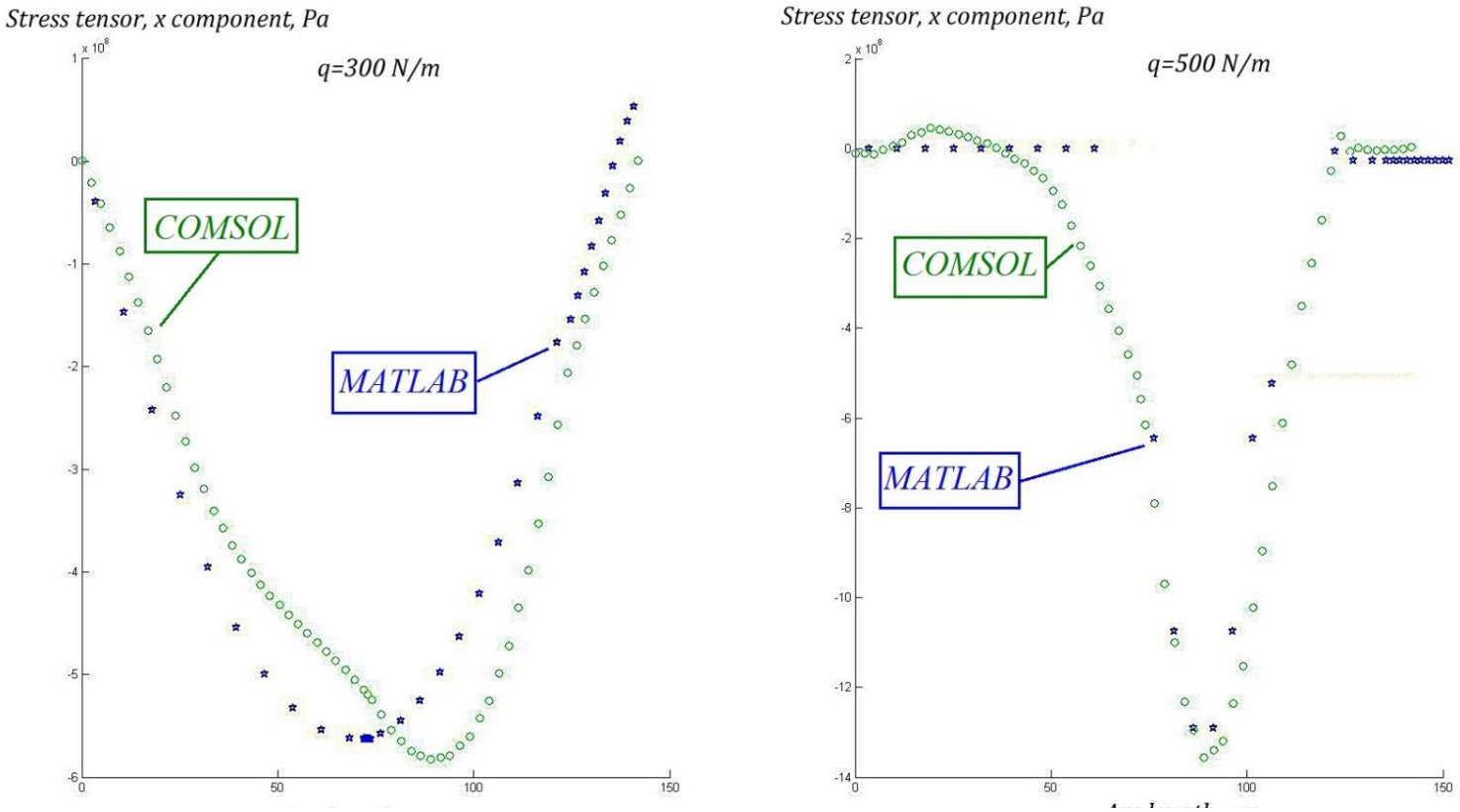

Fig. 3.10. Validation of the simplified model (HTS_Analysis): Distribution of the shear stress in the section l = 35 μm at q = 300 and 500 N/m.

Fig. 3.11 shows the variation of the beam deflection in the section *l = 35 μm* with the increase in *q*. We observe a good agreement between COMSOL and HTS_Analysis. The deflection varies linearly with the linear force (*q*) up to *q = 300 N/m*, then we observe a non-linear variation with an increase in the rate of deflection with the augmentation of the load. This increase results from the development of the plasticity in the beam.

This validation example shows that the simplified model globally well agrees with the results of the complex finite element analysis. It could be easily implemented in industrial environment and used in the HTS design.

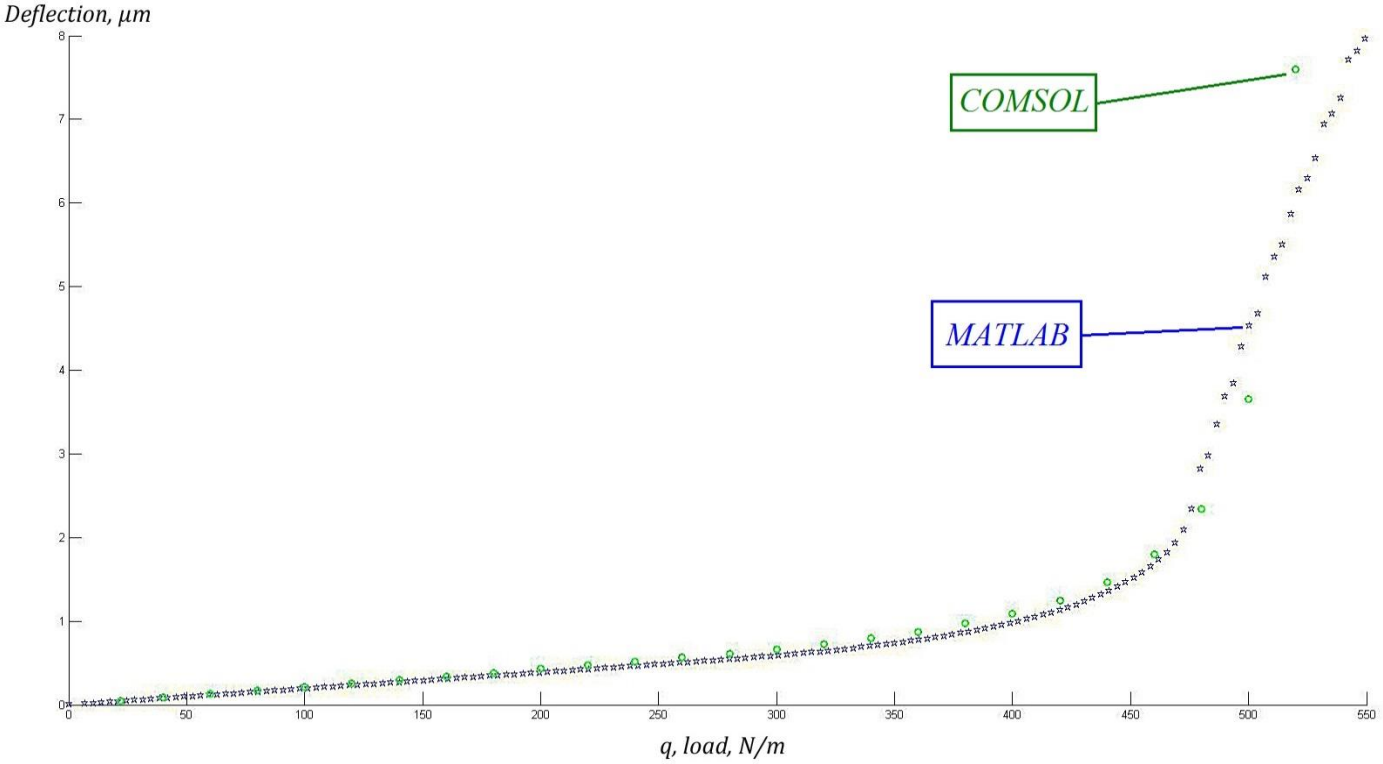

Fig. 3.11. Validation of the simplified model (HTS_Analysis): Variation of the deflection in the section l = 35 μm with the load.

3.5. Application to the optimal design of HTS

In this section, the simplified model (HTS_Analysis) is used for the optimal design of HTS. The criteria used in this analysis concern the position of the neutral axis regarding the YBCO layer. The neutral axis during the process of bending should remain close to the YBCO layer in order to reduce the stresses in this fragile layer.

In the following we analyze different configurations proposed by the industry.

Analyses were conducted with three materials in the third layer: Hastelloy, NiW5 and Stainless steel, whose properties are summarized in Table 3.2. The Young's modulus of Hastelloy and Stainless steel are close (around *192 GPa*) and higher than

that of NiW5 (*111 GPa*), while the axial strength of the stainless steel is about 62% of that of the Hastelloy and the axial strength of NiW5 is about 25% of that of Hastelloy.

For each material we have analyzed 4 cases, which correspond to different values of the thickness of the layers of the HTS proposed by the industry.

Table 3.2: Mechanical properties of the materials used in the 3rd layer

	Young's modulus (GPa)	Axial strength stress (MPa)
Hastelloy	192	478
NiW5	111	121
Stainless steel	193	300

Table 3.3 summarizes the configurations analyzed with Hastelloy. The variation of the position of the neutral axis during bending is illustrated in Fig. 3.12. We observe that in the first configuration (Case 1), the natural axis is far away from the YBCO layer, while in the 3rd and 4th configurations, the neutral axis is below the YBCO layer in the elastic domain and then, it translates towards the upper surface and exceeds the YBCO layer by about 5% of the beam thickness. In the second configuration, the neutral axis is below the YBCO layer in the beginning of the loading and then it translates towards the upper part of the beam and stays close to the YBCO layer. This configuration is the best one, because the neutral axis remains close to the YBCO layer.

Table 3.3:Configurations analyzed with Hastelloy

Case / (Layer)	1 (Cu)	2 (Cu)	3 (YBCO)	4 (Hastelloy)	5 (Cu)	Total Height (µm)
Case 1: height (µm)	18	52	2	50	18	140
Case 2: height (µm)	*30*	*55*	*2*	*25*	*30*	142
Case 3: height (µm)	*18*	*45*	*2*	*25*	*18*	108
Case 4: height (µm)	*18*	*50*	*2*	*25*	*18*	113

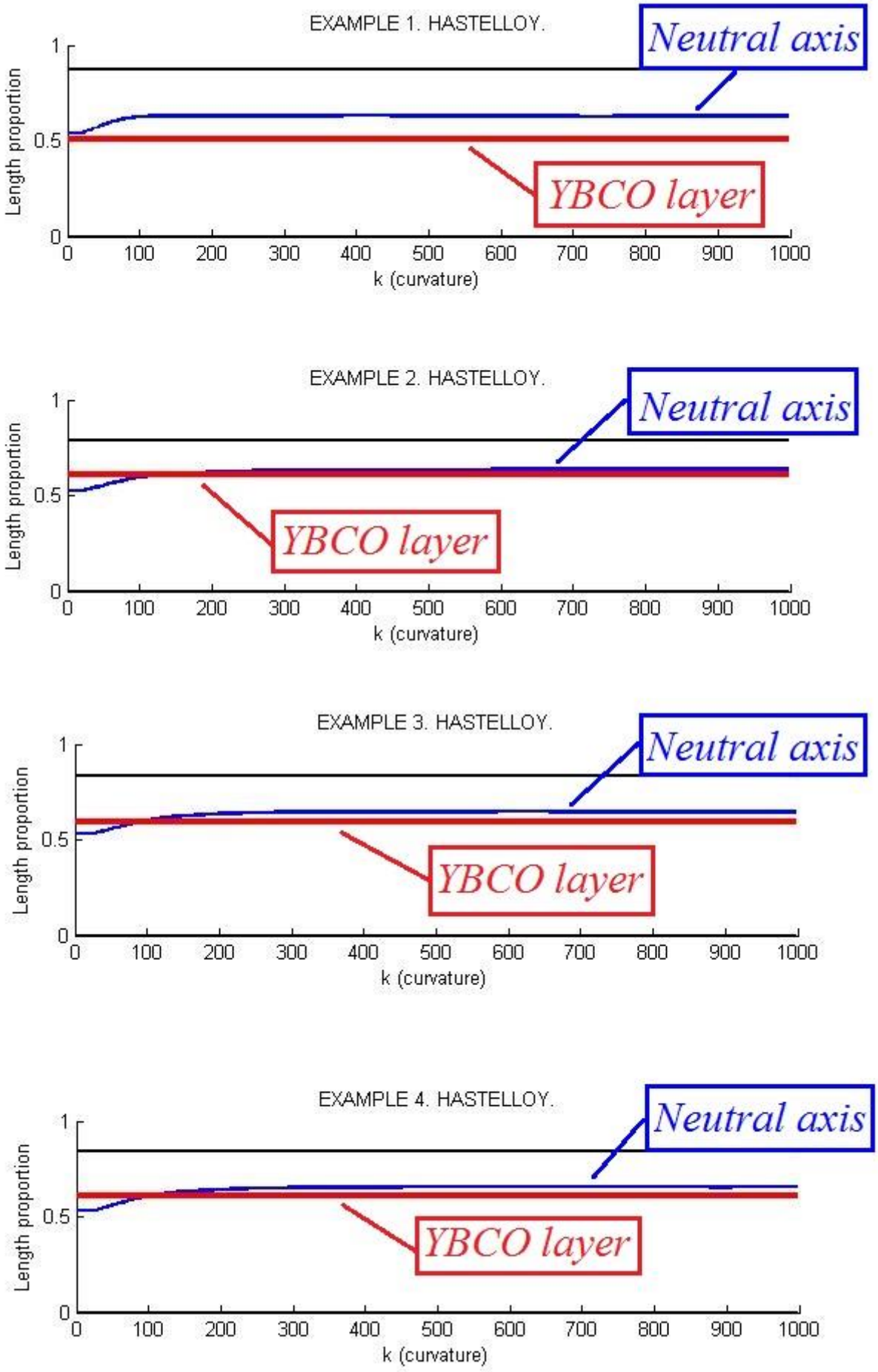

Fig. 3.12. Variation of the position of the neutral axis during bending - HTS with Hastelloy layer; the characteristics of the 4 cases are summarized in table 3.3.

Table 3.4 summarizes the configurations analyzed with NiW5. The total thickness of the beam varies from *90 μm* (Case 2) to *203 μm* (Case 4); this large variation results from the large variation in the thickness of the 2nd and 4th layers.

The variation of the position of the neutral axis during bending is illustrated in Fig. 3.13. We observe that in the configurations 1, 2 and 3, the neutral axis remains close to the YBCO layer, while in the 4th configuration; the neutral axis is below the YBCO layer by about 10% of the beam thickness. This configuration should not be used.

Table 3.4: Configurations analyzed with NiW5

Case / (Layer)	1 (Cu)	2 (Cu)	3 (YBCO)	4 (NiW5)	5 (Cu)	Total Height (μm)
Case 1: height (μm)	18	52	2	50	18	140
Case 2: height (μm)	*18*	*27*	*2*	*25*	*18*	90
Case 3: height (μm)	*18*	*82*	*2*	*80*	*18*	200
Case 4: height (μm)	*18*	*90*	*2*	*75*	*18*	203

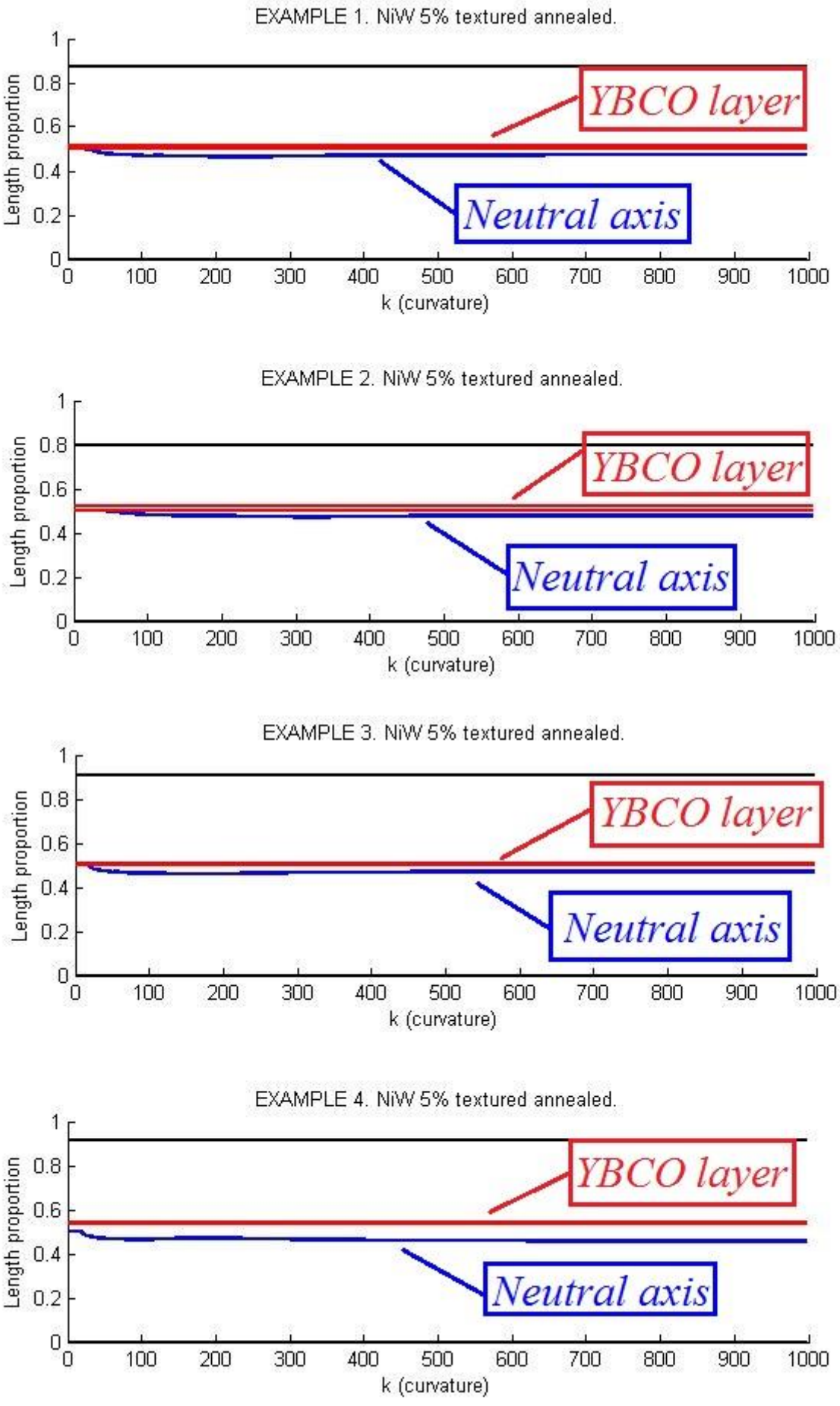

Fig. 3.13. Variation of the position of the neutral axis during bending - HTS with NiW5 layer; the characteristics of the 4 cases are summarized in table 3.4.

Table 3.5 summarizes the configurations analyzed with stainless steel. The total thickness of the beam varies from *108 μm* (Case 3) to *142 μm* (Case 2).

The variation of the position of the neutral axis during bending is illustrated in Fig. 3.14. We observe that in the configurations 2, 3 and 4, the neutral axis remains close to the YBCO layer in the plastic area, while in the 1st configuration, the neutral axis is above the YBCO layer by about 10% of the beam thickness. This configuration is then not recommended.

Table 3.5: Configurations analyzed with stainless steel

Case / (Layer)	1 (Cu)	2 (Cu)	3 (YBCO)	4 (Stainless steel)	5 (Cu)	Total Height (μm)
Case 1: height (μm)	18	52	2	50	18	140
Case 2: height (μm)	*30*	*55*	*2*	*25*	*30*	142
Case 3: height (μm)	*18*	*45*	*2*	*25*	*18*	108
Case 4: height (μm)	*18*	*50*	*2*	*25*	*18*	113

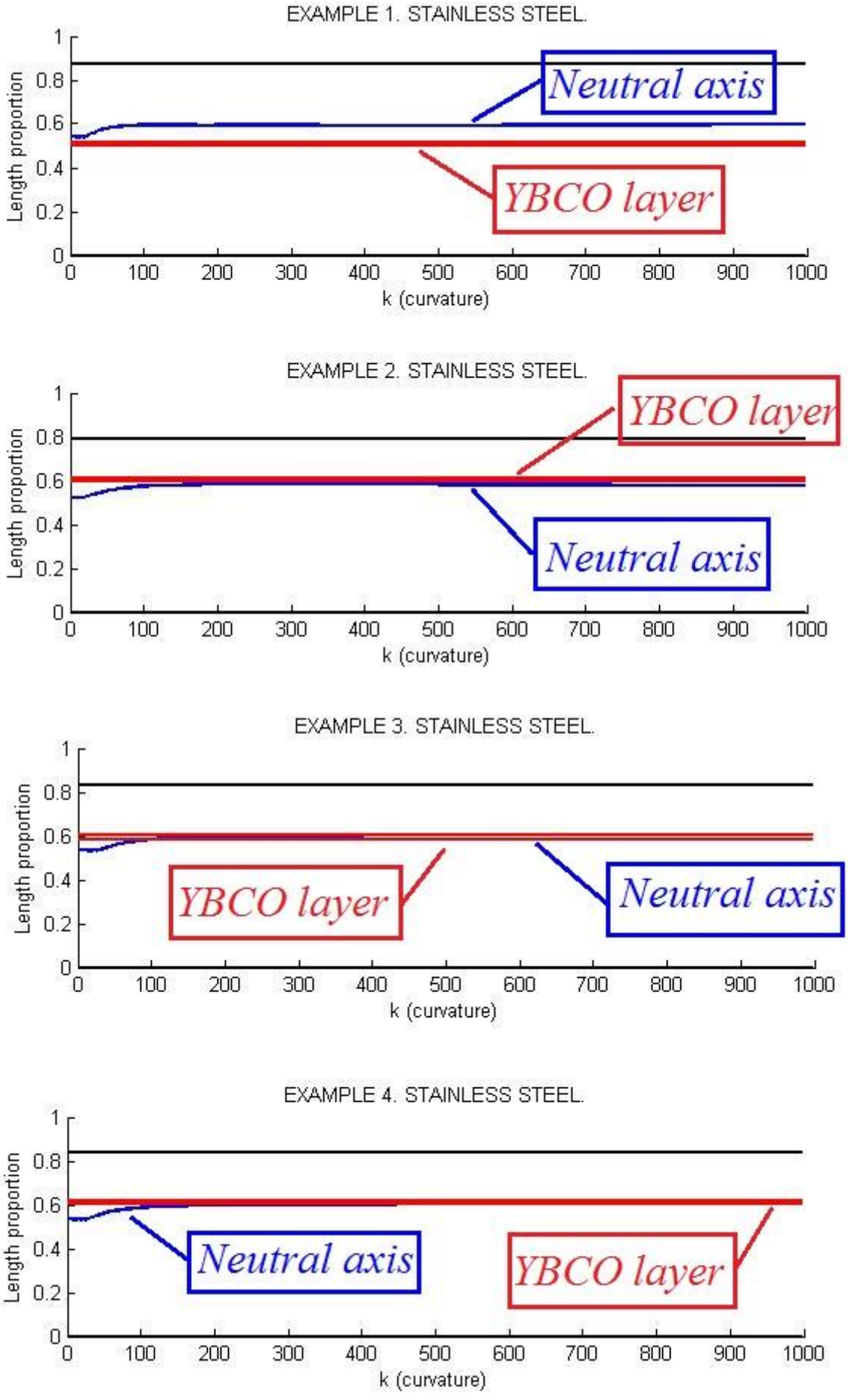

Fig. 3.14. Variation of the position of the neutral axis during bending - HTS with stainless steel; the characteristics of the 4 cases are summarized in table 3.5.

3.6. Conclusion

The fabrication of 2G high-temperature superconductors (HTS) includes a phase of large bending, which induces both axial and shear stresses in the HTS. The optimal design requires keeping the neutral axis close to the super-conductive substrate. The use of finite element method for the analysis of this complex material requires large meshes and computation time, because of the ultra-small thickness of the supra-conductive substrate. In this chapter we presented a simplified model, which is based on the classical beam theory together with the discretization of each layer in small sub-layers working under purely axial stresses. This model takes into consideration the plastic behavior of the HTS constitutive materials. The model was validated by its confrontation to finite element analyses. The validation test gave satisfactory results. In addition, this model could be easily implemented and used in industrial environment.

The model was used for the optimal design of HTS by the analysis of different industrial configurations. Analysis resulted in recommendations for the optimal configurations that reduce stresses in the superconductive substrate.

CHAPTER 4. Validation of the HTS numerical model on experimental tests

The chapter presents the verification of the numerical model presented in the previous chapter for high-temperature multilayer 2G. The verification is carried out on a bending beam test conducted on a high-temperature superconductor tape. The test will be first presented.

The numerical modelling includes two phases. The first one concerns the construction of the global behaviour of the beam using the model presented in chapter 3 and then the calculation of the beam deflection using both the conventional structure theory together with the nonlinear relationship between the bending moment and the curvature as determined in the first phase.

The comparison of the numerical and experimental results will allow analysing the performances of the numerical model developed in the previous chapter and its use in practical applications.

4.1. Introduction

One of the oldest disciplines in the area of studying behaviour of the material is mechanical-technological testing. Since 15th and 16th century the greatest scientist such as Leonardo da Vinci and Galileo Galilei were trying to explain the behaviour of materials in the elastic state but with taking into account flexural stressing. They were creating special devices in order to study more. The further knowledge was received with time and as a result finally the first testing machines appeared in France in the 18th century. Since 1920 the material testing become a business where has been involved such company as Roell & Korthaus, Mohr & Federhaff, Carl Benz, Zwick Roell Group, etc. These and all other companies know how to create an "intelligence" modern testing system or machine with a wide range of high-performance products – from the economical standard machine up to special versions and designs for special test jobs (Zwick Roell Group, 2015). Being a leading company or being an expert in the test systems for different materials this is a big responsibility. And also this means that you can predict a future, because everything that surrounds us – is a big variety of materials.

The high quality manufacturing standards are strongly required during production of 2G high-temperature superconductor tape; otherwise, manufacturing defects may have a big influence in the HTS structure performance. That's why to have a good knowledge of the materials as well as technological process and their influence on the structure is essential. Also it should be taken into account that during the designing process of these complex multilayer tapes, the designer has also to consider such selection of constituents as type of material, their proportion, distribution of the layers and their orientation. All of these constituents depend on the properties required as well as selection processes that are depends on the shape and production requirement. And finally, the mechanical properties of these tapes are playing the major role.

In the following section, the experimental study of the HTS tape during their mechanical bending process is given.

4.1.1. Experiment description

Tests were conducted using the texture analysis machine (Fig. 4.1). Usually these machines are used for investigation the mechanical and physical property of raw ingredients like food structure or/and designs of specific samples, what means that this machine is a well-established technique for the testing unusual samples. Our sample has a very small and specific thickness; as a result the texture of this sample is related to the sense of touch. So, with help of mechanical methods in units such as force, it can be measured. Also this machine can conduct standard test as compression, tension, and flexure.

Fig. 4.1. Test machine.

The machine software allows monitoring the test and data collection. It provides the variation of both the force and displacement. The test was conducted on a beam with simple supports subjected to a concentred force in the middle (Fig. 4.2.)

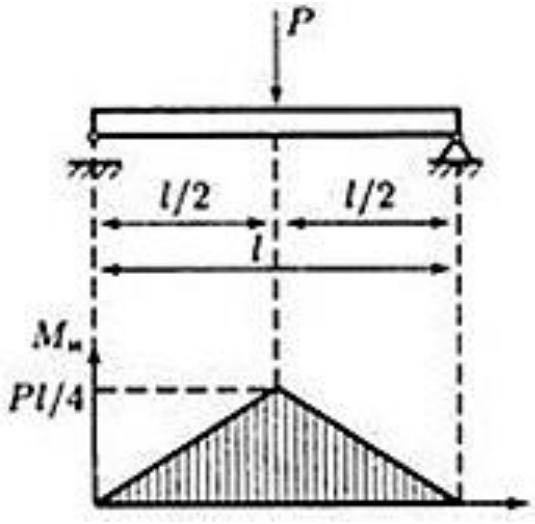

Fig. 4.2. Scheme of loading the sample.

4.1.2. Sample description

Tests were conducted on the high-temperature superconductor tape, which is shown in Fig. 4.3. Table 4.1 and Table 4.2 summarize the geometrical and mechanical characteristics of the tape, respectively.

Table 4.1: Geometrical characteristics of the sample

Number of layers	*4*
Length of the sample (mm)	*70*
Total height (µm)	*140*
Width of the sample (mm)	*5.95*

Table 4.2: Mechanical properties of the sample

Layer Number	1	2	3	4
Material	Cu	YBCO	NiW5	Cu
Height (µm)	*70*	*2*	*50*	*18*
Young's modulus (GPa)	*110*	*128*	111	*110*
Axial strength stress (MPa)	*150*	*260*	121	*150*

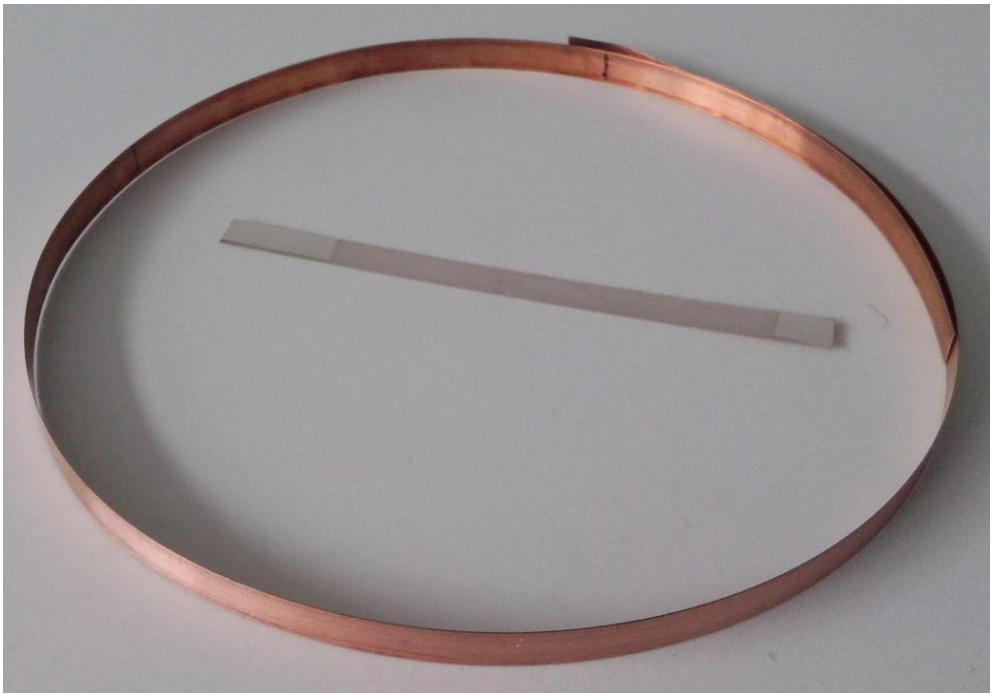

Fig. 4.3. Example of the HTS test sample.

4.1.3. Experimental results

The test was conducted by increasing the beam deflection up to the bearing capacity of the beam. The test was repeated 4 times. Figure 4.4 shows the results of these tests. We can observe a good agreement between these tests, which confirms the reliability of both the experimental setup and experimental procedure. In the following, we will consider the average value of these tests.

The load-deflexion curve shows first a quasi-linear variation up to $P = 0.15\ N$, followed by a nonlinear variation, then by quasi-stabilization. The maximum load is around $0.24\ N$ the corresponding deflection is equal to $20\ mm$.

During the test, we did not observe the destruction by delamination of the tape.

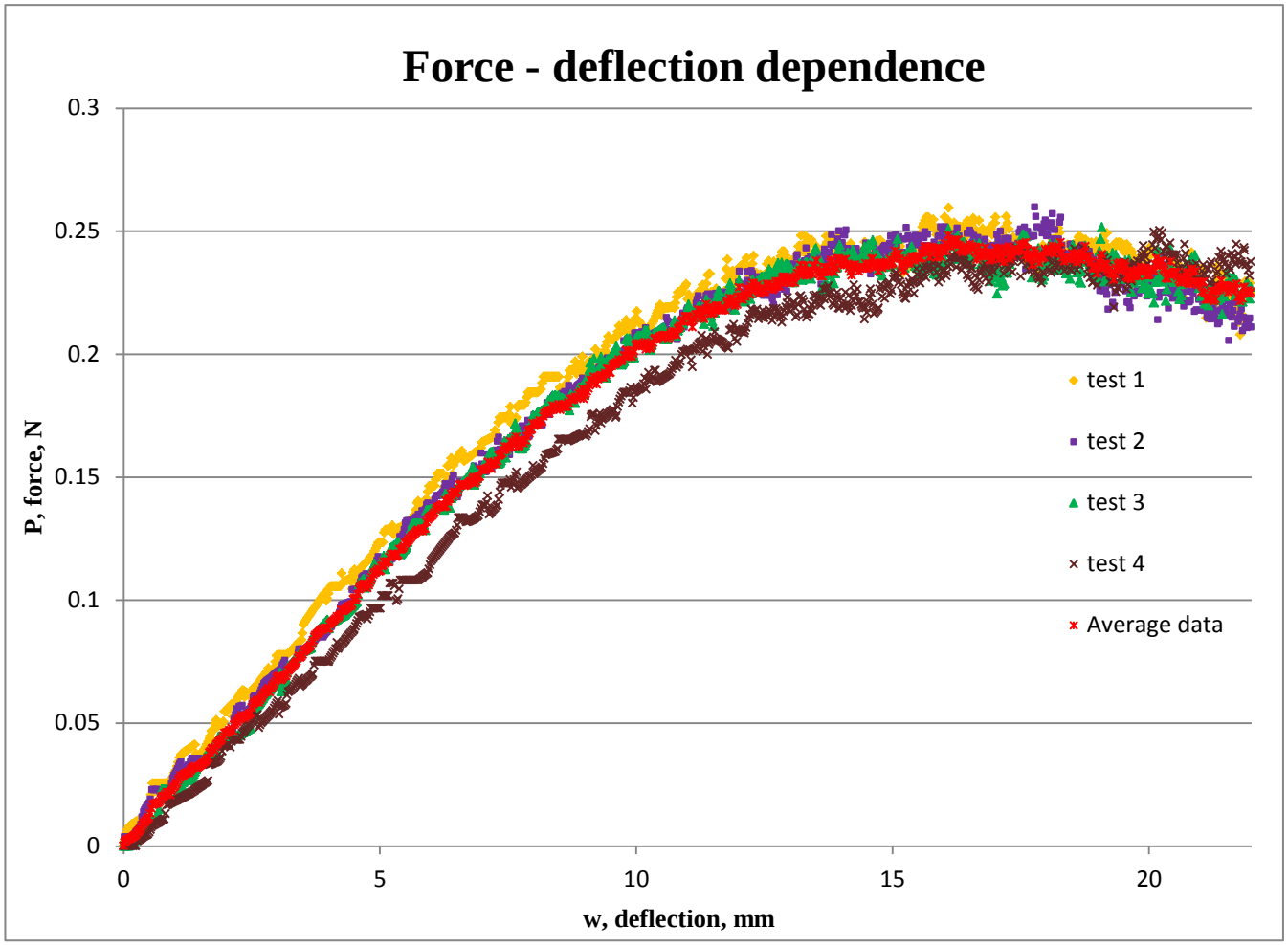

Fig. 4.4. Test result dependence.

4.2. Numerical modeling

4.2.1. Beam behavior

The program presented in chapter 3 is used in this section for the determination of the beam response to the load described in section 4.1.2.

Analyses were conducted with the geometrical and mechanical properties summarized in Table 4.1 and Table 4.2.

Fig. 4.5 shows the variation of the bending moment with the beam curvature. It shows first a linear variation, followed by a non-linear variation, and finally a

stabilization of the bending moment, which corresponds to full plasticity. The maximum bending moment is around $4 \cdot 10^{-3}$ $N \cdot m$.

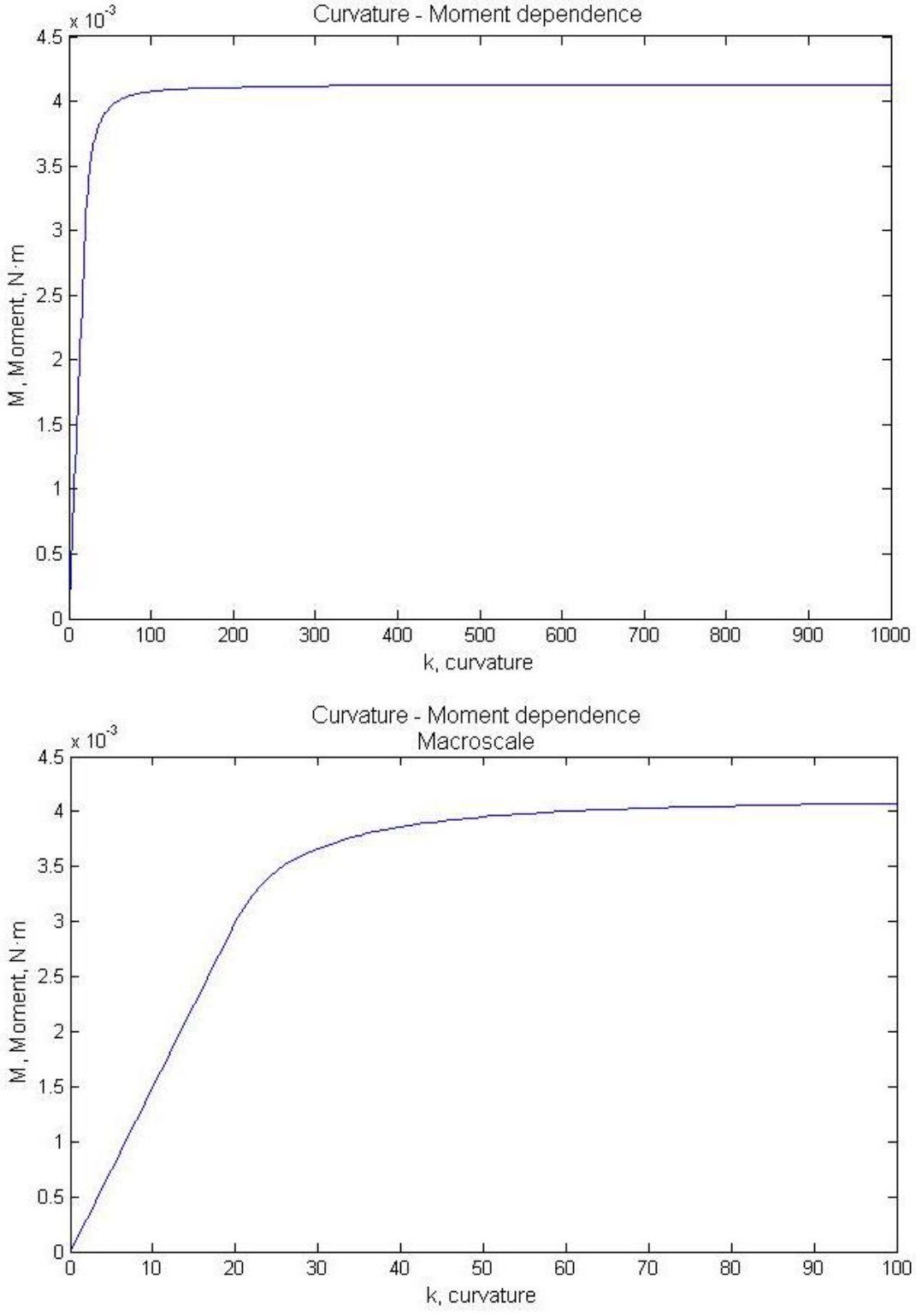

Fig. 4.5.HTS_Analysis calculation: Curvature – moment dependence.

Fig. 4.6 shows the variation of the position of the neutral axis during the increase of the moment. We observe that the neutral axis is first located in the YBCO layer, then it moves below the YBCO layer by about 3.5% of the beam thickness.

It should be taken into account that with such amount of the bending moment the diameter of wire from 2G HTS tape can reach *1 mm* (curvature 250 till 1000).

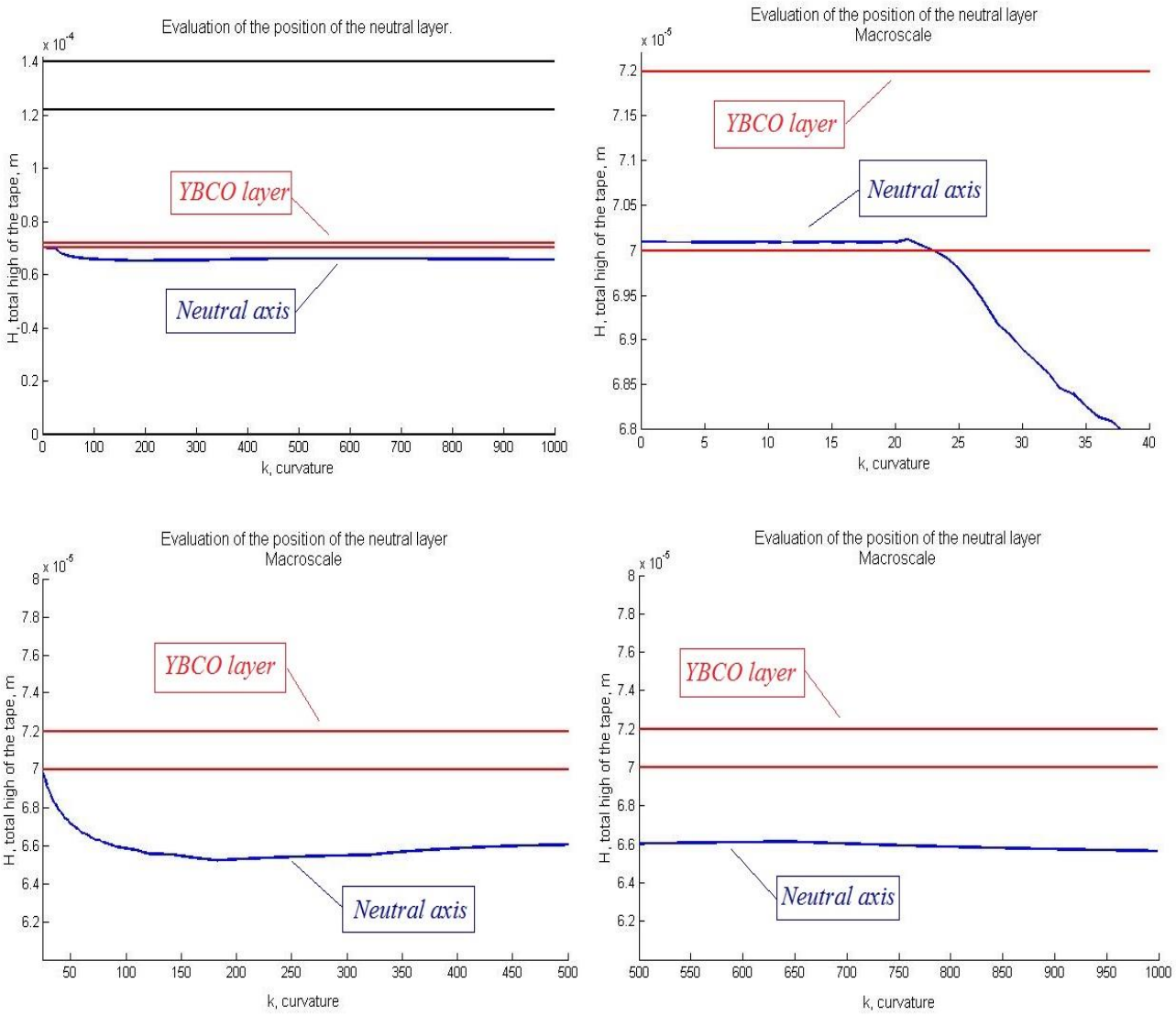

Fig. 4.6. HTS_Analysis calculation: Evaluation of the position of the neutral layer.

Fig. 4.7 shows the bending moment at different levels of the concentrated force.

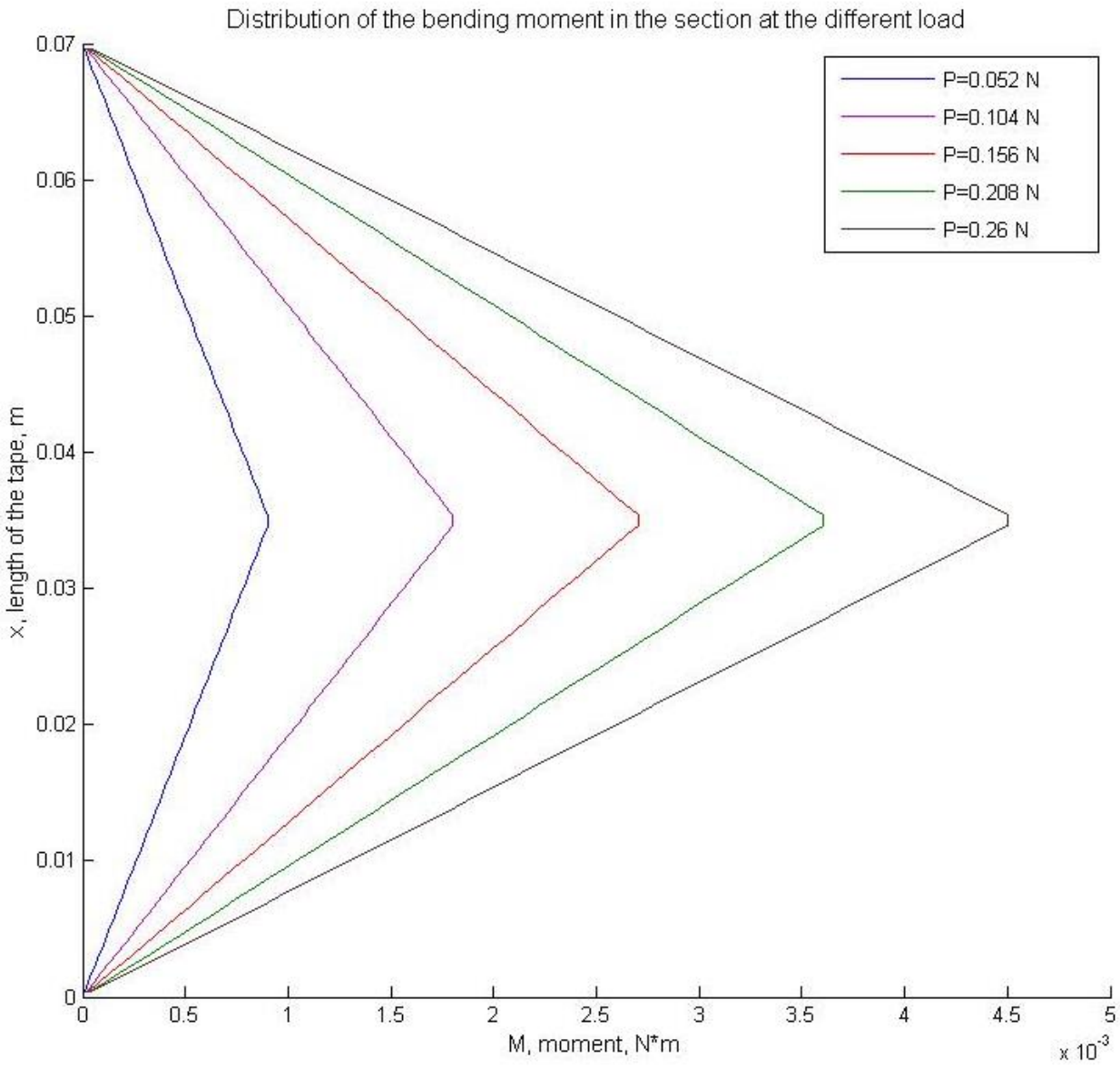

Fig. 4.7.HTS_Analysis calculation: Distribution of the bending moment in the section at the different forces.

The distributions of the normal and shear stresses in the section $x = 35\ mm$ under different forces are shown in Fig. 4.8. A linear variation of the normal stress in each layer is observed under the force $P = 0.0026\ N$. With the increase in the force, plasticity appears in the extreme layers (1st and 4th layers).

Concerning the shear stress, we observe first a ($P = 0.0026\ N$) a conventional distribution of the shear stress. With the increase in the load, we observe a concentration

of the shear stress in the central part (around the neutral axis), which results mainly from the plasticity.

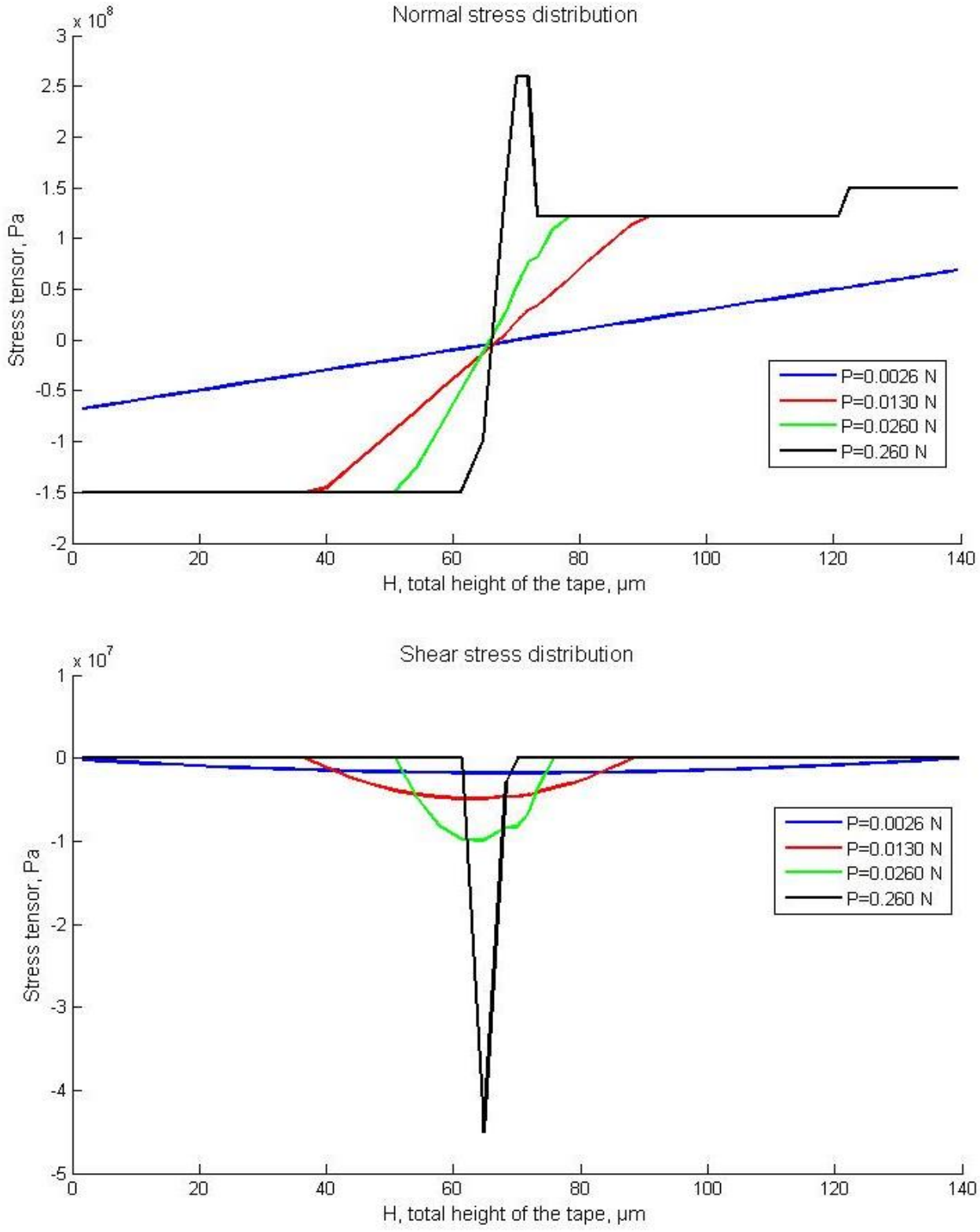

Fig. 4.8. HTS_Analysis calculation: Normal and shear stress distribution.

4.2.2. Beam deflection

The beam deflection was determined using the classical theory of beams together with the relationship between the bending moment and the beam curvature determined in the previous section (Fig. 4.5). We can observe a very good agreement between these results.

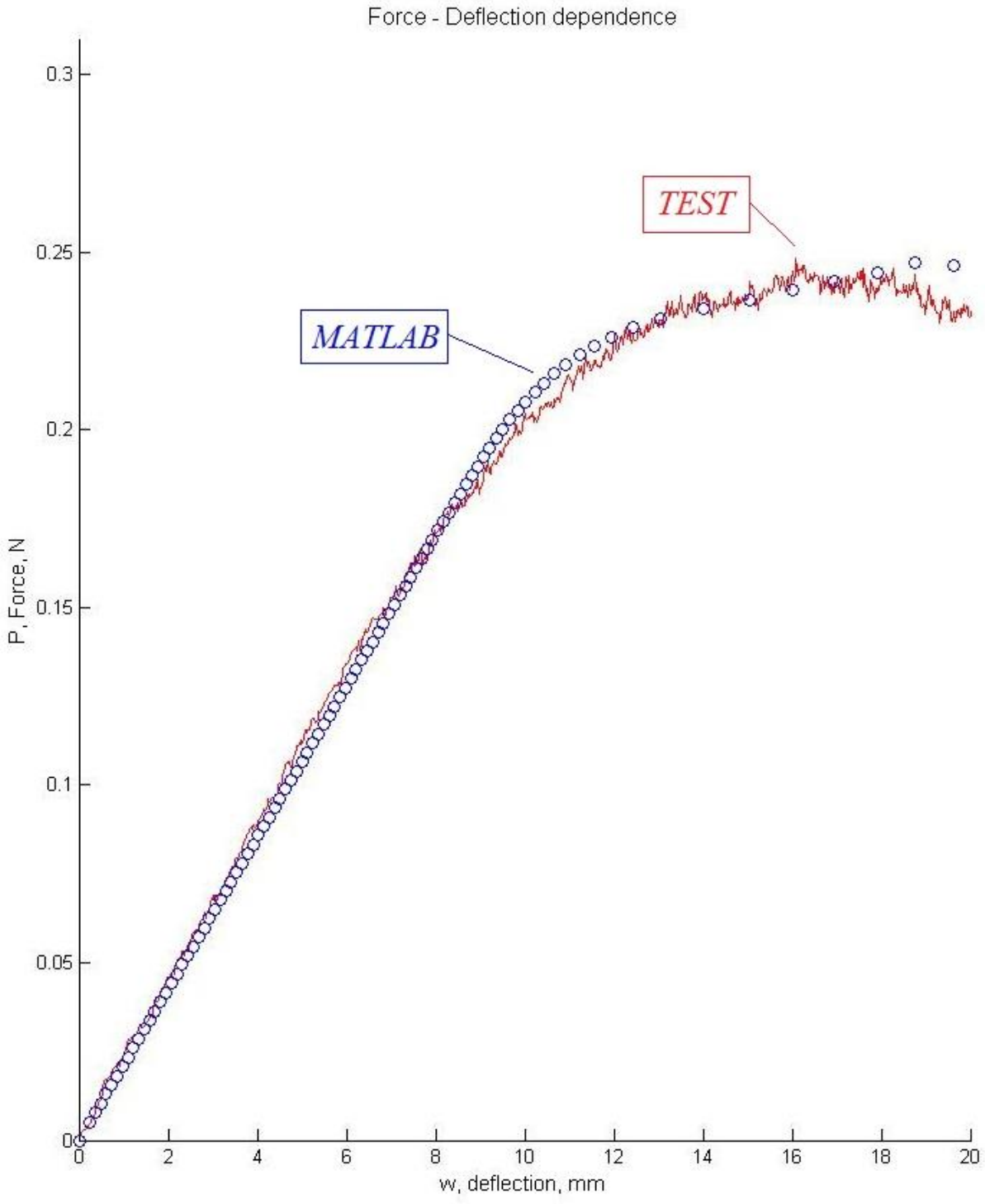

Fig. 4.9. Matlab - test result comparison.

The numerical model reproduces well the different phases of the beam response: the linear phase, the nonlinear one and finally the stabilisation phase at $P = 0.20\ N$. This good agreement shows the performance of the numerical model developed in the previous chapter and its ease use in practical applications.

4.3. Conclusion

The chapter included the verification of the numerical model developed in the previous chapter for the complex behaviour of high-temperature multilayer 2G tape. The verification was conducted on a bending beam test conducted within this thesis. The test was performed on a high-temperature superconductor tape composed of 4 layers.

The numerical modelling included two phases. The first one concerned the construction of the global behaviour of the beam (relationship between the bending moment and the curvature) using the model presented in chapter 3 and then the calculation of the beam deflection using both the conventional structure theory together with the nonlinear relationship between the bending moment and the curvature. Analysis was conducted using a step-by-step analysis with an actualisation of the beam behaviour at the beginning of each step.

The comparison of the numerical and experimental results showed excellent agreement, which confirms the performance of the numerical model developed in the previous chapter and its ease use in practical applications.

GENERAL CONCLUSIONS

The optimization process of the low-temperature superconductor and high-temperature superconductor for the International thermonuclear experimental reactor (ITER) is shown.

The main problem for the LTS materials that was caused by the plastic deformation and realized by pressing and drawing are shown. With help of thermo-elasticity equations, the temperature modes resulting in the appearance of thermoplastic deformations and the possible residual stresses formation are established. The critical drawing velocities are determined from the conditions of contact heating, in order to prevent the residual stresses in the wire. For some kind of metals as copper, titanium, zirconium the critical drawing velocities were given a recommendation that can be applied for development of the drawing technology.

The optimal angles of matrixes for pressing of mono-, bi- and trimetal blank were determined with the conditions of minimum compacting force. The compacting force components containing the cone angle of the technological tool are taken into account. The process parameters affecting the compacting force are revealed. The effect of the elongation and the friction coefficient to the optimal angles is shown. Application of the matrix with the optimal cone angle allows to reduce pressing energy intensity during production of the low-temperature superconducting products.

The main problems in the optimization of the fabrication of 2G high-temperature superconductors (HTS) were shown. The manufacturing of 2G HTS are required the special conditions, in order to decrease the axial and shear stresses in the HTS. The difficulties of usage of finite element method for solving this challenge task were described.

The simplified model that allows to find the optimal design was created. The main condition that requires keeping the neutral axis close to the superconductive layer were taken into consideration. The main principle of this model is the combination of the classical beam theory with the discretization of each layer in small sub-layers working under purely axial stresses. This model was implemented using MATLAB

software. The plastic behavior of the HTS constitutive materials were taken into consideration by this model. The validation of the model was successfully done by its confrontation to finite element analyses.

The best geometry of the HTS tape with the condition of reducing the mechanical stresses was found. Analysis resulted in recommendations for the optimal configurations that reduce stresses in the superconductive layer.

The validation experimental test on the real sample of 2G high-temperature superconductor tape was done. The validation test gave satisfactory results in comparison with prediction of numerical model (HTS_Analysis program) that was implemented using MATLAB software. As a result a number of experiment can be reduce, because the program allows to make a simulation of bending process in order to satisfy the high quality manufacturing standards as well as reduce the possibility of manufacturing defects. Prediction and analysis such important characteristics as critical forces, deflection, influence of boundary condition will help to construct the HTS tape with condition of respect of the high quality manufacturing standards. The recommendation about improvement and optimization the fabrication process can be easily given after HTS_Analysis program simulation.

In addition, this model could be easily implemented and used in industrial environment, in particular to make a prediction and to find a right geometry for the HTS materials of second generation for different industrial applications.

PUBLICATIONS

1. G. Kolmogorov, **N. Kosheleva**, “Rate limit of plastic deformation of rod products” (In Russian: Predel'nye rezhimy plasticheskogo deformirovaniya prutkovykh izdelii), *Collection of theses “Applied Mathematics and Mechanics”, Perm State Technical University,* Perm. 2010. P. 68-70.
2. G. Kolmogorov, **N. Kosheleva**, T. Chernova, “Temperature conditions in manufacturing of superconducting nanocomposites” (In Russian: Temperaturnye usloviya pri proizvodstve sverkhprovodnikovykh nanokompozitov), *Collection of scientific works “New material, nanosystems and nanotechnology” (RAM disk),* Perm. 2010.
3. G. Kolmogorov, **N. Kosheleva**, T. Chernova, “Temperature conditions and forming techniques of residual stresses in wire drawing” (In Russian: Temperaturnye usloviya i rezhimy formirovaniya ostatochnykh napryazhenii pri volochenii provoloki), *Izvestiya VUZ. Nonferrous metallurgy*. 2011. No. 3. P. 23-26.
4. G. Kolmogorov, **N. Kosheleva**, E. Kusnetsova, T. Chernova, “Temperature conditions and models of formation of residual stresses in wiredrawing”, *Russian Journal of Non Ferrous Metals*, 2011. Vol. 52. No. 3. P. 227-229.
5. G. Kolmogorov, **N. Kosheleva**, T. Chernova, “Optimization of geometry of the technological tool at pressing” (In Russian: Optimizatsiya geometrii tekhnologicheskogo instrumenta pri pressovanii), *Vestnik PSTU. Applied Mathematics and Mechanics*. 2011. No. 9. P. 116-120.
6. **N. Kosheleva**, G. Kolmogorov, “Rate limit of plastic deformation and residual stress” (In Russian: Predel'nye skorosti plasticheskogo deformirovaniya i ostatochnye napryazheniya), *Collection of theses of VI Russian Conference of talented young people in Russia, "National treasure of Russia"*. 2012. P. 1003.
7. G. Kolmogorov, **N. Kosheleva**, “Optimization of geometry of the technological tool at pressing bimetallic billet” (In Russian: Optimizatsiya geometrii tekhnologicheskogo instrumenta pri pressovanii bimetallicheskoi zagotovki),

Abstracts collection of the scientific and technical conference of students and young scientists. Perm. PNRPU. 21-27 May 2012. P. 37-38.

8. G. Kolmogorov, **N. Kosheleva**, "Problems of optimal design process of the technological tool for pressing the low-temperature superconducting products" (In Russian: Voprosy optimal'nogo proektirovaniya tekhnologicheskogo instrumenta pri pressovanii nizkotemperaturnykh sverkhprovodnikovykh izdelii), *The collection of materials works of winners of Russian competition of research works of students and phD students in the field of technical science*, Publishing House of St. Petersburg. 2012. P. 249-251.
9. G. Kolmogorov, **N. Kosheleva**, T. Chernova, "Questions of optimization of the technological tool for pressing low-temperature superconductors" (In Russian: Voprosy optimizatsii tekhnologicheskogo instrumenta pri pressovanii nizkotemperaturnykh sverkhprovodnikov), *Materials of the Russian scientific conference of young scientists "Science. Technologies. Innovations"*, Publishing house Novosibirsk. 29 November-02 December 2012. P. 184-188.
10. G. Kolmogorov, **N. Kosheleva**, T. Chernova, "Technological tool geometry optimization during production low-temperature superconductors" (In Russian: Optimizatsiya pressovogo instrumenta pri proizvodstve nizkotemperaturnykh sverkhprovodnikov), *XVIII Winter School on continuum mechanics. Abstracts*, Perm. 2013. P. 185.
11. G. Kolmogorov, **N. Kosheleva**, T. Chernova, "Optimization of technological tool geometry in the production low-temperature superconductors" (In Russian: Optimizatsiya pressovogo instrumenta pri proizvodstve nizkotemperaturnykh sverkhprovodnikov), *Vestnik of Perm National Research Polytechnic University. Mechanics*. 2013. No. 1. P. 106-120.
12. G. Kolmogorov, **N. Kosheleva**, T. Chernova, "Optimization of technological tool geometry in forming bimetallic piece parts" (In Russian: Optimizatsiya geometrii tekhnologicheskogo instrumenta pri pressovanii bimetallicheskoi zagotovki), *Izvestiya VUZ. Nonferrous metallurgy.* 2013. No. 4. P. 19-21.

13. G. Kolmogorov, **N. Kosheleva**, T. Chernova et al, "Technological Basics for Production of Low-Temperature Superconductors", *Open Journal of Metal*. 2013. No. 3. P. 19-22.
14. G. Kolmogorov, **N. Kosheleva**, T. Chernova, "Optimization of technological tool geometry in forming trimetallic piece parts" (In Russian: Optimizatsiya geometrii tekhnologicheskogo instrumenta pri pressovanii trimetallicheskoi zagotovki), *Izvestiya VUZ. Nonferrous metallurgy.* 2014. No. 1. P. 55-58.
15. G. Kolmogorov, **N. Kosheleva**, T. Chernova, "Optimization of geometry of process tool for pressing trimetal billet", *Russian Journal of Non-Ferrous Metals*. 2014. Vol. 55. No. 2. P. 154-156.
16. **N. Kosheleva**, "Technological features of fabrication high-temperature superconductors" (In Russian: Tekhnologicheskie osobennosti proizvodstva vysokotemperaturnykh sverkhprovodnikov), *Innovation Technologies: Theory, instruments, practices*, PNRPU, Perm. 2014. No. 1. P. 341-346.
17. G. Kolmogorov, Yu. Burdina, **N. Kosheleva**, T. Chernova, "Technological tool for low-temperature superconductor fabrication" (In Russian: Tekhnologicheskii instrument dlya proizvodstva nizkotemperaturnykh sverkhprovodnikov), *XIX Winter School on continuum mechanics. Abstracts*, Perm. 2015. P. 155.
18. **N. Kosheleva**, G. Kolmogorov, "The calculation theory of a flexible tape from HTS using Ritz-Timoshenko method" (In Russian: Teoriya rascheta gibkoi lenty VTSP metodom Rittsa-Timoshenko), *Building mechanics and calculation of structures*. 2015. No. 1(285). P. 11-14.
19. **N. Kosheleva**, I. Shahrour, G. Kolmogorov, "The questions of finding the optimal geometry of 2G HTS using simplified mechanical model" (In Russian: Optimal'naya geometriya 2G VTSP provodov s ispol'zovaniem uproshchennoi mekhanicheskoi modeli), *The problem of deformation and fracture of materials and structures. Abstract collections of Russian scientific conference*, PNRPU, Perm. 17-19 June 2015. P. 59.

Patents

1. Methods of billets extrusion. Abstract of invention №2526346 RF application 2013113441/02, 26.03.2013. Date of publication: 20.08.2014 Bull. №23. G. Kolmogorov, V. Trofimov, **N. Kosheleva**, T. Chernova.
2. Methods of pressing of bimetallic billets. Abstract of invention №2528302 RF application 2013118316/02, 19.04.2013. Date of publication: 10.09.2014 Bull. №25. G. Kolmogorov, **N. Kosheleva**, T. Chernova.
3. Pressing method of trimetallic workpiece. Abstract of invention №2544320 RF application 2013148752/02, 31.102013. Date of publication: 20.03.2015 Bull. №8. G. Kolmogorov, **N. Kosheleva**, T. Chernova.

Submitted papers

1. **N. Kosheleva**, I. Shahrour, "A simplified mechanical model for the optimization of the fabrication process of high-temperature superconductors", *International Conference on Mechanics of Complex Solids and Fluids*, Lille, France, May 17-22, 2015.
2. **N. Kosheleva**, I. Shahrour, C. E. Bruzek, G. Vega, G. Kolmogorov, "Development of a simplified numerical model for the design of 2G HTS", *The International Journal of Multiphysics*.
3. **N. Kosheleva**, I. Shahrour, C. E. Bruzek, G. Vega, G. Kolmogorov, "Development of a simplified numerical model for the design of 2G high-temperature superconductors", *IEEE Transactions on Applied Superconductivity.*

References

Attarnejad, R., Semnani, S. J. & Shahba, A., 2010. Basic displacement functions for free vibration analysis of non-prismatic timoshenko beams. *Finite Elements in Analysis and Design,* 46(10), p. 916–929.

Aymar, R., 2002. Status of ITER. *Fusion Engineering and Design,* 61-62(2012), pp. 5-12.

Bansal, G., 2008. *Feasibility studies on large- current capacity HTS conductors for fusion magnets.* Japan, Thesis. The Graduate University for Advanced Studies.

Bareisis, J. & Kleiza, V., 2009. Effect of Layer Geometry and Stiffness on the Fields of Normal Stresses in Multilayer Beams Under Asymmetric Bending. *Journal of mechanics of composite materials,* 45(4), pp. 399-406.

Bauer, M., Semerad, R. & Kinder, H., 1999. YBCO films on metal substrates with biaxially aligned MgO buffer layers. *IEEE Transactions Applied Superconductivity,* 9(2), pp. 1502-1505.

Benamar, R., Bennouna, M. K. & White, R. G., 1991. The effects of large vibration amplitudes on the mode shapes and natural frequencies of thin elastic structures. part i: simply supported and clamped-clamped beams.. *Journal of Sound and Vibration,* 149(2), pp. 179-195.

Bernoulli, D., 1751. *De vibrationibus et sono laminarum elasticarum.*. Petropoli: Commentarii Academiae Scientiarum Imperialis Petropolitanae.

Bhattacharjee, P. P., Ray, R. K. & Upadhyaya, A., 2007. Nickel base substrate tapes for coated superconductor applications. *Journal of Materials Science,* 42(6), pp. 1984-2001.

Bhattacharya, R. S. & Xu, Y., 2005. Development of textured buffer layer on metal tapes for oxide superconductors. *Nat. Lab. UES Materials Laboratory Report. Argonne National Laboratory.*

Bolotin, V. & Novikov, J., 1980. *Mechanics of Multilayer Constructions (in Russian: Mechanika mnogosloinuh construkcii).* Moscow: Mashinostroenie.

Bruzek, C., Allais, A., Morice, S. & et al., 2012. New HTS 2G round wires. *IEEE transactions on applied superconductivity,* 22(3), p. 5800204.

Bruzek, C., Allais, A., Theune, C.-F. & et al., 2011. *New HTS 2G Round wires.* Marseille, MT22.

Carrera, E., Giunta, G. & Petrolo, M., 2011. *Beam Structures: Classical and Advanced Theories, Wiley Series in Computational Mechanics.*. 1 ed. United Kingdom: John Wiley and Sons.

Christensen, R., 1982. *Mechanics of composite materials (in Russian:Vvedenie v mekhaniku kompositov).* Moscow: Mir.

De Borbon, F. & Ambrosini, D., 2010. On free vibration analysis of thin-walled beams axially loaded. *Thin-Walled Structures,* Volume 48, p. 915–920.

De Lorenzis, L., Miller, B. & Nanni, A., 2001. Bond of FRP Laminates to Concrete. *ACI Materials Journal*, 8(3), p. 256–264.

Eickemeyer, J. et al., 2007. Elongated grains in textured substrate tapes and their effect on transport currents in superconductor layers. *Horst Wendrock, Jens Hänisch, Bernhard Holzapfel, L. Schultz, A. Güth, Applied Physics Letters,*, 90(1), pp. 012510-012510-3.

Euler, L., 1744. *Methodus inveniendi lineas curvas maximi minimive proprietate gaudentes, sive Solutio problematis isoperimitrici latissimo sensu accepti. Appendix "De curvis elasticis".* Lausanne: Geneva.

Feodosyev, V. I., 1999. *Strength of Materials (in Russian: Soprotivlenie materialov).* Moscow: MGTU Baumen.

Foner, S., 1987. *Superconductor materials science: metallurgy, fabrication, and applications. (in Russian: Translation from English.Metallovedenie i tekhnologia sverkhprovodiaschikh materialov).* Moscow: Metallurgia.

Fujino, K., Hasegawa, K., Mukai, H. & et al., 1996. 1 meter long thin film tape with high Je of 1.5 X 10 Ncm fabricated by pulsed Iaser deposition. *Adv. Supercond,* Volume VIII, p. 675.

Garuckas, D. & Bareisis, J., 2003. Influence of Different Factors on the Stiffness and Strength of Multilayer Composite Elements. *Journal of mechanics of composite materials*, 39(2), pp. 153-164.

Ginzburg, V., 1999. What problems of physics and astrophysics on the boundary of the twenty-first century, are the most important and interesting?. *Science and life,* Issue 11, pp. 14-21.

Ginzburg, V. & Andrushin, E., 2006. *Superconditivity (in Russian: Sverhprovodimost).* Moscow: Alfa-M.

Golas, J., Podhorenka, A. & et al., 2002. On an Approach to the Solution of the Bending Problem for Laminated Plates. *Mechanics of Composite Materials*, 38(3), p. 252–263.

Gorospe, A., Nisay, A. & Shin, H.-S., 2014. Delamination behaviour in differently copper laminated REBCO coated conductor tapes under transverse loading. *Physica C,* Volume 504, p. 47–52.

Groves, J. R., Hammond, R. H., Depaula, R. F. & Clemens, B. M., 2008. Investigation of early nucleation events in magnesium oxide during Ion Beam Assisted Deposition. *MRS Proceedings*, Volume 1150.

Hazelton, D. W., 2014. *SuperPower 2G HTS Conductor*, Hamburg: BIT's 4th New Energy Forum-2014 (NEF2014).

Hühne, R., Fähler, S., Schultz, L. & Holzapfel, B., 2005. Thin biaxially textured MgO and TiN films prepared by ion-beam assisted pulsed laser deposition for coated conductor applications. *Physica C: Superconductivity,* Volume 426-431. Part 2, p. 893–898.

Iijima, Y., Tanabe, N., Ikeno, Y. & Kohno, O., 1991. Biaxially aligned YBa2Cu3O7−x thin film tapes. *Physica C: Superconductivity*, Volume 185–189. Part 3, p. 1959–1960.

Jeong, H., Park, H., Kim, S. & et al., 2012. Delamination characteristics of coated conductor for conduction cooled HTS coil. *IEEE Transaction on applied superconductivity,* 22(3).

Jonas, B., 2006. Stiffness and Strength of Multilayer Beams. *Journal of Composite Materials,* 40(6), pp. 515-531.

JSC «Chepetsky Mechanical Plant», 2014. *Production of Superconducting Materials (SCM) (in Russian: Proizvodstvo sverkhprovodiaschikh materialov (SPM)) [electronic resource].*. [Online]
Available at: http://www.chmz.net/product/sp/

JSC «Federal grid company of unified energy system», 2011. *Equipment based on high-temperature superconductivity (in Russian).* [Online]
Available at: http://www.fsk-ees.ru/eng/

Kaizhong, D., Yanfang, B. & et al., 2012. Development of ITER HTS current lead at ASIPP. *Physics Procedia,* Issue 36, pp. 931-936.

Kannberg, L. D. et al., 2003. *GridWiseTM: The Benefits of a Transformed Energy System,* Washington: Pacific Northwest National Laboratory.

King, J. L., 1990. On the Flexure of Uniform Anisotropic Beams of Rectangular Section. *Composite Structures,* 14(2), p. 125–150.

Kolmogorov, G. L., 1986. *Hydrodynamic Lubrication in Metal Forming (in Russian: Gidro Dinamicheskaya smazka pri obrabotke metallov davleniya).* Moscow: Metallurgiya.

Kolmogorov, G. L., Filippov, V. B. & Latysheva, T. V., 2007. On Optimal Geometry of Drawing Tool (in Russian:Ob optimalnoi geometrii volochilnogo instruments). *Izvestia VUZov. Chernaia metallurgia,* Issue 4, pp. 41-43.

Kolmogorov, G. L., Kosheleva, N. A. & Chernova , T. V., 2013. Optimization of Technological Tool Geometry at Pressing of Bimetal Blank (in Russian: Optimizatsiia geometrii tekhnologicheskogo instrumenta pri pressovanii bimetallicheskoi zagotovki). *Izvestiia VUZov. Tcvetnaia metallurgia,* Issue 4, pp. 19-21.

Kolmogorov, G. L., Kosheleva, N. A. & Chernova, T. V., 2011. Optimization of Geometry of Technological Tool at Pressing (in Russian: Optimizatsiia geometrii tekhnologicheskogo instrumenta pri pressovanii). *PSTU bulletin. Applied mathematics and mechanics,* Issue 9, pp. 116-120.

Kolmogorov, G. L., Kosheleva, N. A. & Chernova, T. V., 2013. Optimization of Technological Tool Geometry at Pressing of Bimetal Blank (in Russian: Optimizatsiia geometrii tekhnologicheskogo instrumenta pri pressovanii bimetallicheskoi zagotovki). *Izvestiia VUZov. Tcvetnaia metallurgia,* Issue 4, pp. 19-21.

Kolmogorov, G. L., Kosheleva, N. A. & Chernova, T. V., 2014. Optimization of geometry of process tool for pressing trimetal billet. *Russian Journal of Non-Ferrous Metals.,* 55(2), pp. 154-156.

Kolmogorov, G. L., Kosheleva, N. A. & Chernova, T. V., 2014. Optimization of geometry of process tool for pressing trimetal billet. *Russian Journal of Non-Ferrous Metals.,* 55(2), pp. 154-156.

Kolmogorov, G. L., Kosheleva, N. A., Kusnetsova, E. V. & Chernova, T. V., 2011. Temperature conditions and models of formation of residual stresses in wiredrawing. *Russian Journal of Non-Ferrous Metals,* 52(3), p. 227–229.

Kolmogorov, G. L. & Kuznetsova, E. V., 2000. On Degree of Deformation at Axisymmetric Deformation (in Russian: O stepeni deformatsii pri osesimmetrichnom deformirovanii). *Izvestia VUZov. Chernaia metallurgia.,* Issue 11, pp. 31-33.

Kolmogorov, G. L., Mikhailov, V. G., Barkov, U. L. & Karlinskii, V. L., 1991. *Hydraulic Forging of Hardly-Deformed and High-Melting Metals and Alloys (in Russian: Gidropressovanie trudnodeformiruemykh tugoplavkikh metallov i splavov).* Moscow: Metallurgia.

Kolmogorov, G. L., Shevliakov, V. U. & Orlov, S. I., 1992. *Tool for Drawing (in Russian:Instrument dlia volochenia).* Moscow: Metallurgia.

Kolmogorov, G. L. & Shirobokov, S. E., 1995. Temperature Conditions and Mode of Formation of Residual Stresses in Wiredrawing (in Russian:Temperaturnye uslovia i rezhim formirovania ostatochnykh napriazhenii pri volochenii provoloki). *Izvestia VUZov. Chernaia metallurgia,* Issue 1, pp. 49-52.

Kolmogorov, G. L. et al., 2013. Technological Basics for Production of Low-Temperature Superconductor. *Open Journal of Metal,* Issue 3, pp. 19-22.

Kolmogorov, G. L., Trofimov, V. N., Shtutca, M. G. & Chernova, T. V., 2011. *Mechanics of Plastic Deformation of Transversely Isotropic Composite Superconducting Materials (in Russian:Mekhanika plasticheskogo deformirovania transversalno-isotopnykh kompozitsionnykh sverlhprovodnikovykh materialov).* Perm: PNRPU.

Krasilcikov, A., 1991. *Sailplanes USSR (in Russian: Planeru SSSR).* Moscow: Mashinostroenie.

Lehner, T. F., 2013. *Production of 2G HTS Conductor at SuperPower: Recent Progress and Ongoing Improvements.* Aix-en-Provence, France, 7th MEM Workshop (Mechanical and Electromagnetic Effects in Superconductors).

Maeda, H. & Yanagisawa, Y., 2014. Recent developments in High-Temperature Superconducting magnet technology (review). *IEEE Transactions On Applied Superconductivity*, 3(24).

Malinin, N. N., 1975. *Applied Theory of Plasticity and Creep (in Russian: Prikladnaia teoria plastichnosti i polzuchesti).* Moscow: Mashinostroenie.

Markiewicz, W. D. & Swenson, C. A., 2010. Winding strain analysis for YBCO coated conductors. *Superconductor Science and Technology*, Issue 23, pp. 1-12.

Matsunaga, H., 1996. Free vibration and stability of thin elastic beams subjected to axial forces.. *Journal of Sound and Vibration,* 191(5), p. 917–933.

Miyata, S., Ibi, A., Izumi, T. & Shiohara, Y., 2011. Surface roughness of MgO thin film and its critical thickness for optimal biaxial texturing by ion-beam-assisted deposition. *J. Appl. Phys.*, Volume 109, p. 113922.

Myazato, T., Hojo, M. & et al., 2011. Mode I type delamination fracture toughness of YBCO coated conductor with additional Cu layer. *Physica C,* Volume 471, p. 1071 – 1074.

National research centre "Kurchatov institute", 2007. *Superconductors in Electrical PowerIndustry. Metal base of HTS wire of second generation(in Russian)..* [Online]
Available at: http://perst.isssph.kiae.ru/supercond/bulletein/bulletein_v4_n3_2007.pdf

National research centre "Kurchatov institute", 2012. *Superconductors in Electrical PowerIndustry. Heavy-current-carrying elements of the HTS tapes of 2nd generation and their perspectives(in Russian).* [Online]
Available at: http://perst.isssph.kiae.ru/supercond/bulletein/bulletein_v9_n3_2012.pdf

National research centre "Kurchatov institute", 2013. *Superconductors in Electrical Power Industry. Investigation of delamination of HTS conductors 2nd generation (in Russian).* [Online]
Available at: http://perst.isssph.kiae.ru/supercond/bulletein/bulletein_v10_n2_2013.pdf

National research centre "Kurchatov institute", 2014. *Superconductors in Electrical Power Industry. HTS materials of second generation (in Russian).* [Online]
Available at: http://perst.isssph.kiae.ru/supercond/bulletein/bulletein_v11_n1_2014.pdf

Nexans, 2015. *Superconductors in the round.* [Online]
Available at: http://www.nexans.com/eservice/Corporate-en/navigatepub_167338_-32549/Superconductors_in_the_round.html

Nishijima, G. & Kitaguchi, H., 2012. Transport and mechanical property evaluation for Cu stabilized PLD-GdBa CuO coated conductor. *IEEE Transactions on applied superconductivity,* 22(3).

Obradors, X. & Puig, T., 2013. Superconductivity Web 21. *International Superconductivity Technology Center, ISTEC,* pp. 2-14.

Perlin, I. & Ermanuk, M., 1972. *Theory of Drawing (in Russian: Teoria volochenia).* Moscow: Metallurgia.

Perlin, I. & Reitbarg, L., 1975. *Theory of Metal Pressing (in Russian: Teoria pressovania metallov).* Moscow: Metallurgia.

Saint-Venant, A. D., 1856. Memoire sur la flexion des prismes. *Journal de Methematiques pure et appliqu´es,* Volume 1, p. 89–189.

Sarma, V. S., De Boer, B. & Holzapfel, B., 2003. On the development of high strength and bi-axially textured Ni–3%W/Ni–10%Cr–1.5%Al composite substrate for coated conductor application. *Scripta Materialia,* Volume 48, p. 1167–1171.

Scanlan, R. M., 2001. *Conductor cost/performance status report for Snowmass.* s.l., LBNL SCMAG 737.

Schnabl, S., Saje, M., Turk, G. & Planinc, I., 2007. Analytical Solution of Two-Layer Beam Taking into account Interlayer Slip and Shear Deformation. *ASCE Publication, Journal of Structure Engineering,* 133(6), p. 886–894.

Selvamanickam, V., 2011. *Second-generation HTS wires for wind energy applications.* Houston, Texas Center for Superconductivity&SuperPower Inc.

Selvamanickam, V. et al., 2010. *Progress in research and development of IBAD-MOCVD based superconducting wires.* Washington D.C., Applied Superconductivity Conference.

Sherbakov, V., Novikov, M., Shykov, A. & et al., 2012. Superconductors in Electrical Power Industry. Beginning ITER in Russia (in Russian: Stanovlenie ITER v Rossii). *Superconductors in Electric Power Industry,* 9(3), pp. 2-13.

Shikimachi, K. et al., 2009. System coordination of 2 GJ class YBCO SMES for power system control. *IEEE Transactions on Applied Superconductivity,* 19(3), p. 2012.

Shikov, A. K., Nikulin, A. D., Silaev, A. G. & et al., 2003. Development of Superconductors for Magnetic System of ITER in Russia (in Russian: Razrabotka sverkhprovodnikov dlia magnitnoi sistemy ITER v Rossii). *Izvestia VUZov. Chernaia metallurgia,* Issue 1, p. 36 – 43.

Song, H. et al., 2012. 2G HTS coil technology development at SuperPower. *IEEE/CSC & ESAS European superconductivity news forum,* Volume 22.

Superconductor Technologies Inc, 2013. *Investor Presentation.* Chicago, IL.

Timoshenko, S. P., 1921. On the corrections for shear of the differential equation for transverse vibrations of prismatic bars. *Philosophical Magazine,* Volume 41, p. 744–746.

Timoshenko, S. P., 1922. On the transverse vibrations of bars of uniform cross section. *Philosophical Magazine,* Volume 43, p. 125–131.

Timoshenko, S. P. & Goodier, J., 1975. *Theory of Elasticity (in Russian: Teoria uprugosti).* Moscow: Nauka.

Tret'yakov, A. V. & Zyuzin, V. I., 1973. *Mechanical Properties of Metals and Alloys under Pressure Treatment (in Russian: Mekhanicheskie svoistva metallov i splavov pri obrabotke davleniem).* Moscow: Metallurgiya.

Usoskin, A. & Kirchhoff, L., 2008. In-plane texturing of buffer layers by alternating beam assisted deposition: large area and small area applications. *Mater. Res. Soc. Symp. Proc.,* Volume 1150.

Van der Laan, D. C., 2009. YBa2Cu3O7−δ coated conductor cabling for low ac-loss and high-field magnet applications. *Superconductor Science and Technology,* Issue 22, pp. 1-5.

Van der Laan, D. C., Eckin, J. W., Clickner, C. C. & Stauffer, T. C., 2007. Delamination strength of YBCO coated conductors under transverse tensile stress. *Superconductor Science and Technology,* Issue 20, pp. 765-770.

Van der Laan, D. C. & Ekin, J. W., 2007. Large intrinsic effect of axial strain on the critical current of high-temperature superconductors for electric power applications. *Applied physics letters,* Issue 90, pp. 1-3.

Van der Laan, D. C. & Ekin, J. W., 2008. Dependence of the critical current of YBa2Cu3O7−δ coated conductors on in-plane bending. *Superconductor Science and Technology,* Issue 21, pp. 1-6.

Van der Laan, D. C. et al., 2010. Effect of strain, magnetic field and field angle on the critical current density of YBa2Cu3O7−δ coated conductors. *Superconductor Science and Technology,* Issue 23, pp. 1-7.

Van der Laan, D. C., Goodrich, L. F. & Haugan, T. J., 2012. High-current dc power transmission in flexible RE-Ba2Cu3O7-δ coated conductor cables. *Superconductor Science and Technology,* 58(1), p. 014003.

Van der Laan, D. C., Lu, X. F. & al., e., 2011. *RE-Ba2Cu3O7-δ coated conductor helical cables for electric power transmission and SMES.* Tallahassee, Florida, EPRI Superconductivity Conference.

Van Rensburg, N. F. J. & Van der Merwe, A. J., 2006. Natural frequencies and modes of a Timoshenko beam.. *Wave Motion,* 44(1), p. 58–69.

Vasil'ev, V. & Protasov, V., 1990. *Composites Materials (in Russian: Compozicionnie materialu).* Moscow: Mashinostronie.

Voros, G. M., 2009. On coupled bending-torsional vibrations of beams with initial loads.. *Mechanics Research Communications,* Volume 36, p. 603–611.

William, D. & Callister, J., 2007. *Materials Science and Engineering – An Introduction.* 7th ed. New York: John Wiley and Sons, Inc..

Xiea, Y., Knolla, A., Maiorov, B. & et al., 2005. Progress in scale-up of second-generation high-temperature superconductors at SuperPower Inc. *Physica C: Superconductivity*, Volume 426–431. Part 2, p. 849–857.

Yaghoobi, H. & Fereidoon, A., 2010. Influence of Neutral Surface Position of Functionally Graded Beam under Uniformly Distributed Load. *IDOSI Publications, World Applied Sciences Journal,* 10(3), pp. 337-341.

Yamada, Y. et al., 2003. Present status and perspective of IBAD and PLD system in SRL and self-epitaxy in PLD-CeO2 on IBAD seed layer. *Physica C: Superconductivity*, Volume 392–396. Part 2, p. 777–782.

Yanagisawa, Y., Nakagome, H., Nakagome, H. & et al., 2011. Remarkable weakness against cleavage stress for YBCO-coated conductors and its effect on the YBCO coil performance. *Physica C,* Volume 471, p. 480 – 485.

Yu, L. S., Harper, J. M. E., Cuomo, J. J. & Smith, D. A., 1986. Control of thin film orientation by glancing angle ion bombardment during growth. *Journal of Vacuum Science & Technology A*, 4(443).

Zhang, Y., Duvall, J., Knoll, A. & et al., 2011. *Development of testing method for adhesion strength characteriza-tion of 2G HTS wire.* Osaka, The 15th Japan – US Workshop on Advanced Superconductors.

Zwick Roell Group, 2015. *Testing systems.* [Online] Available at: www.zwick.com